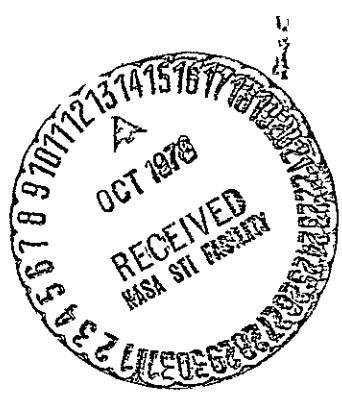

(NASA-CR-159418) STUDY OF DYNAMIC EMISSION SPECTRA FROM LUBRICANT FILMS IN AN ELASTOHYDRODYNAMIC CONTACT USING FOURIER TRANSFORM SPECTROSCOPY Final Report, 1 Jan. 1976 - 31 Dec. 1977 (Suntech, Inc., Marcus

N78-32809

Unclas
G3/70 31590

Suntech Group

NASA CR-159418

STUDY OF DYNAMIC EMISSION SPECTRA FROM LUBRICANT FILMS IN AN ELASTOHYDRODYNAMIC CONTACT USING FOURIER TRANSFORM SPECTROSCOPY

by James L. Lauer

for NATIONAL AERONAUTICS & SPACE ADMINISTRATION
NASA LEWIS RESEARCH CENTER

1. Report No.	2. Government Accession No.	3. Recipient's Catalog No.
NASA CR-159418		

4. Title and Subtitle	5. Report Date
STUDY OF DYNAMIC EMISSION SPECTRA FROM LUBRICANT FILMS IN AN ELASTOHYDRODYNAMIC CONTACT USING FOURIER TRANSFORM SPECTROSCOPY	August 28, 1978
	6. Performing Organization Code

7. Author(s)	8. Performing Organization Report No.
J. L. Lauer	
	10. Work Unit No.

9. Performing Organization Name and Address	11. Contract or Grant No.
Sun Oil Company Marcus Hook Pennsylvania	NAS3-19758
	13. Type of Report and Period Covered
12. Sponsoring Agency Name and Address	Contractor Report
National Aeronautics and Space Administration Washington, D. C. 20546	14. Sponsoring Agency Code

15. Supplementary Notes

Project Manager, William R. Jones, Jr., Lubrication Branch, NASA Lewis Research Center, Cleveland, Ohio

16. Abstract

Infrared emission spectra were obtained through a diamond window from lubricating fluids in an operating sliding elastohydrodynamic contact and analyzed by comparison with static absorption spectra under similar pressures. Different loads, shear rates and temperatures were used. Most of the spectra exhibited polarization characteristics, indicating directional alignment of the lubricant in the EHD contact. Among the fluids studied were a "traction" fluid, an advanced ester, and their mixtures, a synthetic paraffin, a naphthenic reference fluid (N-1), both neat and containing 1% of p-tricresyl phosphate as an anti-wear additive, and a C-ether. "Traction" properties were found to be nearly proportional to mixture composition for traction fluid and ester mixtures. The anti-wear additive reduced traction and fluid temperature under low loads but increased them under higher loads, giving rise to formation of a friction polymer.

17. Key Words (Suggested by Author(s))	18. Distribution Statement
Elastohydrodynamic lubrication; infrared emission spectroscopy; traction; glass transitions; high pressures.	Unclassified - Unlimited

19. Security Classif. (of this report)	20. Security Classif. (of this page)	21. No. of Pages	22. Price*
Unclassified	Unclassified	120	$3.00

* For sale by the National Technical Information Service, Springfield, Virginia 22161

CONTRACT NO. NAS-3-19758

STUDY OF DYNAMIC EMISSION SPECTRA FROM LUBRICANT FILMS IN AN ELASTOHYDRODYNAMIC CONTACT USING FOURIER TRANSFORM SPECTROSCOPY

FINAL REPORT

To: NASA-Lewis Research Center
Cleveland, Ohio 44135

By: JAMES L. LAUER
Research Professor
Department of Mechanical Engineering,
Aeronautical Engineering & Mechanics
Rensselaer Polytechnic Institute
Troy, N.Y. 12181

EXPERIMENTAL WORK DONE AT SUNTECH, INC.,
from January 1, 1976 to December 31, 1977

May 23, 1978

SUMMARY

Infrared emission spectra were obtained through a diamond window from lubricating fluids in an operating sliding elastohydrodynamic contact and analyzed by comparison with static absorption spectra under similar pressures. The fluids were (i) a traction fluid, (ii) an advanced ester, (iii) mixtures of traction fluid and ester, (iv) a synthetic paraffin, (v) a naphthenic reference fluid (N-1), (vi) the same fluid containing 1% of p-tricresyl phosphate as an anti-wear additive, and (vii) a C-ether. Average Hertzian pressures of 630, 763, and 865 MPa, corresponding to loads of 108, 191, and 279N were used. Temperatures in the fluid reservoir ranged from 30 to 70°C and surface speeds were 0.72, 1.08, and 1.44 m/sec.

The spectra were analyzed for fluid film and metal surface temperatures in the contact and for polarization as an indicator of molecular alignment. Most fluids appeared to be oriented as they pass through the EHD contact, as shown by polarization of their spectra. The anti-wear additive reduced traction and fluid temperature under low loads, but increased them under high loads, giving rise to formation of a friction polymer. The inlet temperature at the contact was not changed by the additive, but the solid surface temperature (determined from the continuous background in the infrared emission spectrum from the contact region) was raised significantly.

Whenever it was possible to compare different fluids under the same shear rate, the traction fluid film temperature was the highest. Film temperatures and traction of traction fluid/ester mixtures were nearly proportional to the traction fluid concentration under otherwise constant conditions even though (calculated) film thicknesses were hardly changed. The polarization ratios of two intense traction fluid bands also varied parallel to mixture

composition. While the data are inadequate for a definitive correlation, traction appears to be a function of a molecular property in the liquid state.

In a later phase of the program, fluids will be analyzed that were specially synthesized to provide information from their infrared spectra. This approach should be very helpful in finding the best fluids for given operations. The next phase of the program will also be carried out under different auspices as the senior investigator has transferred to Rensselaer Polytechnic Institute.

TABLE OF CONTENTS

I. INTRODUCTION

The work reported here represents the third phase of a program of applying infrared spectroscopic techniques to the analysis of lubricants in bearings[1]. Infrared spectroscopy is one of the most powerful techniques of chemical analysis both for the nature of the molecular species present and for their state and environment. As a matter of fact, infrared spectroscopy has been used quite a bit for the analysis of lubricants, but in all cases samples of lubricant were withdrawn and analyzed. By applying the spectroscopy to lubricants in operating bearings, the composition is observed where and when it counts, and changes due to deterioration are recognizable. This was the stated objective when this program was originally started in late 1973. At that time the modern Fourier techniques of infrared spectroscopy -- which are basically interferometry -- made it possible to apply infrared spectroscopy to this area, because it was recognized from the beginning that the signal level available from the very thin lubricant films, as they occur during bearing operation, especially under EHD conditions, would be too low for dispersive techniques to work. The project was divided into several phases all of them having the objectives of (i) relating the spectral changes observed to fluid performance, (ii) finding relations between molecular structure and performance -- perhaps being able to deduce a mechanism of traction from a molecular structure point of view -- (iii) determining how boundary additives work under real conditions, (iv) determining film temperatures, surface temperatures and states of aggregation of the fluid, (v) gaining some insight into the adsorption/desorption behavior of additives, etc. In short, many questions that are being asked regarding the lubricant during operation should be answerable by this technique.

We realized, of course, from the start that the experimental techniques would present problems because of the weakness of the signal. Even the Fourier techniques would have to find means of discriminating against the high background resulting from the hot solid surfaces. It appeared clearly difficult to apply a transmission method for operating bearings. However, both reflection and emission techniques appeared potentially useful for the very thin films of lubricant. Both techniques were tried in the early phases of this work but emission techniques were more productive sooner because of simpler equipment. So, essentially all the work reported here deals with emission techniques.

The first phase of the program,[1a] showed that emission infrared spectroscopy is possible of the very small volumes of lubricant fluid contained under very high pressure in the diamond cell. The diamond high pressure cell simulated the situation in the operating bearing. In the second and longer phase,[1b] it was shown that infrared emission spectra could be obtained from an EHD sliding contact through a diamond window and a number of fluids were analyzed by this technique. However, apparatus limitations, in addition to the fundamental limitations of temperature and other operating parameters, made it necessary to add to every fluid under investigation a reasonably large amount of an aromatic additive (usually one-third of polymethylstyrene) to obtain a spectrum for analysis. While the addition of one-third of extraneous material was not negligible and seriously changed the properties of the fluids, it was thought that the essential differences between fluids analyzed would still show. In the determination of fluid film temperature it was possible to calibrate for the same infrared emission band intensity regardless of the composition of the material and, therefore, compare lubricant temperatures under equal operating conditions.

Even though the addition of the aromatic material had certain advantages, as just pointed out, nevertheless the fact that such a large addition very likely changed the properties of the fluid, made it necessary to improve the apparatus to the point where all fluids could be examined by their own infrared bands, and this was done in the work reported here. Still, not every fluid can be analyzed equally well by infrared emission, for the accessible frequency range depends very much on temperature; the Planck radiation law is very definitely a limiting factor. Secondly, the film thickness in an operating contact is determined by properties of the fluid, such as viscosity and viscosity/pressure coefficient, and not by the requirements for good spectrum analysis. Finally, a fluid may not have suitable bands for analysis; aromatic materials have the strongest bands in the accessible region but aromatic fluids are, from an operational point of view, usually not the most desirable.

In the work discussed here, the apparatus developments and the advances of the basic techniques will be discussed but briefly, as most of this work was funded by simultaneous contracts from the Air Force Office of Scientific Research (F44620-74-C-0038 and F49620-76-C-0042). This report will concentrate on the results obtained with fluids supplied to us by NASA and which were studied in pure form.

II. TEST FLUIDS

The fluids tested during the program period are listed in Table 1, where the pertinent properties of these fluids are also shown. In addition, one of these fluids was used with para-tricresyl phosphate additive in a concentration of one percent. Mixtures of the advanced ester and the traction fluid were also analyzed and the results are reported here. On the other hand, the results on polyphenyl ether (5P4E) which was also studied, were separately reported in a report[2] to the Air Force Office of Scientific Research. All these fluids were studied "neat"; there was no longer a need for the addition of polymethylstyrene to bring out the aromatic bands which, in our previous work, were the only ones accessible to us by infrared spectroscopy.

III. APPARATUS

Though the improvements of the apparatus, which were very important for the success of this work, were carried out under simultaneous contracts with the Air Force Office of Scientific Research, it is essential to mention some of the new features here just briefly.

3.1 Spectrometer Modifications

In order to cover a wider wavelength range a number of changes had to be made on our Beckman-RIIC FS-720 Interferometer-Spectrometer. They are outlined below.

3.1.1. Beamsplitter

The FS-720 instrument was originally designed for the far infrared, the frequency range of 10-600cm^{-1}. It is a Michelson interferometer with replaceable beamsplitters, which consist of Mylar film of different thicknesses. With an ultrathin Mylar film beamsplitter the accessible infrared range could be extended to 1000cm^{-1}. The beamsplitter is four inches in diameter and all the limiting optics is of this diameter so that the radiation-gathering power of the interferometer corresponds to $f/2$ speed and is, therefore, superb. The weak signal strength of the far infrared requires high radiation-gathering power and so does the weak emission signal from our lubricating contacts even in the mid-infrared. By locating an equally dimensioned salt plate with a germanium coating in the beamsplitter position, the mid-infrared range, 600-4000cm^{-1}, became accessible. However, a Mylar beamsplitter is easily re-inserted, so that both the mid-and the far infrared are obtainable.

3.1.2 Moveable-Michelson Mirror Positioner

The new beamsplitter alone does not access the mid-infrared: readings must be taken at interferometer mirror displacements not farther apart than

one-quarter of the smallest wavelength to be scanned (or at optical retardation intervals equal to half of the smallest wavelength to be scanned). Since the Moiré gratings used as positioners are ruled at 4 micrometer intervals, it is necessary to provide triggering pulses asking the detector to read amplitudes at accurate fractions of the basic interval (the smallest wavelength accessible now is 2 μm). An electronic circuit was designed and built for this purpose. (It should be noted that the interferometer presents a plot of detector amplitude versus mirror displacement -- not time, because it is impossible to move the mirror at constant speed). This circuit works quite well to record mirror displacements as small as 0.5μm.

Because of grating imperfections it would be impossible to obtain readings at even closer spacings by this method. The obvious way to do that is by a reference interferometer with a laser source. All the parts for such a system are already in our hands and the conversion will be made some time in the near future. While further reductions of the interval are not needed to cover the mid-infrared, they are very desirable to reduce background noise at low signal levels.

3.1.3 Inlet System

The new inlet system shown schematically in Fig. 1 constitutes a considerable improvement over our earlier version. While the principal reason for the change was the wider transmission region of the new beamsplitter -- which made it impossible to balance the radiation from the solid surfaces in the conjunction region of the operating bearing by the radiation emanating from the chopper disc--the new referencing system, consisting of a temperature-controlled radiant heater and a new tuning fork chopper located ahead of the entire optical train, provides additional advantages. Before discussing them, it should be pointed out that the lubricant film in an

operating bearing is not, in general, at the same temperature as the bearing surfaces, since heat is generated in the fluid by viscous friction and transported to the solid surfaces. Furthermore, bearing surfaces have relatively high (0.2-0.3) thermal emissivities, so that the radiation from the fluid film, though discrete, would be swamped by graybody radiation, were it not for the fact that much of the latter is balanced by chopper or reference radiation. Among the additional advantages of the new inlet system is the ability of making polarization measurements, for both the source and the reference radiation traverse an essentially identical optical path -- which was not true before -- and the ability of calibrating the bearing surface temperature by means of the reference source supply voltage.

As Fig. 1 shows, the radiation transmitted through the diamond window is collected by a wide-angle all-reflecting microscope objective lens (Beck lens). This causes no difficulty, for one of the principal advantages of interferometers over dispersive spectrometers is their ability to accommodate radiation of relatively large solid angle without appreciable losses or wavelength distortions that cannot be corrected. This advantage, in addition to the well-know sensitivity advantages, makes an interferometer indispensable for these applications. However, before the radiation can enter the lens, it is (in our present design) periodically interrupted by the reflecting blades of a tuning fork, which are located above the Beck lens and as close to the diamond window as possible. A small flat disc is also attached by a thin rod to each of the tuning fork tines below the reflecting blade. Just above the downward-facing convex mirror of the Beck lens, which is designed similarly to a Cassegrainian telescope, is a reference source in the form of a disc equal in diameter to that of the convex

Beck mirror. This disc is a standard thermoelectric heater or cooler, operable in either the heating or cooling mode,depending on the electrical connections. The geometry of the system is such that 1) the upper reference surface is just covered by the small disc of the chopper whenever the reflecting blades are separated,in order to permit source radiation to enter the Beck lens and 2) the upper reference surface is exposed to the lower (reflecting) surface of the reflecting chopper blades whenever they are overlapping, thus preventing source radiation from entering the lens. In this way reference radiation cannot mix with source radiation, e.g. by reflection from the lower surface of the diamond window.

The electronics of the amplifier (a lock-in, which is tuned and phased to the tuning fork chopper) is such that only the difference between source and reference energies falling on the detector is amplified. Since the upper (radiating) surface of the reference can be made of the material of one of the radiating components of the source, such as the metal of the ball, it is possible to subtract the latter's contribution from the source radiation and obtain essentially only the radiation from the thin film of lubricant. This feature of the entrance optics is very important.

3.1.4 Processing of Spectral Data

The Fourier spectrometer requires extensive data processing and, as a matter of fact, its very existence today is a consequence of the advances in computer technology. For the work described in this report the data were collected on punched paper tape, sent to a central data processing unit by teletypewriter and then returned for plotting on another teletypewriter-plotter. While this procedure works well, the turn-around time is long, (about one hour per spectrum) so that spectral averaging could only be done in a few instances. By contrast, a new system consisting of a dedicated

minicomputer is now available to the Principal Investigator (at Rensselaer Polytechnic Institute) and final spectra can be obtained in less than two minutes after completion of an experiment.

3.1.5 Field of View

In some instances a series of spectra was obtained along the conjunction line of the Hertzian contact region. Size and location of the field of view were determined by a diaphragm at an image position within the interferometer. Since the energy level is already very low, this further reduction of the energy incident on the detector is not helpful. Replacement of the present Beck lens (15X magnification) by one of higher power (not entailing a radiation loss because of its greater numerical aperture) has been contemplated for some time but was not carried out because the smaller working distance would necessitate a relocation of the chopper. However, since the present Golay detector (a pneumatic detector which is very sensitive but of slow response) will soon be replaced by a solid state (Hg-Cd-Te) detector of much faster response and a new faster chopper will have to be installed just ahead of the new detector, the change to a different lens will be carried out then also.

3.2 Bearing Contact

The mechanical arrangement was essentially the same as before -- a rotating ball over a diamond window in the bottom of a cup filled with fluid -- except for one major improvement: loading of the ball was accomplished by a platform resting on the ball at contacts formed by two rollers instead of the previous contacts consisting of three sapphire surfaces. The rollers make contact on the ball along the periphery in a vertical plane which also contains the diamond sliding contact. Since rolling friction is much smaller than sliding friction, this arrangement permits reasonably

accurate estimates of traction from the current through the dc motor which is driving the ball. Above all, however, there are less failures, since scoring of the ball would occur most frequently at the sapphire contacts.

A frequent serious problem was vibration from the mechanical drive being transmitted to the interferometer. The problem's magnitude increased with increased severity of operating conditions. The rollers were better than the sapphire sliders in this respect, but only slightly so. New sponge rubber pads under the interferometer helped, but again not very much. The best temporary solution turned out to be the selection of ball speeds for which the vibrational interaction was minimized. This is the reason for the particular speeds used, which the reader might find arbitrary. If speeds were used which fell between the values normally selected, apparent signal amplitudes were obtained which could be many times greater than the true ones. They could be recognized by their periodicity. It is expected that the vibration problem will be very much improved (at Rensselaer Polytechnic Institute) by a vibration-resistant table, consisting of a heavy granite slab resting on air cushions.

IV. THEORETICAL BACKGROUND AND DATA REDUCTION

4.1 Wavelength Calibration

After all the changes and improvements of the equipment, especially the spectrometer, the obvious question to be asked is: "How good are the spectra obtained?". Is it really possible to cover the entire wavelength range normally covered by infrared radiation? Fig. 2 shows a comparison between a spectrum of polystyrene obtained with our interferometer and a standard spectrum published by the International Union of Chemistry. It can be seen that every band of the standard spectrum is reproduced in our spectra. The intensities are, however, different, which is not surprising since the reference spectra are two-beam whereas our spectrum is single-beam, taken with a continuous source of relatively low temperature. Therefore, a background slope is evident in our spectrum. We believe from a comparison of these calibration spectra that our results, when calculated in the same way as the reference spectrum, should be good to about $5cm^{-1}$. The shape of the spectral bands is also reproduced quite well so that the resolution calculated theoretically at about $5cm^{-1}$ is also very close to the actual resolution. We have not -- for this work -- tried to increase the resolution. It is not necessary here because our liquids do not require it; but we did obtain some gas spectra where we could increase the resolution to one wave number or better.

4.2 Apparent Spectral Peak Inversion

It was said earlier that our spectra are really differences between those of a reference and of a source, and our inlet system to the spectrometer is always carefully balanced so that the background and the reference spectra nearly cancel each other and the film spectrum remains. The question might be asked: "What happens when the reference emission is of greater intensity than the

source radiation?" In that case, since only the absolute value of the difference spectrum is recorded, an emission spectrum can show up as an absorption spectrum, and the other way around when the reference is much less intense. Since some of our spectra could indeed show up as absorption spectra, even though obtained as emission spectra (because of a temperature gradient through the fluid), it is very important to know that one does not deal with an artifact of this nature. Fortunately the check can be made quite easily by computation. It is possible to add to the original interferogram the interferogram of a simulated reference at higher temperature or at any temperature desired; the resulting spectrum will have the reference artifically raised or lowered as the case may be. If the original spectrum was obtained properly, then a change of the reference level obtained artifically in this manner will not change the structure of the spectrum. In general, the balancing is quite good so that only a slight addition or subtraction of a mathematical reference will suffice to carry out this test. All our spectra were so adjusted so that there should be no question as to artifacts produced in this manner. It turns out that all one has to do to obtain an artifical reference is to increase or decrease by a calibrated amount the magnitude of the central burst in the original interferogram. This is done quite easily and when the spectra are thus recalculated the check can be done.

Figure 3 shows a plot of the relation between the reference voltage and the central bursts for a blackbody -- or essentially a blackbody -- spectrum, furnished by a hot plate at known temperature. As can be seen, the magnitude of the central burst decreases as the reference potential increases. This is expected, since the interferogram is the difference between the source interferogram and the reference interferogram. When the reference potential

keeps increasing, inversion takes place and the center burst can actually assume a value lower than the basic dc level of the interferogram. In other words, the center burst points in a negative direction. Over quite a stretch this calibration is a straight line but for low reference potentials the slope is much lower than for most. Presumably the reason for this behavior is that at low reference potentials other contributions to the interferogram become important, such as general background reflections which contribute similar to an increase of reference potential. Figure 4 shows a similar calibration against reference potential, except that this time instead of the center burst intensity the greatest unnormalized amplitude is plotted. This curve is perhaps more of a straight line than the center burst curve although from a theoretical point of view the center burst should be preferable. It should be pointed out, however, that while theoretically the center burst of a spectrum is equal in magnitude to the entire area under the curve in the spectrum, in reality this is not quite so, so that it is not unreasonable for the greatest unnormalized amplitude in a given spectral region to be a better measure than the central burst.

4.3 Cleanliness

The hot plate that was used for reference in the preceding section was actually a copper oxide-coated copper plate. It had been assumed that it would show only a continuous spectrum through the diamond window. As can be seen from the spectra from Fig.5 the hot plate was evidently not clean because a number of spectral bands are showing through, especially the very strong hydrocarbon bands at 1380 and 1460cm^{-1}. These bands undoubtedly were contributed by a thin adsorbed film inevitably formed in the atmosphere of a petroleum laboratory. At zero reference potential only slight indications of bands are seen at these two wave numbers but, as is always the case, the band

at 1460^{-1} is considerably stronger than the one at $1380cm^{-1}$. At a reference voltage of 2 volts these bands are smoothed out and essentially the curve is that of a blackbody. There is, of course, a slight slope present as would be expected from the emission of such a material at temperatures about $60^{o}C$. In other words, a reference potential of 2 volts just about balanced the radiation from the plate. When the reference potential was increased to 4 volts more structure became evident. A careful study of the spectrum shows the presence of an emission band sitting in a trough of an absorption band so that what is seen here is indeed a rather broad absorption band extending from 1400 to about $1500cm^{-1}$, and in its middle the emission peak is showing through. As the reference voltage was increased further, the absorptions at $1460cm^{-1}$ and the one at $1380cm^{-1}$ became much stronger and under these conditions we see apparent strong absorption corresponding to the emission*. The presence of these hydrocarbon bands showed to us very clearly that very strong precautions must be taken for cleanliness. The problem probably would not arise in the case of our runs under EHD, for then the diamond is entirely covered by the fluid under investigation. To ascertain this more carefully, we then put the diamond window between the copper source and the chopper and after cleaning the copper plate source very carefully we found at first that there were absorption due to hydrocarbons but when the diamond was cleaned very carefully, with all sorts of solvents, then as shown in Fig. 6, all hydrocarbon absorption was removed.

* These transitions from apparent emission to absorption, which depend on the relative radiant powers of source and reference can be very helpful for temperature measurements but can complicate spectral analyses. They must be kept in mind whenever weak sources are analyzed, but can be clearly identified by running spectra at more than one reference voltage. This problem can be avoided by reflection techniques (ATR, attenuated total reflection, for example) or by cooling the entire spectrometer to liquid nitrogen temperature (which has been done by Russian investigators). Reflection techniques will be given another look, but they entail other difficulties.

4.4 Polarized Emission Spectra

Since the interferometer optics with the germanium beamsplitter is essentially non-polarizing (the difference in overall intensity between incident radiation polarized in the plane of incidence to the beamsplitter and polarized perpendicular to it is less than 10%) and not a sharply changing function of wavelength, and since, furthermore, the optics is symmetrical about the optic axis -- the major exception being the beamsplitter -- any polarization of emitted radiation is likely to originate in the source. The ball/plate contact does have a preferred direction -- the conjunction line -- whenever the ball is turned. Indeed, the emitted background or graybody radiation then becomes somewhat polarized, but the discrete fluid radiation may become considerably polarized in the neighborhood of infrared bands. The changes of refractive index become quite large near absorption bands so that this behavior is not unexpected. The theory is quite complicated, if a detailed analysis is required (anomalous dispersion, large unknown parameters), but for our purposes the variation of band intensity with polarization and with the various mechanical parameters is most important.

Figure 7 shows the situation in the contact region with representative values for the reflectivities at the interfaces. These reflectivities were calculated for average indices of refraction and for the acceptance angle of 30° of the 15X Beck lens used. (There is a distribution of angles, of course). Because of the cylindrical symmetry of the optics the polarizations have meaning only when "plane of incidence" is defined, say in terms of the plane containing the conjunction line of the contact and the center of the ball. For the purpose of later discussion "polarizer vertical" means that radiation is transmitted whose electric vector is oscillating parallel to this plane. Evidently the reflectivities for the two planes of polarization are

significantly different at the diamond/air interface so that peaks in a spectrum of one polarization can correspond to valleys in the orthogonal polarization, provided the reference source intensity level is intermediate between the intensity levels of the two polarization spectra.

Accordingly, as long as an anisotropy exists in the fluid film, the ratio or the difference between two emission spectra of mutually perpendicular polarization can provide a spectrum that is more highly structured, more sensitive, and more noisefree than either of the two emission spectra. Such a spectrum would ideally be obtained with a polarizing chopper, but the effect is shown even by carrying out the ratioing on sequentially obtained spectra, such as those of Fig. 8. The discrimination in favor of the -- polarized -- spectral bands in the ratioed spectrum is very clear. To use this effect for superior spectra from weak sources, it is not necessary to know the reason for the polarization. As long as some bands are polarized, noise and other imperfections in the spectra which are not polarized are discriminated against. After this observation was made and applied to a number of instances, similar to that shown in Fig. 8, it was found that Overend[3] and his coworkers at the University of Minnesota had used a similar idea for the detection of very weak emitted infrared signals from adsorbants. They recorded emission spectra from materials adsorbed on solid surfaces and used polarizing choppers to get much enhanced discrimination. They were able to get respectable spectra from a few as 9 layers of stearate films on a gold substrate using the above-described double-beam mode. Their sample temperature was around 100^{o}. Much better spectra were obtained with 17 and 33 layers. (The layers were prepared by the Langmuir-Blodgett technique). It is of interest here to note that the wavelength region these authors explored was very closely the same as that used in our case (CH deformation

region) and that their sample thickness was almost exactly the same as that for the advanced ester just shown in Fig. 8. In this manner, therefore, the work by Overend and his coworkers is a confirmation of our work, though under entirely different conditions. Overend and coworkers claimed that the reason for the polarization is the stacking of the films in alternate layers oriented in opposite directions. It is interesting that the stacking occurs on an inert surface such as gold. The implications to our work are quite obvious and it is our intention to pursue these ideas with bearing balls coated with gold and other metal layers to find out whether analogous effects can be obtained. Overend suggests that it might be possible by this method to improve the signal-to-noise ratio to such an extent that monolayers could be observed. It should also be pointed out that Overend's work, which is shown in Fig. 9, was carried out with a dispersive spectrometer and that emission was superior in many ways to reflection.

The reason for the alignment of the molecules of the advanced ester has not been clearly established. As noted, there is evidently a preferred direction which can be identified with the conjunction plane. Possible reasons for the alignment are a flow polarization, stress polarization, solidification, glass formation and stress in the glass, crystallization, and various others, and considerably more work will have to be done to differentiate between possibilities. For example, if flow polarization is the dominant cause, then the dichroic ratio, i.e. the ratio between the spectral intensities for mutually perpendicular directions of polarization, should vary linearly with the flow velocity. However, this is not easily determined, because a change in flow velocity also changes the temperature and thickness of the fluid film and these factors also have to be taken into account. More polarization spectra will be shown in a later section.

4.5 Diamond Cell Calibration Spectra

Emission and absorption spectra of the various fluids under investigation were obtained with a diamond cell at thicknesses corresponding to those observed in the contacts under dynamic conditions. The purpose of these spectra was to calibrate or to help interpret dynamic spectra in terms of intensity changes and shifts of absorption bands with pressure. Since dilution of the fluids with solvents to reduce the effective optical pathlength was not possible, because of the potential change of fluid properties with dilution, very thin metal gaskets were required as spacers between the diamonds. Gasket materials thinner than about 200 μm -- certainly less than 25 μm -- are difficult to obtain. We were able to secure some of these gaskets made out of tantalum from a manufacturer of metal foil for nuclear experiments. We used tantalum foil of thickness about 2.5 μm for some of our calibration work. Unfortunately, tantalum is difficult to handle and when the gasket is not exactly aligned and parallel to the planes of the diamond, it is very easy, under pressure, to cause scratches to the diamond. Presumably, the foil shifts in position as pressure is applied and particles of tantalum, which are exceedingly hard, become embedded in the diamond surface. It is also difficult to get an exact measurement of the actual pressure in such thin layers, for ruby crystals of this size, even when they can be located in the cavity of the diamond cell, fluoresce only very weakly. In thicker layers of the fluid some of the absorption bands become of near infinite intensity as far as the spectral recording is concerned and are, therefore, almost impossible to analyze. This work was, therefore, very difficult to do and was not always carried out with the same satisfactory results. Perhaps it will be satisfactory to use the pressure shift of some of the absorption bands in the fluids themselves as measures of the prevailing pressure.

4.6 Thickness of Fluid EHD Films

Probably the best method of obtaining thickness of EHD lubricant films under operating conditions is by optical interference. This method has been established by Cameron and his coworkers[4] and also by Winer[5] and his students. In a few instances we were able to carry out the same procedure using our ball/diamond plate setup separately from the interferometer. The mechanical stand was removed from its normal position above the interferometer and an optical microscope was placed in the location of the Beck lens for observation of the ring pattern at different speeds and loads. The radiation used was visible light or light from a red laser. Because of the high index of refraction of the diamond it was not necessary to provide a chromium coating, such as the one Cameron and other investigators used on sapphire, to make the fringe pattern more pronounced. The fringes we were able to obtain were quite respectable and could be photographed by means of a polaroid camera. Because of lack of time only a few calibration experiments were carried out. In most cases the fluid film thickness was calculated from the viscosity relations and the equations developed by Wedeven in the same manner as described in our earlier report.[1b]

4.7 Glass Formation in an EHD Contact and Stress-Induced Fluidization

In some of our work, we obtained glass transition temperatures at various pressures in the diamond cell using the procedure described by Block, Piermarini and coworkers[6], which we had adapted to our needs as shown in a recent publication[7]. According to these measurements and the results reported by Winer[8], many of our fluids should become glasses under the conditions of operation. The question then is: If this is so, why do they still behave so much as fluids and what is the reason for the polarization of some of the infrared emission spectra[2]. Perhaps the two questions

can be answered by means of a concept developed for plastic materials, viz. stress-induced fluidization. This phenomenon, which has been found for almost all polymers, has been discussed in a recent article by Kambour and Robertson[9] in Polymer Science. The material these authors studied is polycarbonate. One explanation for the yielding of the glass given by these authors is that shear stress induces a liquid-like structure in the material by the unbalancing of atomic forces; the molecules are required to seek a new arrangement. In the course of reaching the new arrangement intermediate liquid-like structures develop. In other words, glass would be formed under the operating conditions but because of shear the glass is again liquified. More about this will have to be investigated.

V. RESULTS

5.1 Static Infrared Spectra of Fluids

Figs. 10-14 contain standard double-beam infrared absorption spectra of the fluids for reference. The relative intensities of the most intense bands are shown schematically in Fig. 15. These intensities are theoretically equal whether absorbances or emittances are plotted; either of these are ratioed, the latter to a blackbody spectrum of the same temperature. Experimentally what counts in emission is the signal strength at a given frequency. Accordingly the band intensities must be corrected for Planck's distribution and, when this is done, the relative intensities (single-beam, for emitter temperatures of 100°C) become the ones of Fig. 16. These intensities are quite different from the usual ones of the analytical spectroscopist; for example, the carbonyl band at about 1750cm^{-1} is weaker than the aromatic band near 700cm^{-1}. The relatively most sensitive region of the spectrum is now the one near 1000cm^{-1} because this frequency corresponds to the peak of the Planck radiation curve. As can be seen from Figs. 10-14, the fluids do not contain many very strong infrared bands. Outstanding ones are the 730cm^{-1} CH_2 rocking mode, the 1160cm^{-1} C-O stretching mode, the

1380/1460cm^{-1} C-H deformation modes, and still the 1750cm^{-1} carbonyl stretching mode.

Static high- and low-pressure absorption spectra were obtained, (at ambient temperature) with diamond cell for all the fluids (Figs. 17-21). As can be seen, there are changes (mostly decreases) with pressure in the relative intensities of many of the bands and there are peak shifts mostly toward higher frequencies. A shift toward higher frequency may be quantitatively interpreted as the result of an increase in the relative importance of repulsive forces of neighboring molecules. Conversely, a shift toward lower frequency indicates that the attractive forces of neighboring molecules are exerting greater influence on the atom or group. Most of the latter shifts have been observed in bands assigned to X-H stretching vibrations in substances whose structures involve hydrogen bonds.

At pressures of the order of 20 kbar, the volume of the fluids studied decreases by about 10%.[10] Since the interatomic body distances are hardly affected, the intermolecular distance changes must be quite large; hence changes to the "glassy" state are very likely. One would expect, therefore, that hydrogen bonds would be good indicators of the glass transition and that one should look for downward shifts of frequency for this purpose. The ester spectra (Fig. 18) show many changes with pressure, but no downward shifts in the frequency range studied. However, the proper spectral regions for this effect to show are the far infrared and the O-H stretching region; Craven[11] has done some pertinent work in the former region, Drickamer and Klaboe[12] in the latter, but neither author has interpreted his results from the point of view of the glass transition. Fig. 22 is a plot of the changes of the spectral shifts, the data having been taken from Drickamer's publication.[12]

The location of maximum slope change is very likely the glass transition. The implications of these ideas to dynamic spectra are obvious.

Our results on the synthetic paraffin appeared strange at first when three new bands were found in the low pressure diamond spectrum (Fig. 20), but not in the high one. Since these (at 900, 1000 and 1100cm^{-1}) did not show up in the standard spectra, they were suspect, even though some authors did refer to new bands appearing in the diamond cell and had various interpretations for them. After a complete realignment of the instrumentation, the "mystery" bands disappeared. Our present interpretation is based on multiple beam interference fringes in the sample, which show up because of the low refractive index of the paraffin. At higher pressure, the fluid's refractive index increases, thereby reducing the reflectivity at the fluid/diamond interfaces sufficiently to make the fringes disappear. Also the effective optical path difference decreases, causing the fringes to broaden. When the optics are properly aligned the source image falls into the sample volume of the diamond cell and the interference is eliminated. This example shows how tricky microtechniques can be.

5.2 Rates of Shear

Before discussing the dynamic emission spectra of the various fluids separately in more detail, an overall view of the differences between the fluids as they affect the spectra is indicated. A considerable amount of effort was expended in calculating various parameters as they refer to the spectral presentations and to the operating variables, for example, temperatures and shear rates for these fluids. The nature of the fluids is such that it is not possible to keep the parameters constant for all the fluids and then just compare the spectra, which is the customary procedure of analytical spectroscopy. Table II gives the parameters of the apparatus as

they relate to the film thickness in our EHD contact. The parameters given in this table are independent of the nature of the fluid but they do depend upon the materials used in the contact, such as the steel of the ball and the mechanical parameters of the diamond, etc. Three speeds and three loads were usually used. As can be seen, the influence of the surface speed of the ball on film thickness is much greater than the influence of load. For example, a change in load by almost a factor of three affects the parameter F (which is proportional to the film thickness) by only about 5%. On the other hand, doubling of the speed changes this parameter by more than 60%. Table I deals primarily with the viscosity parameters and the so-called film-forming capability of the different fluids. The film-forming capability has been defined by Jones and coworkers[13] as the parameter which, when multiplied by the apparatus variable F, shown in the previous table, yields the film thickness. It will be noticed that the viscosity of the different fluids changes by quite a bit and so does the viscosity-pressure coefficient and, therefore, the relative film-forming capability is quite different for these fluids. The thickest films are formed by the synthetic paraffin and some of the thinnest by the ester and it is, therefore, not surprising that even though the ester has very strong infrared bands, especially the one at 1160cm^{-1}, it is relatively difficult to obtain spectra from the ester as good as those from some of the other fluids. Viscosities were calculated by the ASTM procedure at two temperatures from those at the two temperatures for which the viscosities were experimentally determined, namely at 38^{o} and 99^{o}C, following the usual procedure as prescribed by the ASTM. Table III shows a comparison between the film thicknesses and rates of shear that were obtained for the different fluids at various loads and speeds. These are values calculated from the viscosity-pressure coefficient. In some cases spot checks were made

by the optical interference method to obtain film thicknesses at operating conditions. Especially this was done in the case of the traction fluid where two such spot checks were run and reasonable checks were obtained. Since no known data appear in the literature on this particular fluid, work to determine experimental thicknesses for this fluid is planned, especially because of the importance of traction in future EHD lubricant research.

It would have been of advantage to have comparable rates of shear for all the fluids for the comparison of temperatures in the contact region. Unfortunately, the situation is such that this is impossible. For example, the very viscous synthetic paraffin fluid cannot be sheared at the same rates as the other fluids. The thickness of the film is always considerably greater and it would take enormous forces to bring the rate of shear to the values of the ester or the naphthenic reference fluid if, indeed, this could ever be achieved with our apparatus. It can thus be seen that the rates of shear varied between 0.5 and 25 million seconds^{-1}. These are very high rates and it is, therefore, not so surprising that flow polarization can occur similar to that observed for polymers, even though the molecular weight of these fluids is very much lower (generally around 500 in the lubricant range).

The shear rates (linear velocity of the ball surface divided by the average film thickness in the Hertzian region) were plotted against the inlet temperature, in Fig. 23. This temperature was recorded for every experiment by a thermocouple immersed in the cement holding the diamond window and in close contact with the diamond. Because of the very excellent thermal conductivity of Type IIA diamond (the window material; twice that of electrolytic silver), this temperature has been identified with the inlet temperature to the Hertzian contact. The diamond's temperature becomes uniform very quickly and the tiny thermocouple junction used responds with minimal delay. Clearly

the synthetic paraffin temperature changes least, the advanced ester temperature most with rate of shear. Since the rates of shear were determined at the experimental inlet temperatures, these curves show that the traction fluid exists in thicker films under the same operating conditions than the ester, for example, even though its film temperature is higher. The synthetic paraffin is really in a class by itself. There is no apparent difference in this behavior between the naphthenic reference fluid (N-1) in the neat state and the same fluid containing 1.0% of the anti-wear additive p-tricresyl phosphate (TCP).

On the other hand, the plot shown in Fig. 24 shows a difference for N-1 and for N-1 + TCP. Here the Hertzian area metal surface temperature (determinded from the continuous background in the infrared emission spectrum) was plotted against the shear rates. The temperatures are higher when the additive is present! Apparently this is a real effect and not merely a case of enhanced metal surface emissivity because of phosphate deposition (which will be checked more carefully later) because stick-slip motion and bearing failure occurred at the higher shear rates tested (more about this later) and other phenomena occurred. Essentially no correlation between ball surface temperature and rate of shear occurred for the synthetic paraffin and traction fluids. The higher temperatures for these fluids correspond mostly to higher loads.

In Fig. 25 some band strengths along flow are plotted against shear rate. Assuming no dependence of band emissivity or band polarization on temperature, these plots can be interpreted as film temperatures against shear rates. As mentioned in the Introduction, it is not possible to use the same infrared bands for all the fluids because of their different nature. Polarized spectra were used because they showed much sharper bands than unpolarized ones. It will be noticed that for the N-1 fluids the intensity of the 1460 (C-H deformation) cm^{-1} band becomes more negative (i.e. more absorptive) as the shear rate

increases and at a faster rate for the additive-containing fluid. This band is known to be polarized in some polymers and both polarization and thermal gradients could be determining factors for this behavior. More work should help clarify it. There is no dependence of the 1460cm^{-1} band intensity of the synthetic paraffin on shear rate, while the 760cm^{-1} band for this fluid and the 1160cm^{-1} band for the ester fluid became more emissive with increased shear rate.

Calibration data between fluid temperature and bandstrength have been obtained in the diamond cell but not under polarization. The unpolarized spectral bands do not seem strong enough for adequate measurements. However, already the data of Fig. 25 show interesting correlations and better data will be obtained in the near future.

5.3 Mixtures of Traction Fluid and Advanced Ester

In addition to obtaining dynamic emission spectra for the pure traction fluid and the advanced ester, two mixtures of intermediate composition were also studied to help potentially in the interpretation of traction. For convenience, all the results are described in this section.

5.3.1 Polarization of Spectral Bands in the Dynamic Emission Spectra of Traction Fluid

Fig. 26 shows the C-H bending region (1350-1500cm^{-1}) in the emission spectrum of the traction fluid at low load (11 kg) and Fig. 27 at high load (22 kg) for the same rotational speed (240 RPM) in three ways (i) unpolarized, (ii) polarized along the flow, and (iii) polarized perpendicularly to the flow. In both figures closer inspection will show that the unpolarized spectrum is the sum of the two polarized spectra. (Note that all spectra were obtained separately in succession). The 11 kg spectrum polarized along the flow (center spectrum of Fig. 26) is a lowered resolution version of the standard absorption spectrum of Fig. 9 except that the peak frequencies are somewhat

lower than those of the standard spectrum at ambient temperature. Since the theoretical resolution of these dynamic spectra was only $10cm^{-1}$ and the fluid film temperature certainly higher than the measured diamond temperature of $43^{o}C$ for these conditions, these frequency shifts are in the right direction and explainable. The bottom spectrum of Fig. 26 can be derived from the middle one by inverting the central portion of each absorption peak. If the polarization of the dipole moment derivative corresponding to the band peaks is directed normal to the conjunction line (the flow direction) in the Hertzian contacts, then the spectrum observed with the polarizer in a direction normal to the flow direction will show an emission peak and that observed with the polarizer along or parallel to the flow direction will show an absorption peak. The band wings are most likely unpolarized. At the high load (22kg) (Fig. 27) the dipole moment derivatives appear to be rather randomly oriented so that emission (or essentially emission) peaks appear in all three spectra (unpolarized and polarized perpendicular and parallel to the direction of flow). If this picture is contrary to the expectation that more rather than less orientation should occur at higher pressures, it is consistent with Schnur's[14] Raman observation (under static conditions): less orientation at higher pressures.

Table IV presents a very rudimentary analysis of these peak polarizations for the traction fluid under various operating conditions. The second ($1460cm^{-1}$) band is the more intense of the two and the data for it more reliable for this reason. Emission (E) or absorption (A) refer to the analysis just discussed for Figs. 26 and 27; asterisks refer to doubtful situations because of inadequate data. The overall picture appears to be consistent nevertheless: The $1460cm^{-1}$ band moment derivative is oriented with respect to the flow direction at low load (switches A to E with change of polarization), but not at high load.

with respect to the flow direction at low load (switches A to E with change of polarization), but not at high load.

Fig. 29 compares the shapes of the 1450cm^{-1} band for the traction fluid at different loads and speeds at both horizontal and vertical polarization. These plots show rather clearly that under horizontal polarization the band center is pointing upward corresponding to emission but downward in the polarization along the flow corresponding to absorption. As explained earlier the interpretation of this data is that the dipole moment derivative responsible for this infrared band is primarily directed perpendicularly to the direction of flow; under high loads the polarization is greatly reduced. Fig. 30 is a similar comparison of the bands in the deformation region for a somewhat higher speed. Again, under horizontal polarization the 1450cm^{-1} band shows up as emission. The explanation is again that the band derivative is primarily directed perpendicularly to the flow direction.

5.3.2 Polarization of Spectral Bands in the Dynamic Emission Spectra of Advanced Ester

The strongest band in the accessible spectral region of the advanced ester is the carbon oxygen stretch band near 1160cm^{-1}. Figs. 31 and 32 compare the shape, direction, and magnitude of this band for different speeds, loads, and bath reservoir temperatures. These temperatures refer to the heat exchanger and are not the actual temperatures of the fluid in the contact region. Even though this particular band is the strongest for the ester it must still be realized that the film thickness of the ester is considerably thinner than that of the traction fluid, so that the precision of the data is not as good. As can be seen from Fig. 30 under vertical polarization or polarization along the direction of flow, the 1160cm^{-1} band is invariably showing up as absorption. Under polarization normal to the flow direction as shown in Fig. 31, the band is sometimes an emission band and sometimes an absorption band. Only under the conditions where the band is an emission band under polarization normal to the flow, i.e. when the band sense contrasts with

that of the opposite polarization, is there any evidence of alignment of the dipole moment derivative. Figs. 32 and 33 refer to two different situations: same high load, but low speed and low bath temperature in one case and high speed and high bath temperature in the other. The two polarization spectra were plotted and there is good evidence for molecular orientation for the former case, but little for the latter.

The situation, therefore, for the ester fluid can be summarized in this way -- there seems to be some evidence of polarization of the ester C-O linkage in a direction parallel to the flow line but the data are not very firm and some of this work should be repeated. On theoretical grounds, of course, an alignment of the ester is likely, but the effects of speed, load, and fluid temperature are much more difficult to evaluate.

5.3.3 Polarization of Spectral Bands in the Dynamic Emission Spectra of Mixtures between Traction Fluid and Advanced Ester

Figs. 34 and 35 compare the $1160cm^{-1}$ ester and the $1450cm^{-1}$ traction band in 1/3:2/3 and 2/3:1/3 mixtures respectively under various loads and ball speeds. In both mixtures the two bands are essentially directed downward (absorption-like) under polarization in the flow direction for all three operating conditions. Under polarization perpendicular to flow one or both of these bands are sometimes directed in the opposite (emission) direction, thus showing evidence of orientation. In particular, the $1160cm^{-1}$ ester band under high load appears to be polarized at high speed in Fig. 34 (low ester concentration) and at both high and low speeds in Fig. 35. The only clear case of polarization of the $1450cm^{-1}$ traction band occurs in Fig. 35 (low traction concentration) for the low load, high speed case.

Fig. 36 has been included here as an example of the mixture spectra under polarization because it shows some of the features discussed before rather clearly. For example, the most outstanding band in the 630 to $1230cm^{-1}$

spectral region is the 1150/60cm^{-1} ester band in the unpolarized spectrum. Under polarization along the flow direction this band is very much cut down in intensity while the other bands are hardly affected. Under polarization normal to the flow this band is peak-inverted.

It is clear that these data are only a beginning. However, it is also clear that very much can be learned from this approach once the spectroscopic data can be correlated with the operational ones discussed in the next section.

5.3.4 Comparison of Temperatures and Traction of Ester/Traction Mixtures

Table V compares motor current (proportional to traction) and several measured temperatures (T_D, the "diamond" temperatures, T_B, the temperature as measured with a thermocouple near the ball surface, and T_o, the average fluid temperature at some distance from the contact) for a number of loads and ball speeds as function of ester/traction composition ratio (by volume). Figs. 37 and 38 are plots of some of this data. Clearly there is an almost linear effect with concentration, showing that traction is unlikely to be caused by few "glass pebbles" concentrated in the contact zone -- as has been suggested[14] -- but a property of the entire fluid, related to its chemical composition. Better understanding of the traction phenomena from the point of view of finding better fluids must come from studies of the chemistry involved. Perhaps Fig. 39 can add some insight. Here the diamond temperatures are plotted against the motor current (traction) for the different mixtures. Evidently the increase of temperature with increase of traction is highest for the pure traction fluid and lowest for the pure ester. Indeed the ester films are thinner than the traction films under equal conditions and the ester is a better thermal conductor. The near proportionality of slope change with composition points to a "bulk" property of the fluids, not a surface property. (If coating of the surfaces by the ester were involved, a fall-off in slope

with composition would be expected. However, surface saturation might have been present from the beginning -- though unlikely).

5.4 Naphthenic Reference Fluid, both Neat and Containing 1% of p-Tricresyl Phosphate

5.4.1 Dynamic Emission Spectra of N-1

Fig. 12 shows a routine infrared absorption spectrum of N-1. It will be recalled that N-1 is one of the "standard" fluids on which many studies have been performed by a number of laboratories. It is primarily naphthenic in nature. From the point of view of infrared spectroscopy it is, however, not particularly attractive, because even its strongest absorption bands (at 1350 and 1460cm^{-1}) are not outstandingly intense, and moreover, because these bands are due to deformation vibrations characteristic of almost any hydrocarbon or hydrocarbon groupings. For this reason, we took great care in cleaning our system to remove potential contaminants.

In Fig. 40 two sets of spectra (1300-1550cm^{-1}) are compared at two cooling bath temperatures (15° and 25°). The two curves of every one of the four charts refer to a low ball speed (240 RPM) and a high ball speed (480 RPM) respectively; different charts refer to ~low load on the (10 kg) ball and a high load.

At the lower bath temperatures (Figs. 40a and b), the low or high load curves show a 1450cm^{-1} emission peak at low speed, but a corresponding absorption peak at high speed. At the high load the peak intensities are relatively less than at low load, presumably because of smaller film thicknesses. It would appear that the intensities are always lower at the higher bath temperatures (Fig. 41c and d) for the same reason (thinner films because of lower viscosities). Peak/valley reversal with ball speed is less pronounced at the higher bath temperature. A possible explanation for the change of emission to absorption -- or re-absorption -- at higher ball speed (fluid

flow) is the thicker fluid film in the latter instance. A temperature gradient through the fluid film is certainly a reasonable assumption.

The spectra of Fig. 40, as mentioned, were obtained without a polarizer in the optical path. When a polarizer was inserted oriented about the optic axis in such a way as to transmit radiation polarized along the ball/plate conjunction line, the bands became much more structured (Fig. 41 shows the low load case). Emission and absorption seem to occur simultaneously over the bandwidth of approximately $100cm^{-1}$. There seems to be a reversal with ball speed at the lower bath temperature. All the curves shown in Fig. 42 (also low-load) for polarization perpendicular to the flow direction resemble the low load/low speed case for parallel polarization; however, at the lower bath temperature, the band center is shifted about $8cm^{-1}$ higher for polarization normal to the flow direction.

The very high-load spectra of Fig. 43 (without polarization) should be contrasted with the low load spectra of Fig. 40. In general, they show less structure and less difference with speed. The high-load spectra of Fig. 44 (polarization along the flow direction) show phase reversal (absorption/emission) on speed change at the low bath temperature, but at the high bath temperature the band at $1450cm^{-1}$ turned out to be the strongest absorption band of its kind in the entire series; there, it appears that the $1350cm^{-1}$ reversed with speed change, but the $1450cm^{-1}$ did not.

Fig. 45 presents the high-load spectra under polarization normal to the flow direction. Again the band center is shifted toward higher wavenumbers with respect to those at polarization in the flow direction.

Fig. 46 has been included primarily because of the near perfect phase reversal with speed change. It has been taken from our series of intermediate loads (27 kg) and refers to the $15^{o}C$ bath temperature and polarization along the flow direction.

We can summarize our observations as follows:

(a) The 1450/60cm^{-1} band is the most outstanding spectral feature.

(b) Polarization increases the structure of this band.

(c) The band center may point up or down and often reverses with ball speed. The wings may also reverse in this manner.

(d) Polarization normal to the flow direction generally displaces the band center toward higher wavenumbers.

After completion of our work with N-1 fluid, the apparatus was cleaned and filled with N-1 fluid containing 1% of p-tricresylphosphate. The same series of runs was attempted with this fluid as with the neat N-1 fluid, but it was observed that this fluid could not be operated at the higher loads. A load of 26 kg was about the highest possible (compared to easy operation of pure N-1 at 36 kg) and even then the low speed (240 RPM) operation could not be maintained. The entire apparatus went into violent oscillations, a kind of stick-slip motion. We therefore settled on three loads, 10 kg, 20 kg, and 26 kg for this fluid, the last one being only at the higher speeds. As Table VI shows, our measured tractions (d.c. driving motor current) were lower for the TCP fluid than for pure N-1 at the lower loads, but apparently (stick-slip) higher at the higher loads.

Fig. 47 shows a comparison of spectra in the 1300-1500cm^{-1} region, which were obtained without polarizers. In general, the higher speed or the higher load spectra show much less structure than those at lower speed. Fig. 48 shows that, under polarization along the flow direction, the 1450cm^{-1} band shows as emission at the low cooling bath temperature for high and low loads as well as slow and fast speeds except for the low-load/fast speed/-low temperature case. At the higher bath temperature absorption and emission reverse with speed.

The spectra under polarization normal to the flow direction of Fig. 49 exhibit even more structure than those under parallel polarization. The low speed spectra have the sharpest bands; there the simultaneous occurrence of emission and absorption is particularly pronounced. When the corresponding spectra for different polarizations are compared, opposite phases are mostly found. For example, Figs. 48 and 49 have the 1460cm^{-1} band reversed at low speed, while the 1350cm^{-1} bands remain in the same direction. The situation is not as pronounced for the bands at high speed.

The sharpness and consistency of the TCP spectra compared to the neat N-1 spectra was rather remarkable. The low speed results, in particular, showed rather constant features and these would reverse with polarization (at 1460cm^{-1}) as just pointed out. A solid deposit built up on the diamond plate could explain this phenomenon, especially the sharp 1460cm^{-1} band, reversing with polarization. Furthermore, when a spectrum (Fig. 50) was calculated to higher frequencies, apparently self-reabsorbed bands were found at 1625cm^{-1} and 1750cm^{-1}, in addition to the 1460cm^{-1} band. This observation pointed to the presence of some olefinic or aromatic residue (at 1625cm^{-1}), perhaps left from the TCP, and to a carbonyl-containing material.

As further runs showed these features even more strongly, the fluid was removed, the diamond cleaned, and spectra were obtained by placing a heated steel plate above the diamond. Spectra similar to Fig. 50 were still obtained.

By then it was clear that there must have been a deposit on the diamond. Indeed, we found the same "Friction Polymer" we had found once before (at least it looked like the same one). It stuck so tightly to the diamond that it had to be removed with a needle. Further examination of the diamond revealed that its surface had also been damaged by slight scratches.

It is difficult to pinpoint the experiment where the damage occurred. The buildup of deposit must have progressed throughout the N-1 + TCP series. A more careful review of the spectra would seem to indicate this buildup. Although the proper evidence is lacking, it would appear that the deposit is largely hydrocarbon; the CO-band is normally so intense that the amount found in the spectra, e.g. Fig. 50, is relatively very small. Of course, the entire deposit is only visible under a microscope and (what is now left of it) not analyzable by infrared transmission. Better emission spectra should be obtained and compared with a friction polymer deposit kept from earlier work.

It is interesting that the friction polymer should have formed in the presence of the TCP ("anti-wear") additive. No effort was taken to keep out air from the contact region. Perhaps the combination of air and TCP could have been effective. It is certainly apparent that these results require closer study.

During the course of our work with the N-1/TCP combination, a series of spectra was obtained as the polarizer was rotated over incremental angles of 30^{o}. The results of Fig. 51 are consistent with a solid material aligned in a definite direction. This observation also induced us to take the system apart for closer examination.

5.4.2 Discussion of Preceding Data

The deduction from the N-1 + TCP spectra of the presence of a solid deposit on the diamond in the conjunction region may not be obvious. Hence a brief explanation may be in order.

Let us start with the premise that a deposit formed from the organic fluid would also be organic and that it would also have infrared bands corresponding to the C-H bending modes, i.e. at about 1380 and 1460cm^{-1}. Such a deposit would be oriented during its formation on the diamond surface. The

dipole oscillations giving rise to the 1460cm^{-1} band are also oriented with respect to the diamond surface. If emission takes place from the same vibrational mode of the fluid in the conjunction region -- because heat is generated in the fluid by viscous friction --, then part of the emission band is absorbed by the solid, the relative amount being related to film thickness and temperatures. Since a more intense band is also generally broader, emission and absorption in the band envelope may differ from that in the center. Hence ups and downs may occur in the spectra over one bandwidth, depending on operating conditions.

A temperature gradient through a liquid film could give rise to similar spectral phenomena. However, the reason we considered it a solid in the case of the TCP fluid, was the remarkable constancy of the spectral changes, especially under polarization, and the progressive worsening of the complexity of the spectra.

Procedures have been developed by Fourier spectroscopists to separate individual spectra from overlapping spectra (not more than three) by computation for this purpose it is generally necessary to have individual spectra of at least some of the components. If we could get the emission spectrum of the friction polymer alone, we could subtract it from the total EHD spectra and get the film spectra. An approach of this nature will be attempted.

If there were no overlap between fluid film and deposit bands, these problems would not arise. Such a situation exists with an aromatic fluid and a paraffinic deposit. Such a situation will very likely also exist with the "halogen-tagged" fluid, which is now being synthesized for us.

A number of subtractions between spectra to obtain "one" spectrum have been done. An example is shown in Fig. 52. The difference spectrum of Fig. 52 (vertical minus horizontal polarization) is considerably simpler that that of either of the components and all the bands are now absorption bands, 1350cm^{-1},

1460cm^{-1}, bands near 1600cm^{-1}, and a band near 1725cm^{-1}. Is this the spectrum of the friction polymer? There are many assumptions here and since this is only a progress report, it is too early to make a definite statement.

5.5 Synthetic Paraffin (XRM-109)

Fig. 53 shows a series of spectra under different polarization. The only important bands of this fluid are the 1350/1450cm^{-1} C-H deformation modes. This fluid is very viscous and is, therefore, present in rather thick films in the EHD contact: its rates of shear are, therefore, lower and the amount of heat generated is also lower. Nevertheless there appears to be evidence of polarization and, therefore, some alignment.

The spectroscopic data and others for this fluid were summarized in Figs. 24 and 25.

5.6 C-Ether. A Traverse through the Contact Region

The C-ether is one of the newer fluids suggested for high temperature applications because of its stability. As the standard spectrum of Fig. 54 shows, the fluid is highly aromatic. Only a few preliminary experiments were carried out with this material. Thus Fig. 55 records the spectral changes observed on pressurization in the diamond cell; significant spectral changes do occur, whose significance will be studied later with more data.

The following very interesting dynamic spectra were obtained. Fig. 56 shows a spectrum of the central portion of the conjunction region of a low-load (10 kg), high speed (480 RPM) and low temperature (cooling bath temperature 15^{o}C) run. All the three principal infrared bands (compare with Fig. 57) are shown in emission, though there is also some reabsorption ("Bands sit in their own trough"). Since the film temperature is highest in this region, reabsorption is minimized, although even here (film thickness estimated at $\sim$ 0.2 μm) the temperature gradient is unmistakable. A computer program can be employed to fit this spectrum to a temperature gradient in such a way as

to make the "troughs" disappear. Clearly, the EHD film is not isothermal and a proper film temperature profile through the EHD region should include both x,y, and z directions.

Fig. 57 corresponds to the same conditions, except that the region looked at was slightly displaced towards the exit region. The 690cm^{-1} aromatic band is standing out a little more over its background and its peak is displaced toward lower frequency, both observations being in line with somewhat high temperatures. The 745/775cm^{-1} doublet has fused into one band.

Fig. 58 is the spectrum when the observed region was displaced toward the inlet side. The cooler temperature is indicated by (i) the reabsorption of the 690cm^{-1} peak, (ii) higher wavenumbers, and (iii) the (asymmetric) split of the 745/775cm^{-1} doublet.

Fig. 59 corresponds to Fig. 56, but at twice the load. Now the 690cm^{-1} band is much broadened, that at 745cm^{-1} shows evidence of peak reabsorption. However, the 775cm^{-1} partner of the doublet is much enhanced.

The relative intensities of these three bands, and especially of the doublet components, might well correspond to solidification.

Fig. 59 is one of the best emission spectra obtained from an operating bearing.

The overall spectral intensities (GUA's) are all in good agreement with our perception of the situation in regions of the Hertzian area.

VI. DISCUSSION AND CONCLUSION

The data presented should give the reader an overview of the wealth of information that can be gathered from the spectra. In addition to showing (i) effects of temperature, and (ii) pressure, the spectra indicate the existence of (iii) molecular alignment under some conditions, (iv) the existence of a temperature gradient, and (v) chemical changes paralleling the formation of a friction polymer. None of these aspects has been studied in detail; the purpose of the work so far was primarily to identify the areas warranting further research. For this purpose a specially synthesized "tagged" fluid will be most helpful, especially for elucidation of the traction mechanism. Work on it is already underway.

VII. REFERENCES

1. (a) Lauer, J.L., "Study to Define Behavior of Liquid Lubricants in and Elastohydrodynamic Contact," NASA CR-134671, October 1974.

   (b) Lauer, J.L., "Infrared Emission Spectra from Operating Elastohydrodynamic Sliding Contacts," NASA CR-3-18531, March 1976.

2. Lauer, J.L, "Infrared Spectra of Fluid Films under Conditions of Incipient Bearing Failure," Final Report to the Air Force Office of Scientific Research on Contracts F44620-74-C-0038 and F49620-76-C-0042. May 1978.

3. Blanke, J.F., Vincent, S.E., and Overend, J., Spectrochimica Acta, 32A, pp. 163-173, 1976.

4. Westlake, F.J., and Cameron, A., "Fluid Film Interferometry in Lubrication Studies," Nature, 214, pp. 633-634, 1967.

5. Sanborn, D.M., and Winer, W.O., "Fluid Rheological Effects in Sliding Elastohydrodynamic Point Contacts with Transient Loading: 1 - Film Thickness," Transactions of the ASME, Journal of Lubrication Technology, Series F, Vol. 93, pp. 262-271 (1971).

6. Barnett, J.D., Block, S., and Piermarini, G.J., "An Optical Fluorescence System for Quantitative Pressure Measurement in the Diamond Anvil Cell," Rev. of Scientific Instruments, 44, 1-9 (1973).

7. Lauer, J.L., and Peterkin, M.E., "Glass Transition and Fluid Pressure Determinations from the Fluorescence Spectrum of Ruby," Canadian Journal of Spectroscopy, 21, pp. 153-158, (September, October 1976).

8. Alsaad, M., Bair, S., Sanborn, D.M., and Winer, W.O., "Glass Transitions in Lubricants: Its Relation to Elastohydrodynamic Lubrication," Paper No. 77-Lub-3, Presented at the ASLE-ASME Joint Lubrication Conference, Kansas City, Missouri, October 3-7 (1977).

9. Kambour, R.P., and Robertson, R.E., "The Mechanical Properties of Plastics," Chapter II, pp. 687-822, in Polymer Science, Vol. I (A.D. Jenkins, editor). North Holland Publishing Co., Amsterdam, 1972.

10. Lippincott, E.R., Whatley, L.S., and Duecker, H.C., "Microtechniques Using Miniaturized Diamond Optics," Chapter 14, pp. 435-461, in Applied Infrared Spectroscopy (D.N. Kendall, editor). Reinhold Publishing Corporation, New York, 1966.

11. Craven, S.M., and Bentley, F.F., "Far Infrared Group Frequencies. I. Aliphatic Alcohols," Applied Spectroscopy, 26, 242-7 (1972).

12. a) Christian, S.D., Grundnes, J., and Klaboe, P., "High Pressure Infrared Studies of Liquids with the Diamond Anvil Cell," Applied Spectroscopy, 30, 227-229 (1976).

    b) Moon, S.H., and Drickamer, H.G., "Effects of Pressure on Hydrogen Bonds of Organic Solids," J. Chem. Phys. 61, 48-54 (1974).

13. Jones, W.R., Jr., Johnson, R.L., Winer, W.O., and Sanborn, D.M., "Pressure-Viscosity Measurements for Several Lubricants to 5.5 x 10^8 Newtons per Square Meter and 149°C," NASA, TN D-7736 (August 1974).

14. Schoen, P.E., Priest, R.G., Sheridan, J.P., and Schnur, J.M., Nature (London), 1977, 270(5636), 412-414; "Effect of Pressure on Raman Bands of Alkanes".

15. Roelands, C.H.A., Correlational Aspects of the Viscosity-Temperature-Pressure Relationship of Lubricating Oils. O.P. Books Program, University Nicrofilm, Ann Arbor, Michigan, 1966.

VIII. APPENDIX I. INDEX OF MATHEMATICAL SYMBOLS

1. h_o average fluid film thickness
2. u combined surface velocity at contact
3. C motor current (amperes)
4. E' reduced elastic modulus
5. F parameter defined in Table II
6. R ball radius
7. T_B fluid temperature near the ball surface
8. T_D temperature next to diamond window (^oC)
9. T_o fluid reservoir temperature
10. W load
11. α pressure coefficient of viscosity
12. α_{ot} slope of tangent to $\log \eta$ as a function of pressure
13. η_o absolute viscosity of fluid in entrance region
14. $\nu(T)$ kinematic viscosity, a function of temperature

IX. LIST OF TABLES

TABLE I
PROPERTIES OF FLUIDS

Fluid	Temperature (°C)	Kinematic Viscosity m^2/sec	Density kg/m^3	Absolute Viscosity (η) Pa.s	Viscosity-Pressure Index* Z	Viscosity-Pressure Coefficient** α_{oT}	Film-Forming Capability $(\alpha_{oT}\eta)^{5/7}_{s^{5/7}}$
Synthetic	38	443×10^{6}	835.5	370.1×10^{-3}	0.44	1.947×10^{-8}	1.528×10^{-6}
Paraffin	49	250	828.4	207.1	0.44	1.816	0.960
	77	82	810.2	66.4	0.44	1.561	0.383
	99	41	795.9	33.0	0.44	1.468	0.222
Advanced	38	24.8×10^{-6}	969.9	24.02×10^{-3}	0.48	1.454×10^{-8}	0.176×10^{-6}
Ester	49	16.5	962.8	15.89	0.48	1.353	0.124
	77	7.7	944.6	7.27	0.48	1.162	0.064
	99	4.97	930.3	4.62	0.48	1.051	0.043
Sun	38	40.9×10^{-6}	869.2	35.53×10^{-3}	1.06	3.294×10^{-8}	0.417×10^{-6}
Traction	49	23.0	862.1	19.83	1.02	2.991	0.257
Fluid	77	8.0	843.9	6.75	0.92	2.191	0.095
	99	4.49	829.6	3.72	0.85	1.767	0.053
Naphthenic	38	24.1×10^{-6}	904.0	21.75×10^{-3}	0.67	1.996×10^{-8}	0.205×10^{-6}
Reference	49	14.6	896.9	13.09	0.67	1.822	0.134
Fluid	77	6.0	878.7	5.27	0.67	1.511	0.061
(N-1)	99	3.73	864.4	3.222	0.67	1.344	0.040

* based on Roelands, C.H.A. (Ref. 15)
** slope of the tangent to log η as a function of pressure
isotherm at atmospheric pressure

TABLE II

APPARATUS PARAMETER RELATING TO EHD FILM THICKNESS

Ball Rotational Speed (RPM)	240			360			480		
Ball Surface Speed (m/sec)	0.719			1.078			1.438		
Load (N)	108	191	279	108	191	279	108	191	279
Parameter* (F)	1.003	0.979	0.959	1.340	1.304	1.281	1.646	1.602	1.573

*defined according to Wedeven et.al.[15] by

$$h_o = 1.73R\,(u/R)^{5/7}(W/E'R^2)^{-1/21}(\alpha\eta_o)^{5/7}$$

$$= F\,(\alpha\eta_o)^{5/7}$$

TABLE III

CALC. EHD FILM THICKNESSES AND RATES OF SHEAR
UNDER STANDARD CONDITIONS

Fluid	Ball Rotational Speed (RPM) and Surface Speed (m/sec) (in parentheses)	Load (N)	Film Thickness (h) in μm at temperature (°C) 38°	49°	77°	99°	Rates of Shear (U/h) (sec^{-6}) at temperature (°C) 38°	49°	77°	99°
Synthetic Paraffin	240 (0.719)	108	1.53	0.963	0.384	0.223	0.470	0.747	1.872	3.224
		191	1.49	0.940	0.375	0.217	0.483	0.765	1.917	3.313
		279	1.47	0.921	0.367	0.213	0.489	0.781	1.959	3.376
	360 (1.078)	108	2.05	1.287	0.513	0.297	0.526	0.838	2.101	3.630
		191	1.99	1.252	0.499	0.289	0.542	0.861	2.160	3.730
		279	1.96	1.230	0.490	0.284	0.550	0.876	2.220	3.796
	480 (1.438)	108	2.52	1.581	0.630	0.365	0.571	0.910	2.283	3.940
		191	2.45	1.538	0.613	0.356	0.587	0.935	2.346	4.039
		279	2.40	1.511	0.602	0.349	0.599	0.952	2.389	4.120
Advanced Ester	240 (0.719)	108	0.177	0.125	0.064	0.043	4.062	5.752	11.234	16.721
		191	0.172	0.122	0.062	0.042	4.180	5.893	11.597	17.119
		279	0.169	0.119	0.061	0.041	4.254	6.042	11.787	17.537
	360 (1.078)	108	0.236	0.167	0.085	0.058	4.568	6.455	12.682	18.586
		191	0.230	0.162	0.083	0.056	4.687	6.654	12.988	19.250
		279	0.225	0.159	0.082	0.055	4.791	6.780	13.146	19.600
	480 (1.438)	108	0.290	0.205	0.105	0.071	4.959	7.015	13.695	20.254
		191	0.282	0.199	0.102	0.069	5.099	7.226	14.098	20.841
		279	0.277	0.196	0.100	0.068	5.191	7.337	14.380	21.147
Sun Traction Fluid	240 (0.719)	108	0.418	0.257	0.095	0.054	1.720	2.798	7.568	13.315
		191	0.407	0.251	0.093	0.052	1.767	2.865	7.731	13.827
		279	0.400	0.246	0.091	0.051	1.798	2.923	7.901	14.098
	360 (1.078)	108	0.559	0.344	0.128	0.072	1.928	3.134	8.422	14.972
		191	0.544	0.335	0.124	0.070	1.982	3.218	8.694	15.400
		279	0.534	0.329	0.122	0.068	2.019	3.277	8.836	15.853
	480 (1.438)	108	0.686	0.422	0.157	0.087	2.096	3.408	9.159	16.529
		191	0.668	0.411	0.153	0.086	2.153	3.499	9.399	16.721
		279	0.656	0.404	0.150	0.084	2.192	3.559	9.587	17.119
Naphthenic Reference Fluid (N-1)	240 (0.719)	108	0.206	0.134	0.061	0.040	3.490	5.366	11.787	17.975
		191	0.200	0.131	0.060	0.039	3.595	5.489	11.983	18.436
		279	0.197	0.128	0.059	0.038	3.650	5.617	12.186	18.921
	360 (1.078)	108	0.275	0.179	0.082	0.053	3.920	6.022	13.146	20.340
		191	0.268	0.175	0.080	0.052	4.022	6.160	13.475	20.731
		279	0.263	0.172	0.078	0.051	4.099	6.267	13.821	21.137
	480 (1.438)	108	0.338	0.220	0.100	0.065	4.254	6.536	14.380	22.123
		191	0.329	0.215	0.098	0.063	4.371	6.688	14.673	22.825
		279	0.323	0.211	0.096	0.062	4.452	6.815	14.979	23.194

TABLE IV

EMISSION (E) OR ABSORPTION (A) OF
$1375cm^{-1}$ (CH_3 sym) AND $1450/60cm^{-1}$ (CH_2 + CH_3 asym)
BAND CENTERS RESPECTIVELY FOR SUN TRACTION FLUID

Cooling Bath Temp(^{o}C)	← 15 →			← 25 →	
Ball Speed (RPM)	120	240	360	120	240
Load (KG)	← 11 →				
Not Polarized	-	A A	EE	EA	A A
Pol. Along Flow	-	EA	EA	EA	EA
Pol. Normal to Flow	-	EE	EE	EE	EE
Load (KG)	← 22 →				
Not Polarized	EE	EA	-	AA	-
Pol Along Flow	AA	AE	-	AA	-
Pol. Normal to Flow	AA	AE	-	AA	-

AA both peaks pointing down
EE both peaks pointing up
AE first peak pointing down, second up
EA first peak pointing up, second down

TABLE V

MOTOR CURRENT AND TEMPERATURES
OF
ESTER/SUNTRAC MIXTURES

MIX	100% of Ester 0% of Traction Fluid				67 33				33 67				0 100%			
RPM/KG	C	T_D	T_B	T_o	C	T_D	T_B	T_o	C	T_D	T_B	T_o	C	T_D	T_B	T_o
240/11	1.05	29	23	23	1.23	34	25	23	1.36	38	27	25	1.50	41	30	27
240/22	1.50	39	27	25	1.65	46	29	26	1.78	51	32	28	-	54	36	30
360/11	1.08	30	23	22	1.26	34	24	23	1.45	42	29	28	1.59	46	30	28
360/22	1.55	41	27	25	1.77	49	30	29	1.92	57	34	33	2.07	64	39	34

C = motor current related to traction

T_D='diamond'or Hertzian inlet temperature

T_B= temperature measured by thermocouple sliding on ball surface

T_O= temperature measured by thermocouple in a quiet location in the fluid away from the contact

*Note that 240 RPM corresponds to a sliding speed of 0.72m/s, 360 RPM to 1.08m/s and that 11 and 22 kg loads correspond to 108 and 216 N respectively.

TABLE VI

Comparison of Relative Friction (Traction) Data for N-1

and

N-1 + 1%-TCP Fluids

(Current of D. C. Drive Motor in Amperes)

N-1 Fluid and N-1 + 1% TCP Fluid (in parentheses)

	Cooling Bath Temperature, 15°C		Cooling Bath Temperature, 25°C	
Ball Speed (RPM)	230	480	230	480
Load (kg)				
10	0.75 (0.87)	1.09 (1.04,1.02)	.95 (0.85)	1.07 (1.02)
20	1.20*(1.18)	1.37* (1.32)	1.20*(1.17)	1.36*(1.32)
26	1.36 (**)	1.56 (1.66)	1.34 (**)	1.56
36	1.56	1.84	1.67	1.76

*Interpolated

**Slip-stick operation

TABLE VII

COMPARISON OF POLYSTYRENE REFERENCE BANDS

Band	Wavenumber by (a) Interferometer	Band	(b) Grating Spectrometer
A	702	$\bar{A}$	700
B	753	--	--
C	770	$\bar{B}$,$\bar{C}$	760
D	842	$\bar{D}$	845
E	875	--	--
F	908	$\bar{F}$	910
G	940	--	--
H	960	$\bar{H}$,$\bar{I}$	970
I	980	--	--
J	1000	--	--
K	1030	$\bar{K}$	1030
L	1074	$\bar{L}$	1072
M	1155	$\bar{M}$	1157
N	1184	$\bar{N}$	1184
O	1205	--	--
P	1300	--	--
Q	1318	$\bar{Q}$,$\bar{R}$	1330
R	1355	--	--
S	1378	$\bar{S}$	1370
T	1450	$\bar{T}$	1450
U	1493	$\bar{U}$	1490
V	1575	$\bar{V}$	1580
W	1601	$\bar{W}$	1598
X	1635	--	--
Y	1650	--	--
Z	1678	--	--
a	1695	--	--
b	1718	--	--
c	1745	--	--
d	1762	--	--
e	1804	--	--
f	1832	--	--

XI. Captions to Figures

1. Interferometer Emission Optics
   The tuning fork tine vibrate at 15 Hz, alternatingly exposing source and reference.

2. Comparison of Polystyrene Spectra
   The uppertracers are single-beam absorption spectra obtained by the interferometer, while the lower trace is a routine double-beam grating spectrum. Corresponding absorption bands are marked by unbarred and barred letters. Bands listed by letters separated by commas were not resolved in the grating spectrum. The wave numbers corresponding to lettered bands are given in Table VII.

3. Reference Voltage versus Center Burst for a Graybody Spectrum
   The resultant center burst intensity becomes negative when the radiant energy detected from the reference exceeds that from the source.

4. Reference Voltage versus Greatest Amplitude for a Graybody Spectrum

5. a. (Top). Emission Spectrum from a Hot Plate through a Contaminated Diamond Window. b. (Bottom). Spectrum with Cleaned Diamond.

6. Ray Diagram of EHD Contact Region for Orthogonal Polarizations
   Reflectivity differences result in intensity differences between polarized emissions.

7. Spectra of Advanced Ester for Two Orthogonal Polarizations and Their Ratio
   a. Comparison of unpolarized and polarized spectra.
   b. Ratio of polarized spectra, showing enhanced sensitivity.

8. Emission Spectra Taken from Article by Overend et al.[3]

9. Standard Infrared Absorption Spectrum of Traction Fluid

10. Standard Infrared Absorption Spectrum of Advanced Ester

11. Standard Infrared Absorption Spectrum of Synthetic Paraffin

12. Standard Infrared Absorption Spectrum of Naphthenic Reference Fluid (N-1)

13. Standard Infrared Absorption Spectra of Naphthenic Reference Fluid (N-1) Containing 17% (upper trace) and 5% (lower trace) of p-Tricresyl Phosphate.

14. Standard Infrared Absorption Spectrum of p-Tricresyl Phosphate (film)

15. Main Absorption Bands (Schematic)
   The heights of the bars refer to absorptivities. The intensities in emission are quite different (see next figure).

16. Corrected (Single-Beam) Emission Band Intensities

17. Diamond Cell Absorption Spectra of Traction Fluid

18. Diamond Cell Absorption Spectra of Advanced Ester

19. Diamond Cell Absorption Spectra of Synthetic Paraffin

20. Diamond Cell Absorption Spectra of Naphthenic Reference Fluid (N-1)

21. Diamond Cell Absorption Spectra of Naphthenic Reference Fluid (N-1, top traces) and of Naphthenic Reference Fluid (N-1) containing 1% of p-Tricresylphosphate (TCP, bottom traces)
    The two strongest TCP bands are marked. Note that intensity of the one at higher frequency is much reduced by pressure, but that the other one is essentially unaffected.

22. Change of Band Peak Location with Pressure for 2,6-Dichlorophenol (Replotted[12])
    Note the break in the curve of wavenumber against pressure.

23. Hertzian Inlet Temperatures as a Function of Shear Rate.
    The temperatures for the naphthenic reference fluid (N-1) were not changed significantly by the presence of 1% of tricresyl phosphate (TCP).

24. Hertzian Area Ball Surface Temperatures vs. Shear Rate for Different Fluids
    The temperatures were obtained from the graybody emission measured by the infrared detector. The fluids were CASE A-synthetic paraffin, B-traction fluid, C-naphthenic reference fluid N-1 with 1% tricresyl phosphate, D-N-1, and E-pentaerythritol ester.

25. Band Intensities (obtained under parallel polarization) vs. Shear Rate

26. Emission Spectra of Traction Fluid from EHD Contact under Low Load and Low Speed
    The cooling bath temperature was 15°C, the load 11 kg, and the ball's rotational speed 240 RPM (Corresponding to the load and linear speed shown).

27. Emission Spectra of Traction Fluid from EHD Contact under High Load and Low Speed
    The cooling bath temperature was 15°C, the load 22 kg, and the ball's rotational speed 240 RPM (corresponding to the load and linear speed shown).

28. Comparison of Emission Spectra of Traction Fluid from EHD Contacts for Different Loads and Speeds
    A and D - 108N, 0.72m/s
    B and E - 108N, 1.08m/s
    C and F - 216N, 0.72m/s
    The cooling bath temperature was 15°C throughout.

29. Emission Spectra of Traction Fluid from EHD Contacts at Low Load and High Speed
    The cooling bath temperature was 15°C, the load 11 kg, and the rotational speed 360 RPM (corresponding to the load and linear speed shown).

30. Emission Spectra of Advanced Ester, C-O Band, from EHD Contacts under Various Conditions for Polarization in the Flow Direction
    A - 108N load, 1.08m/s sliding speed, 25°C
    B - 108N load, 1.08m/s sliding speed, 15°C
    C - 216N load, 1.08m/s sliding speed, 25°C
    D - 216N load, 0.72m/s sliding speed, 15°C

31. Emission Spectra of Advanced Ester, C-O Band, from EHD Contacts under Various Conditions for Polarization Normal to the Flow Direction
    A - 108N load, 1.08m/s sliding speed, 25°C
    B - 108N load, 1.08m/s sliding speed, 15°C
    C - 216N load, 1.08m/s sliding speed, 25°C
    D - 216N load, 0.72m/s sliding speed, 15°C

32. Emission Spectra of Advanced Ester from EHD Contacts under High Load Low Flow Speed, and Low Cooling Bath Temperature
    The effect of polarization is shown.

33. Emission Spectra of Advanced Ester from EHD Contacts under High Load, High Flow Speed, and High Cooling Bath Temperature
    The effect of polarization is shown.

34. Emission Spectra of Advanced Ester/Traction Fluid Mixtures (1:2) from EHD Contacts
    A - 108N load, 1.08m/s sliding speed, polarization normal to flow
    B - 216N load, 0.72m/s sliding speed, polarization normal to flow
    C - 216N load, 1.08m/s sliding speed, polarization normal to flow
    D - 108N load, 1.08m/s sliding speed, polarization parallel to flow
    E - 216N load, 0.72m/s sliding speed, polarization parallel to flow
    F - 216N load, 1.08m/s sliding speed, polarization parallel to flow

35. Emission Spectra of Advanced Ester/Traction Fluid Mixtures (2:1) from EHD Contacts
    A -108N load, 1.08m/s sliding speed, polarization normal to flow
    B -216N load, 0.72m/s sliding speed, polarization normal to flow
    C -216N load, 1.08m/s sliding speed, polarization normal to flow
    D -108N load, 1.08m/s sliding speed, polarization parallel to flow
    E -216N load, 0.72m/s sliding speed, polarization parallel to flow
    F -216N load, 1.08m/s sliding speed, polarization parallel to flow

36. Comparison of Polarized Emission Spectra of an Advanced Ester/Traction Fluid Mixture (2:1) from EHD Contacts

37. Traction in EHD Contact of Ester/Traction Fluid Mixtures

38. Effect of Traction Fluid Concentration on Diamond (Hertzian Inlet) Temperature of an EHD Contact

39. Relation between Diamond (Hertzian Inlet) Temperature and Traction (Motor Current) for Traction Fluid/Ester Mixtures (A - Traction Fluid, B - Traction Fluid/Ester (2:1), C - Traction Fluid/Ester (1:2), D - Ester)

40. Comparison of N-1 Emission Spectra from an EHD Contact
    A - 15°C Cooling bath, 108N load
    B - 15°C Cooling bath, 292N load
    C - 25°C Cooling bath, 108N load
    D - 25°C Cooling bath, 292N load
    Solid traces represent 0.72m/s sliding speed, broken traces represent 1.44m/s sliding speed.

41. Emission Spectra of N-1, Polarized along the Direction of Flow, from EHD Contact
    Case A - 15°C cooling bath temperature
    Case B - 25°C cooling bath temperature
    The load was 108N and the sliding speeds were 0.72m/s (solid trace) and 1.44m/s (broken trace).

42. Emission Spectra of N-1, Polarized Normal to the Direction of Flow, from an EHD Contact
    Case A - 15°C cooling bath temperature
    Case B - 25°C cooling bath temperature
    The load was 108N and the sliding speeds were 0.72m/s (solid trace) and 1.44m/s (broken trace).

43. Emission Spectra of N-1, not Polarized, from an EHD Contact under High Load (330N)
    Case A - 15°C cooling bath temperature
    Case B - 25°C cooling bath temperature
    The sliding speeds were 0.72m/s (solid trace) and 1.44m/s (broken trace).

44. Emission Spectra of N-1, Polarized along the Direction of Flow, from an EHD Contact under High Load (330N)
    Case A - 15°C cooling bath temperature
    Case B - 25°C cooling bath temperature
    The sliding speeds were 0.72m/s (solid trace) and 1.44m/s (broken trace). The solid trace for Case B was calculated for additional (computed) reference radiation, which was not used in the calculation of the dot-line-dot trace.

45. Emission Spectra of N-1, Polarized Normal to the Direction of Flow, from an EHD Contact under High Load (330N)
    Case A - 15°C cooling bath temperature
    Case B - 25°C cooling bath temperature
    The sliding speeds were 0.72m/s (solid trace) and 1.44m/s (broken trace).

46. Emission Spectra of N-1, Polarized along the direction of flow, from an EHD Contact at 15°C Cooling Bath Temperature and a Load of 292N
    Solid trace - 0.72m/s sliding speed
    Broken trace - 1.44m/s sliding speed

47. Emission Spectra of N-1 Containing 1% of TCP, not Polarized, from an EHD Contact
    Case A - 15°C cooling bath temperature, 108N load
    Case B - 15°C cooling bath temperature, 216N load
    Case C - 25°C cooling bath temperature, 108N load
    Case D - 25°C cooling bath temperature, 216N load
    The sliding speeds were 0.72m/s (solid traces) and 1.44m/s (broken traces).

48. Emission Spectra of N-1 Containing 1% of TCP, Polarized along the Flow Direction, from an EHD Contact
    Case A - 15°C cooling bath temperature, 108N load
    Case B - 15°C cooling bath temperature, 216N load
    Case C - 25°C cooling bath temperature, 108N load
    Case D - 25°C cooling bath temperature, 216N load
    The sliding speeds were 0.72m/s (solid traces) and 1.44m/s (broken traces).

49. Emission Spectra of N-1 Containing 1% of TCP, Polarized Normal to the Flow Direction, from an EHD Contact
    Case A - 15°C cooling bath temperature, 108N load
    Case B - 15°C cooling bath temperature, 216N load
    Case C - 25°C cooling bath temperature, 108N load
    Case D - 25°C cooling bath temperature, 216N load
    The sliding speeds were 0.72m/s (solid traces) and 1.44m/s (broken traces).

50. Emission Spectra over an Extended Range of N-1 Containing 1% of TCP, Polarized Parallel to the Flow Direction, from an EHD Contact
    The cooling bath temperature was 15°, the sliding speed 1.44m/s and the load 108N.

51. Emission Spectra from an EHD Contact of N-1 Containing 1% of TCP
    The load was 108N, the sliding speed 0.72m/s and the cooling bath temperature 25°C.
    A - polarized -30° with respect to the flow direction
    B - polarized along the flow direction
    C - polarized +30° with respect to the flow direction
    D - polarized +60° with respect to the flow direction
    E - polarized normal to the flow direction

52. Emission Spectra from an EHD Contact of N-1 Containing 1% of TCP. The load was 108N, the sliding speed 0.72m/s, and the cooling bath temperature 25°C
    A - polarized along the flow direction
    B - polarized normal to the flow direction
    C - difference between spectrum A and spectrum B

53. Emission Spectra from an EHD Contact of Synthetic Paraffin (XRM-109)
    For cases A,B, and C the polarization was normal to the flow direction for cases D,E, and F along the flow direction. The cooling bath temperature was 50°C throughout. For cases A and D the load was 108N and the sliding speed 1.08m/s. For all the other cases the load was 216N and the sliding speed 0.72m/s.

54. Standard Absorption Spectrum of C-Ether

55. Absorption Spectra of C-Ether in the Diamond Cell at Ambient Temperature
    Continuous trace - 100 MPa pressure
    Broken trace - 1 GPa pressure

56. Emission Spectrum of C-Ether from the Central Portion of an EHD Contact
    The sliding speed was 1.44m/s, the load 108N.

57. Emission Spectrum of C-Ether from the Exist Portion of an EHD Contact
    The sliding speed was 1.44m/s, the load 108N.

58. Emission Spectrum of C-Ether from the Inlet Portion of an EHD Contact
The sliding speed was 1.44m/s, the load 108N.

59. Emission Spectrum of C-Ether from the Central Portion of an EHD Contact
The sliding speed was 1.44ms, the load 216N.

Figure 1

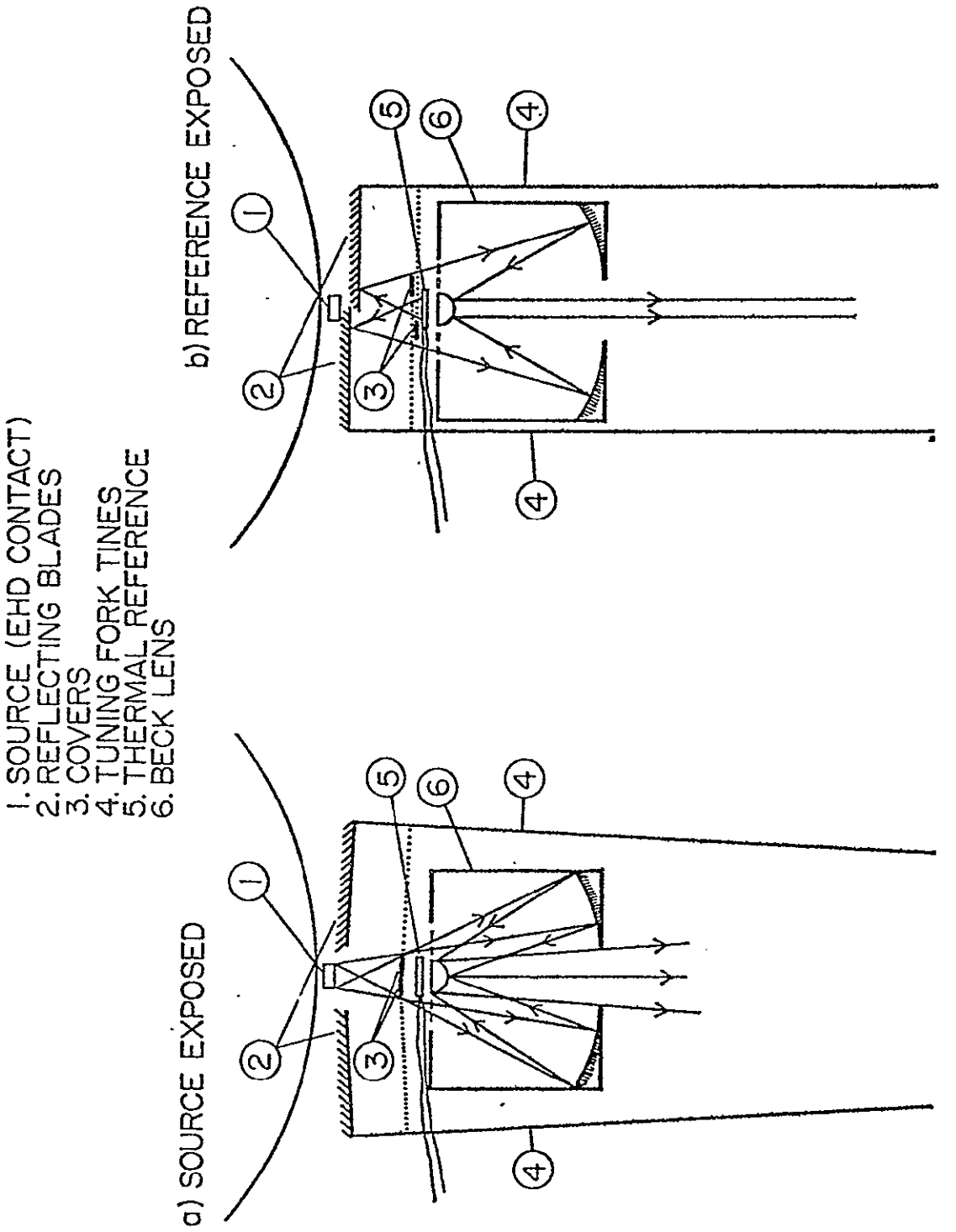

ORIGINAL PAGE IS
OF POOR QUALITY

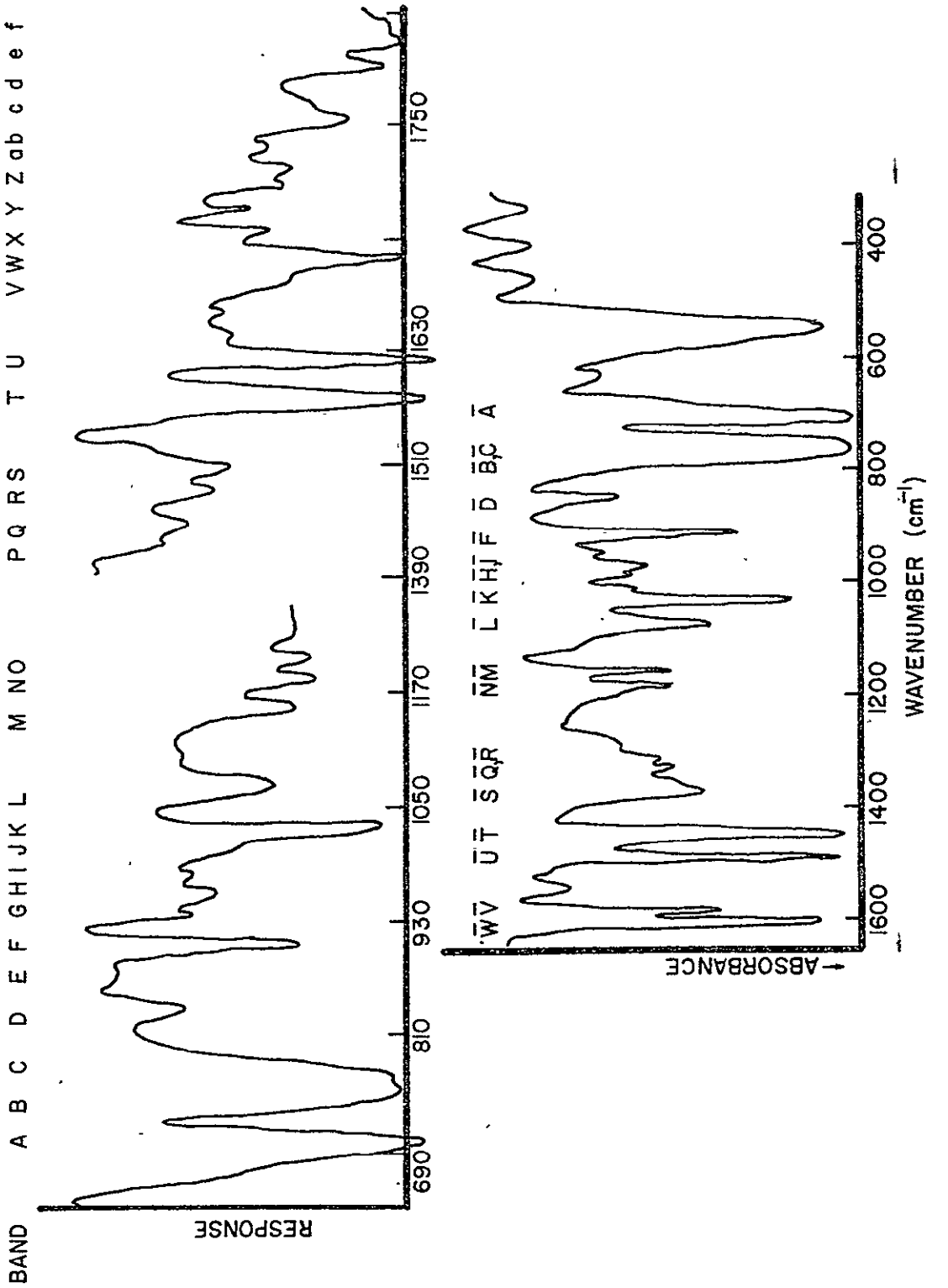

Figure 3

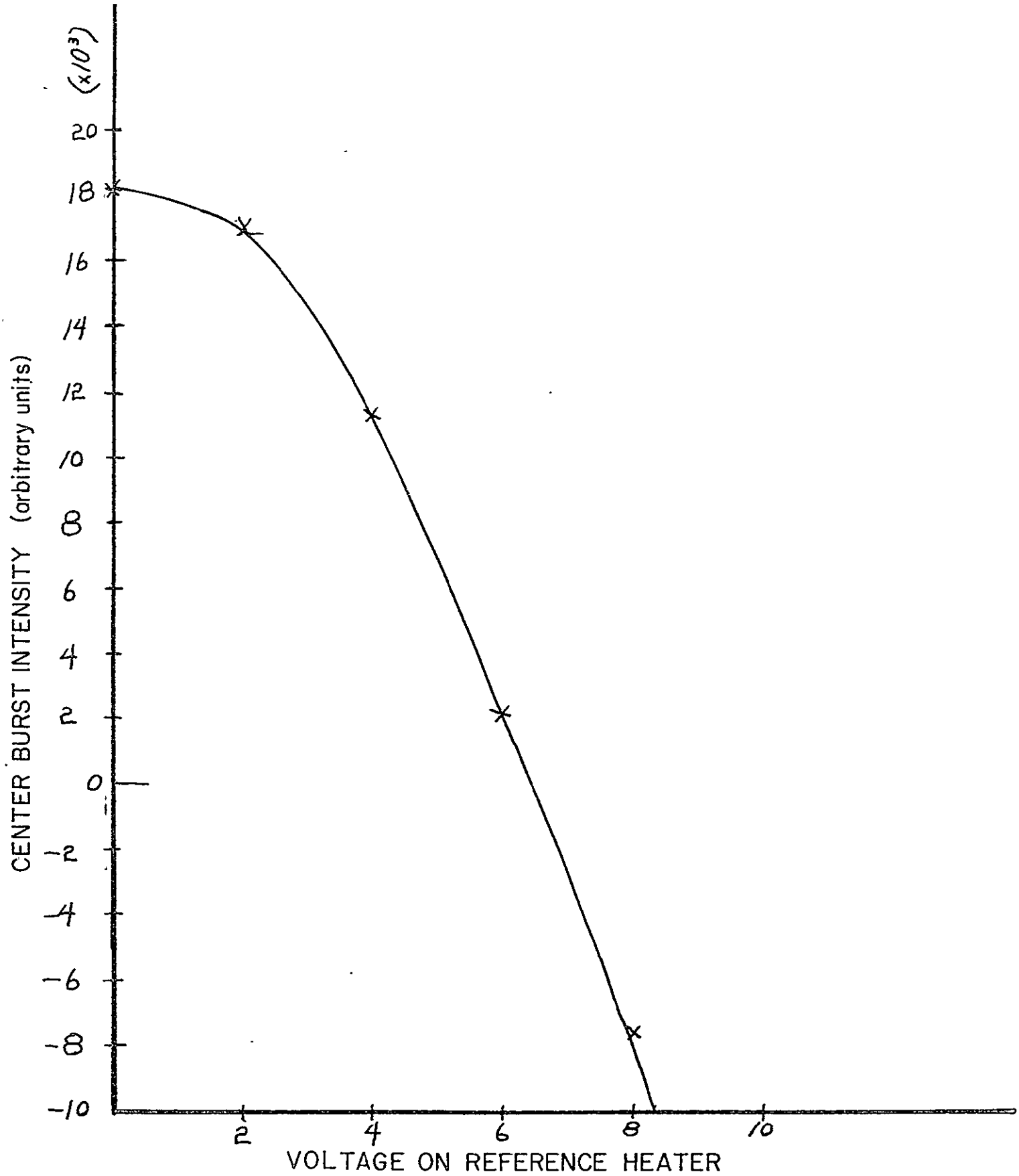
(x10³)
20
18
16
14
12
10
8
6
4
2
0
-2
-4
-6
-8
-10
CENTER BURST INTENSITY (arbitrary units)
2
4
6
8
10
VOLTAGE ON REFERENCE HEATER

Figure 4

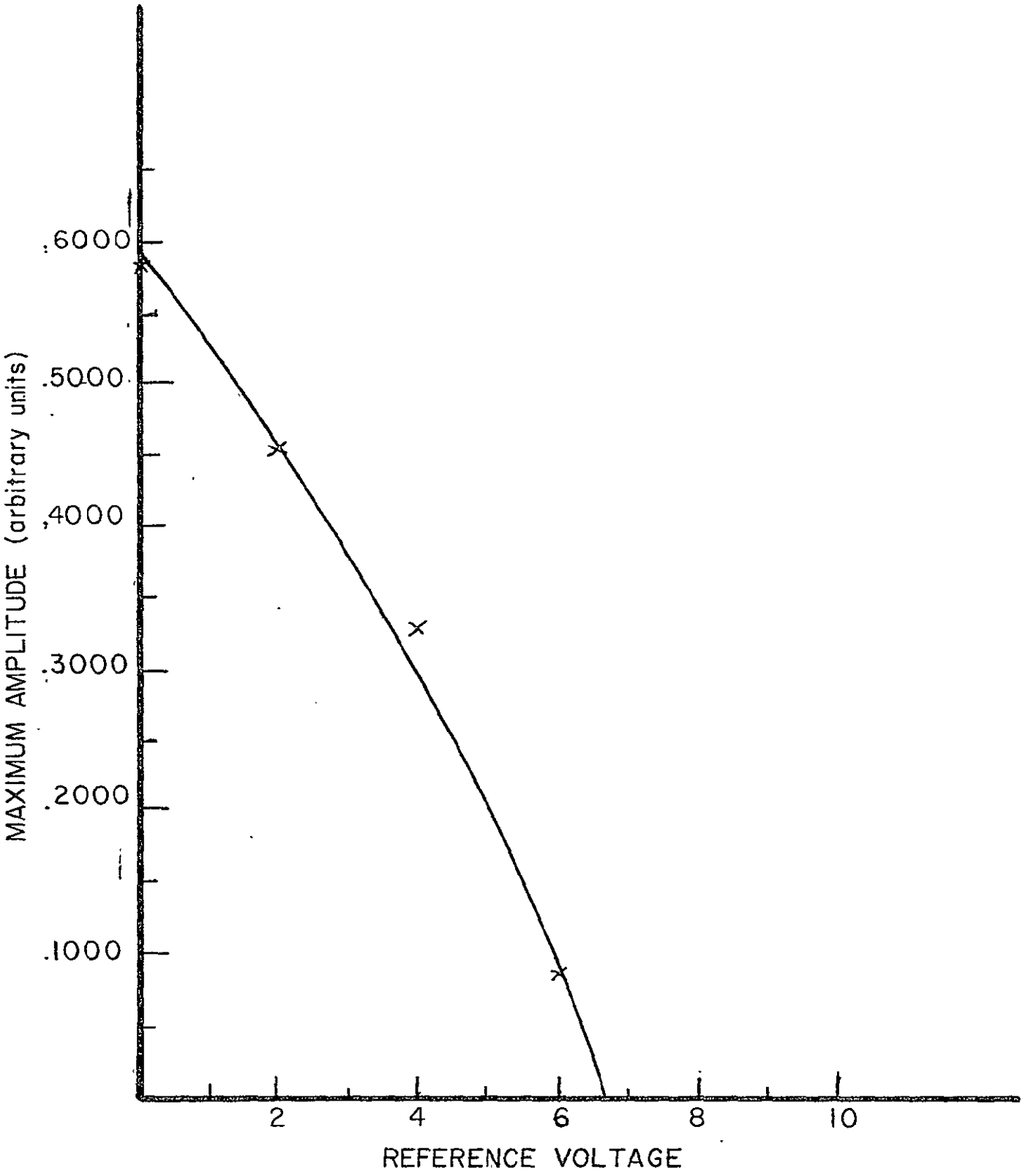
.6000
.5000
.4000
.3000
.2000
.1000
MAXIMUM AMPLITUDE (arbitrary units)
2
4
6
8
10
REFERENCE VOLTAGE

Figure 5

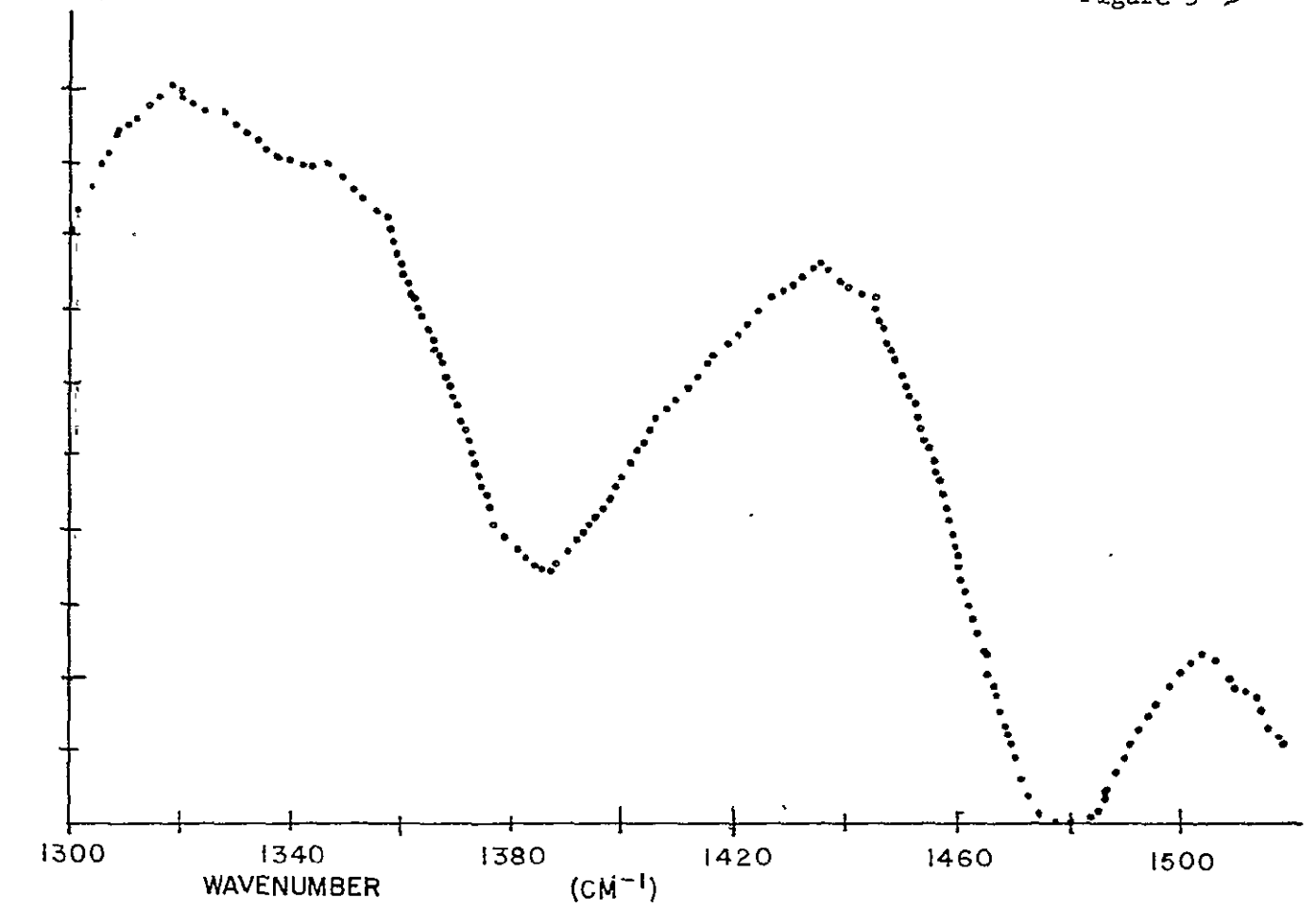
1300
1340
1380
1420
1460
1500
WAVENUMBER
(CM⁻¹)

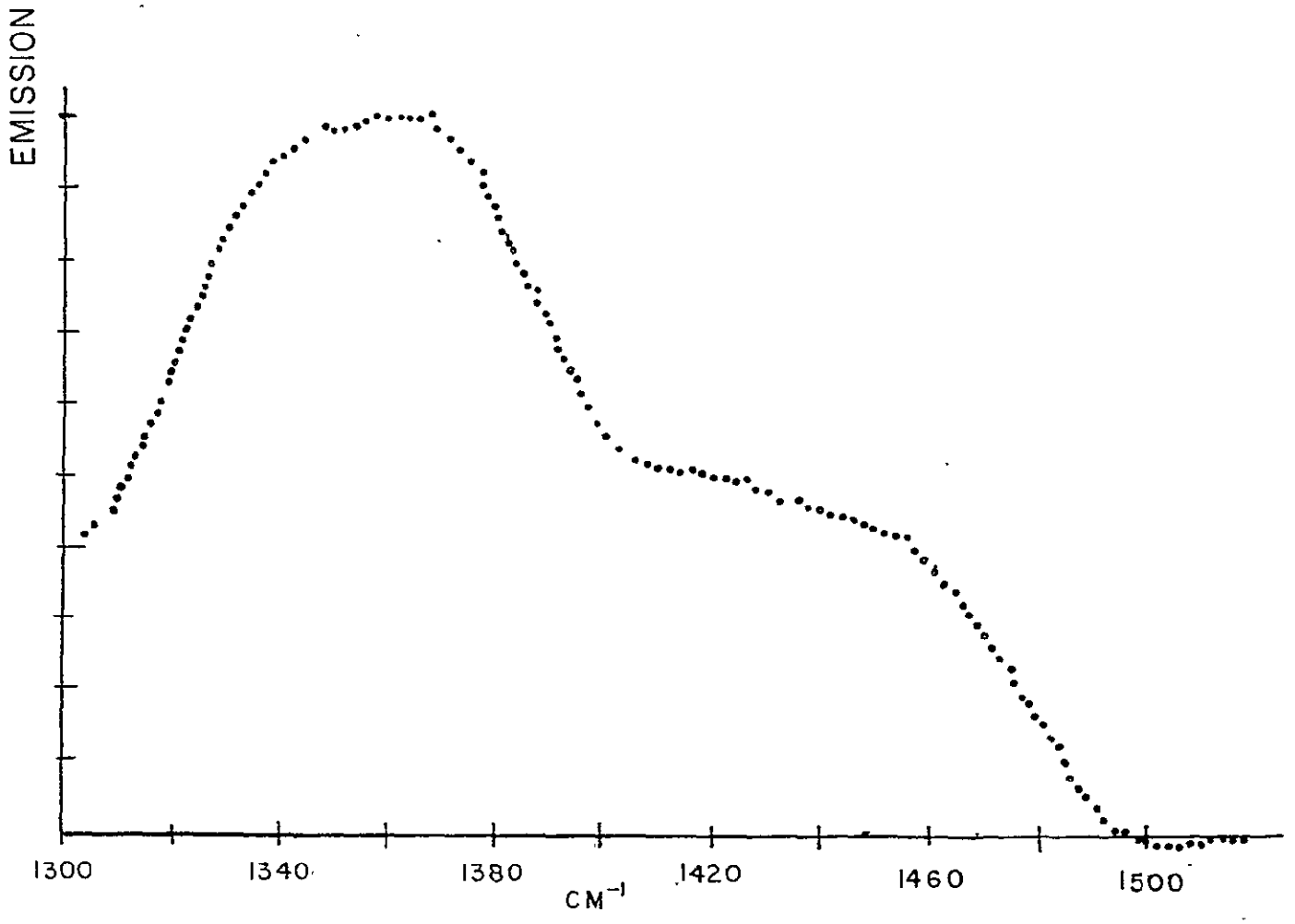
EMISSION
1300
1340
1380
1420
1460
1500
CM⁻¹

Figure 6

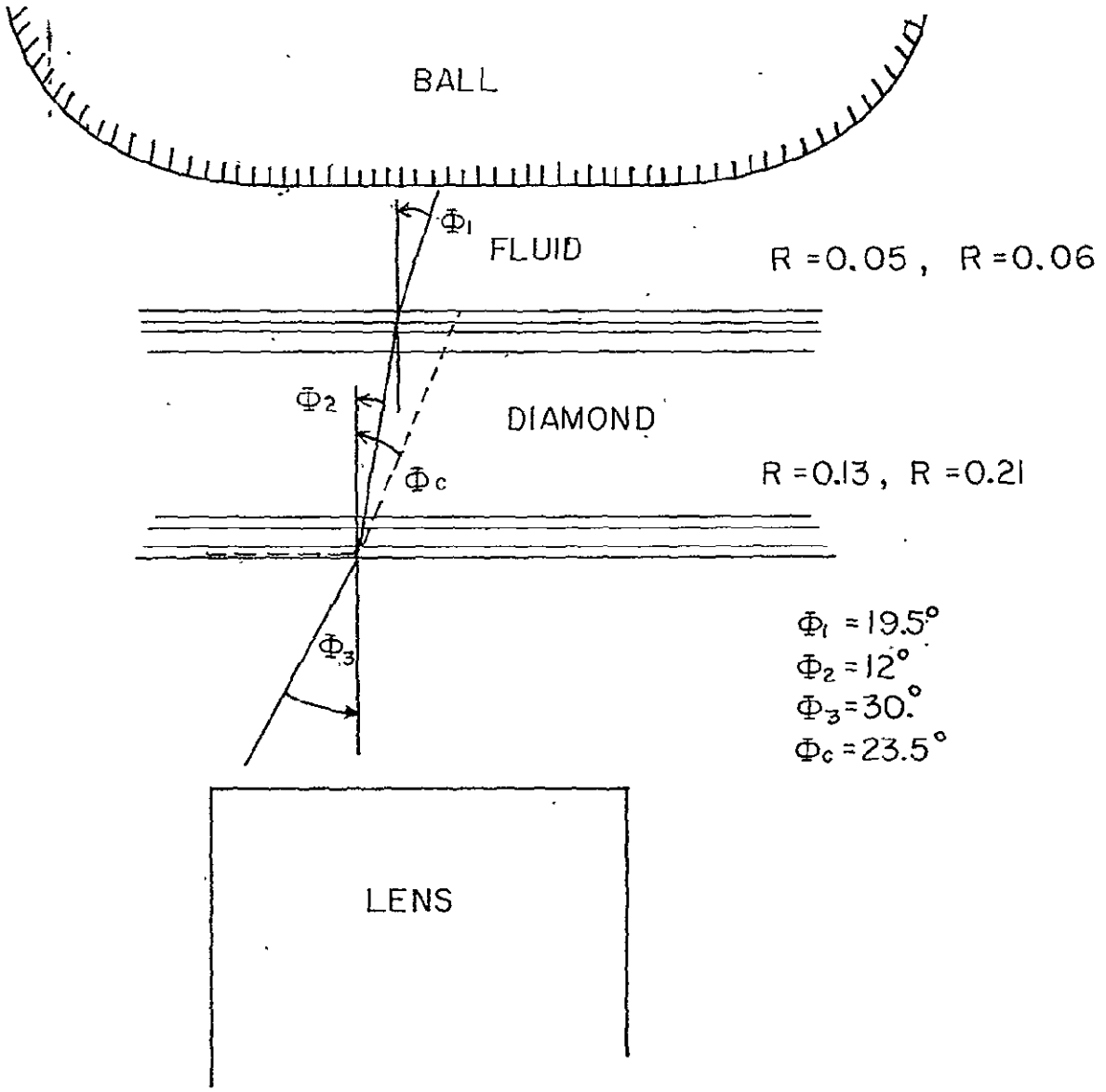
BALL
Φ_1
FLUID
R =0.05 , R =0.06
Φ_2
DIAMOND
Φ_c
R =0.13 , R =0.21
Φ_3
Φ_1 =19.5°
Φ_2 =12°
Φ_3=30.°
Φ_c =23.5°
LENS

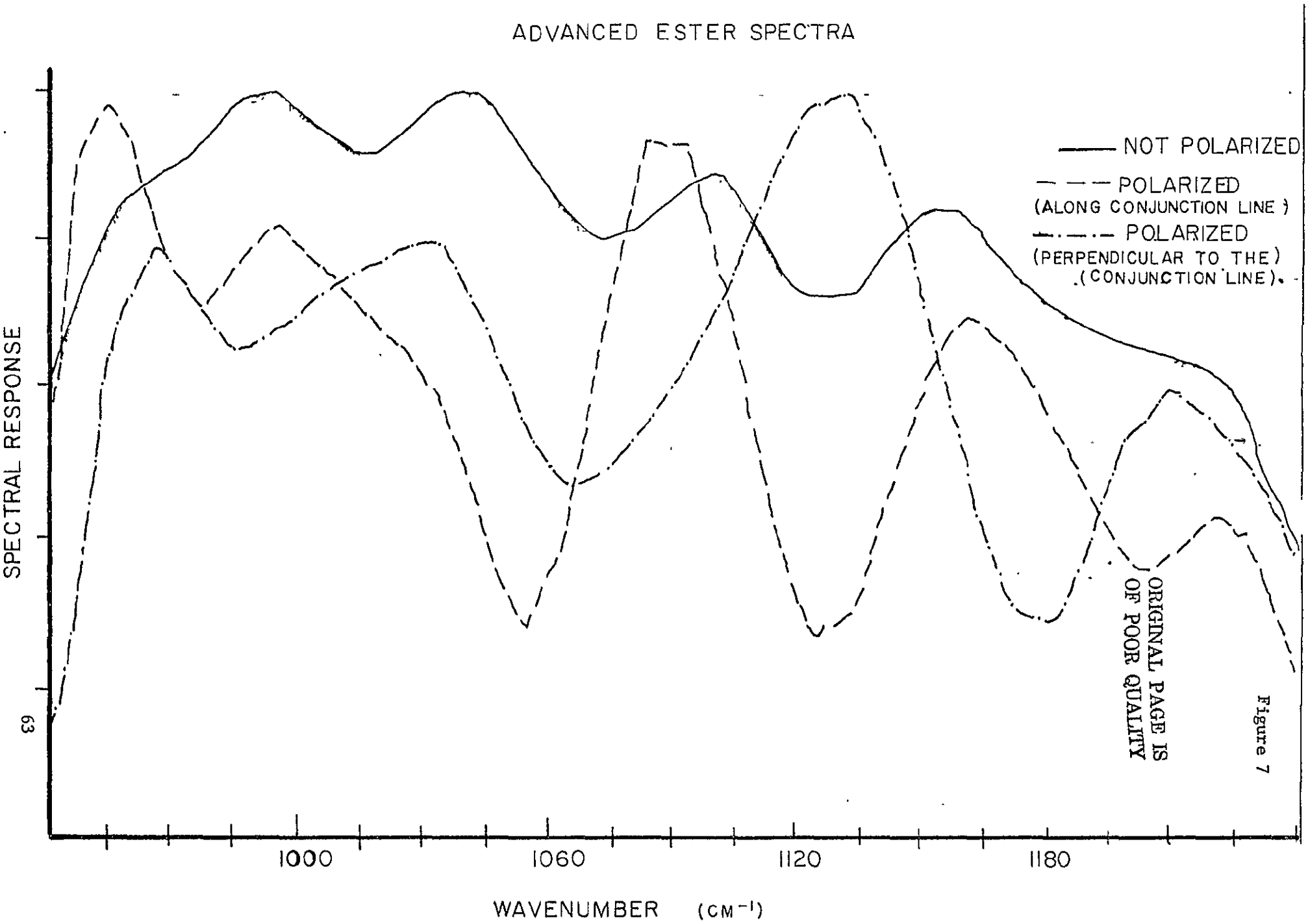

ORIGINAL PAGE IS OF POOR QUALITY

Figure 7

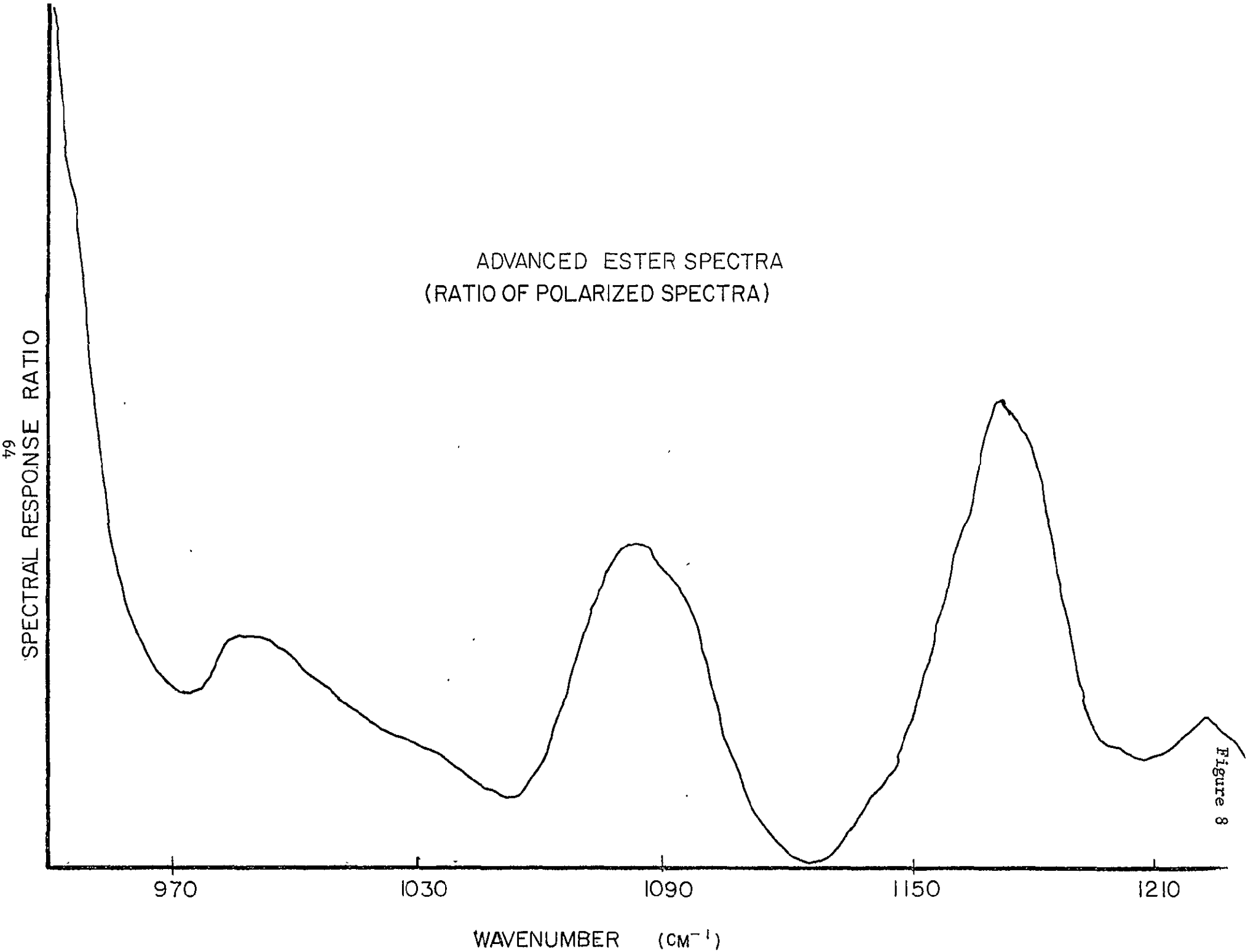
ADVANCED ESTER SPECTRA
(RATIO OF POLARIZED SPECTRA)
SPECTRAL RESPONSE RATIO
970
1030
1090
1150
1210
WAVENUMBER (CM⁻¹)

Figure 8

Figure 9

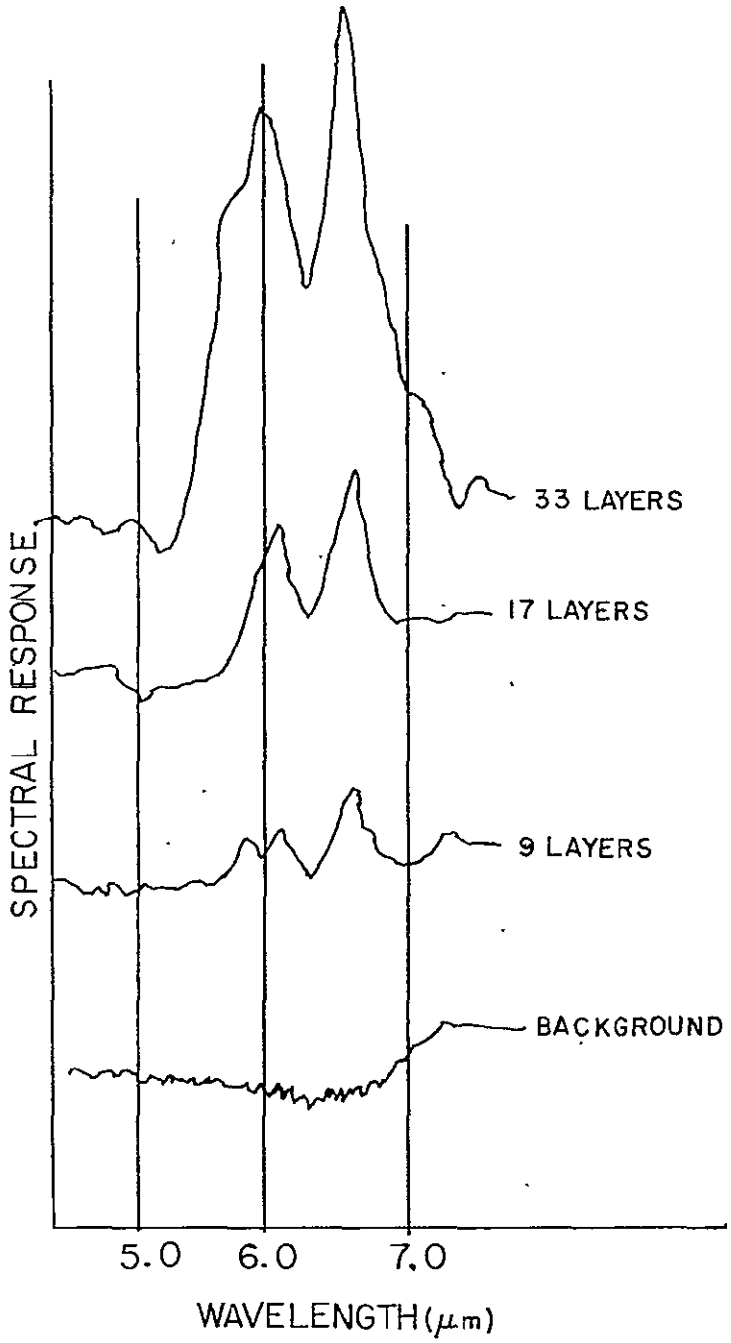
33 LAYERS
17 LAYERS
9 LAYERS
BACKGROUND
SPECTRAL RESPONSE
5.0
6.0
7.0
WAVELENGTH (μm)

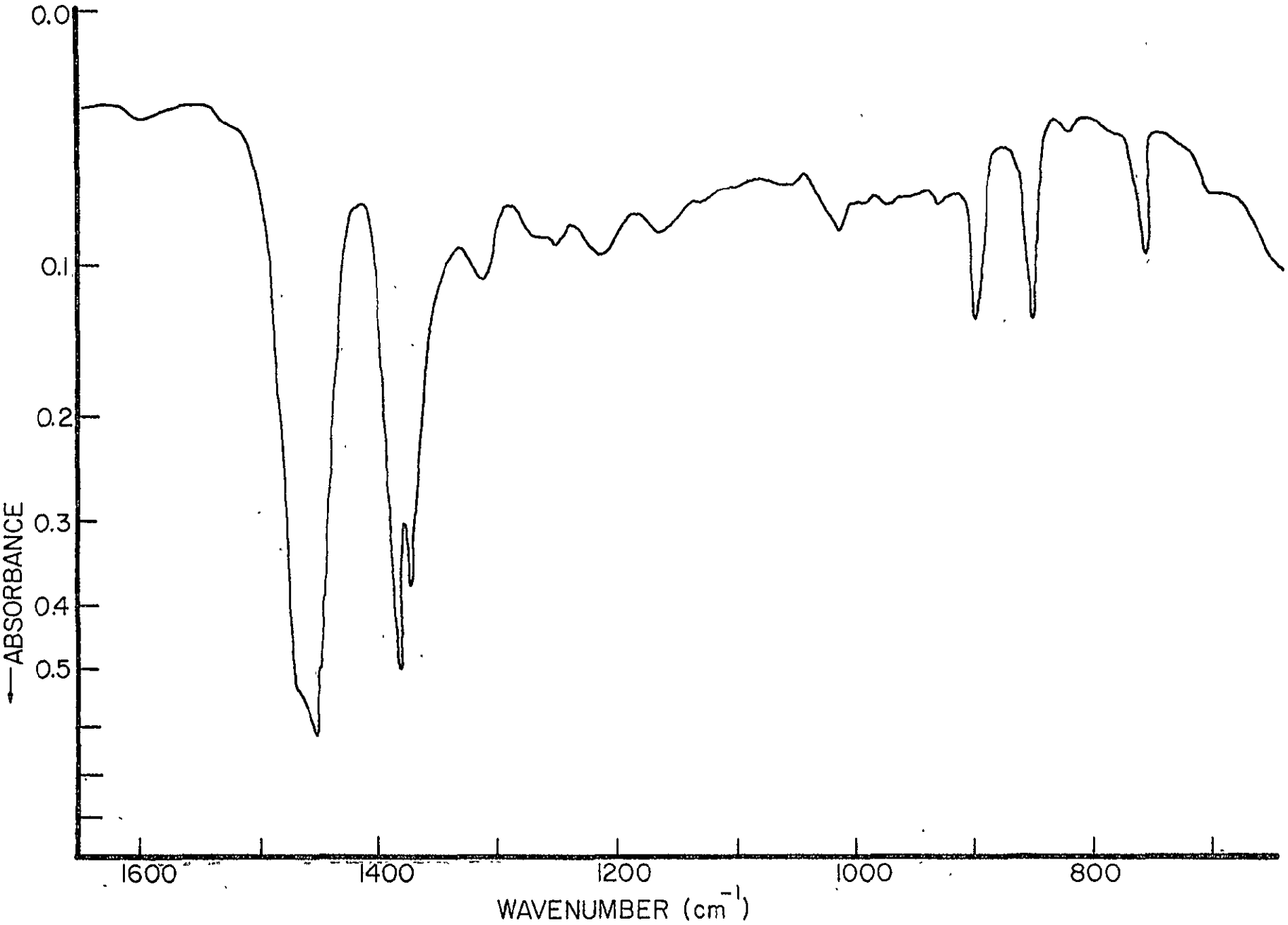
0.0
0.1
0.2
0.3
0.4
0.5
ABSORBANCE
1600
1400
1200
1000
800
WAVENUMBER (cm⁻¹)

Figure 10

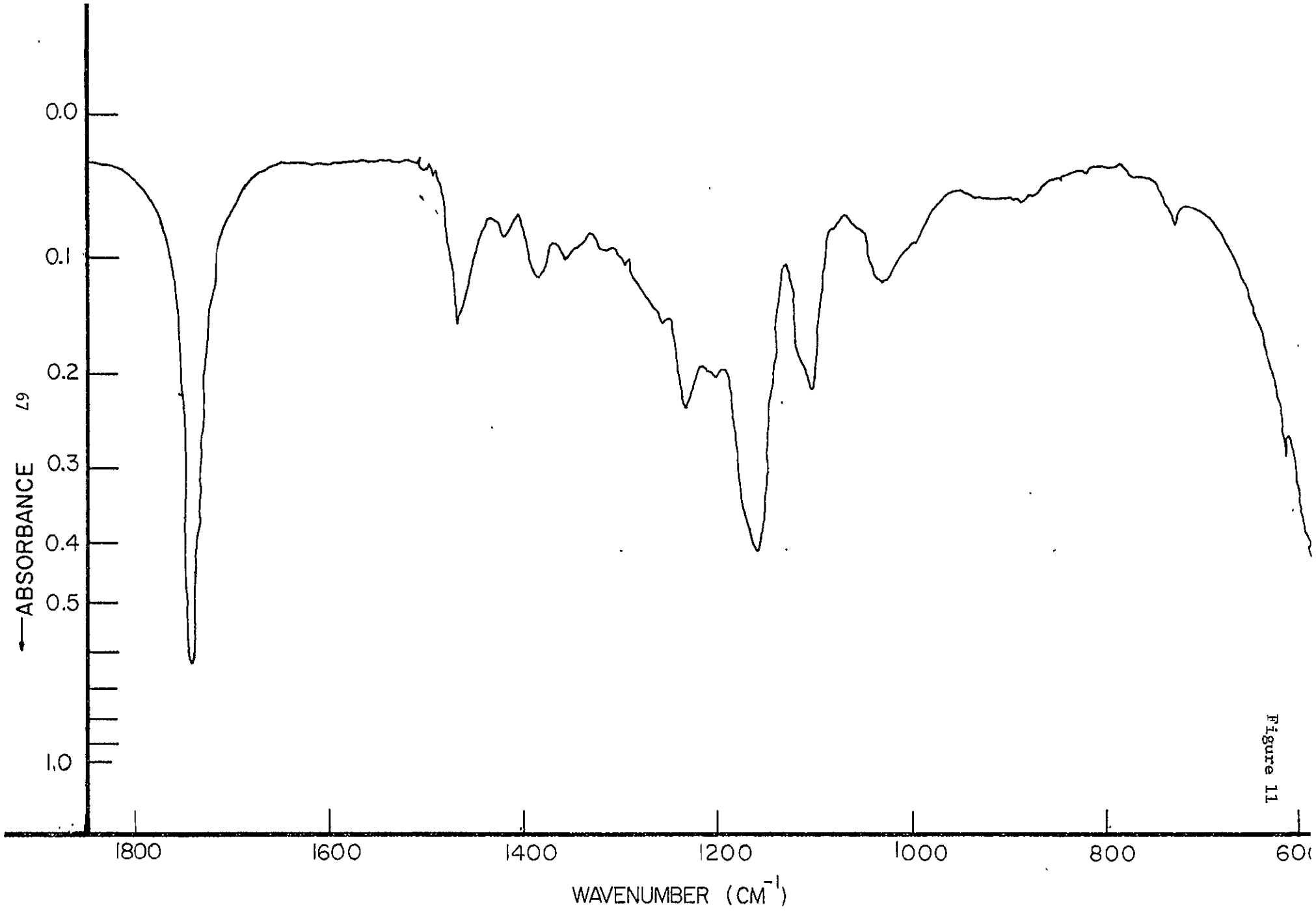
0.0
0.1
0.2
0.3
0.4
0.5
1.0
ABSORBANCE
1800
1600
1400
1200
1000
800
WAVENUMBER (CM⁻¹)

Figure 11

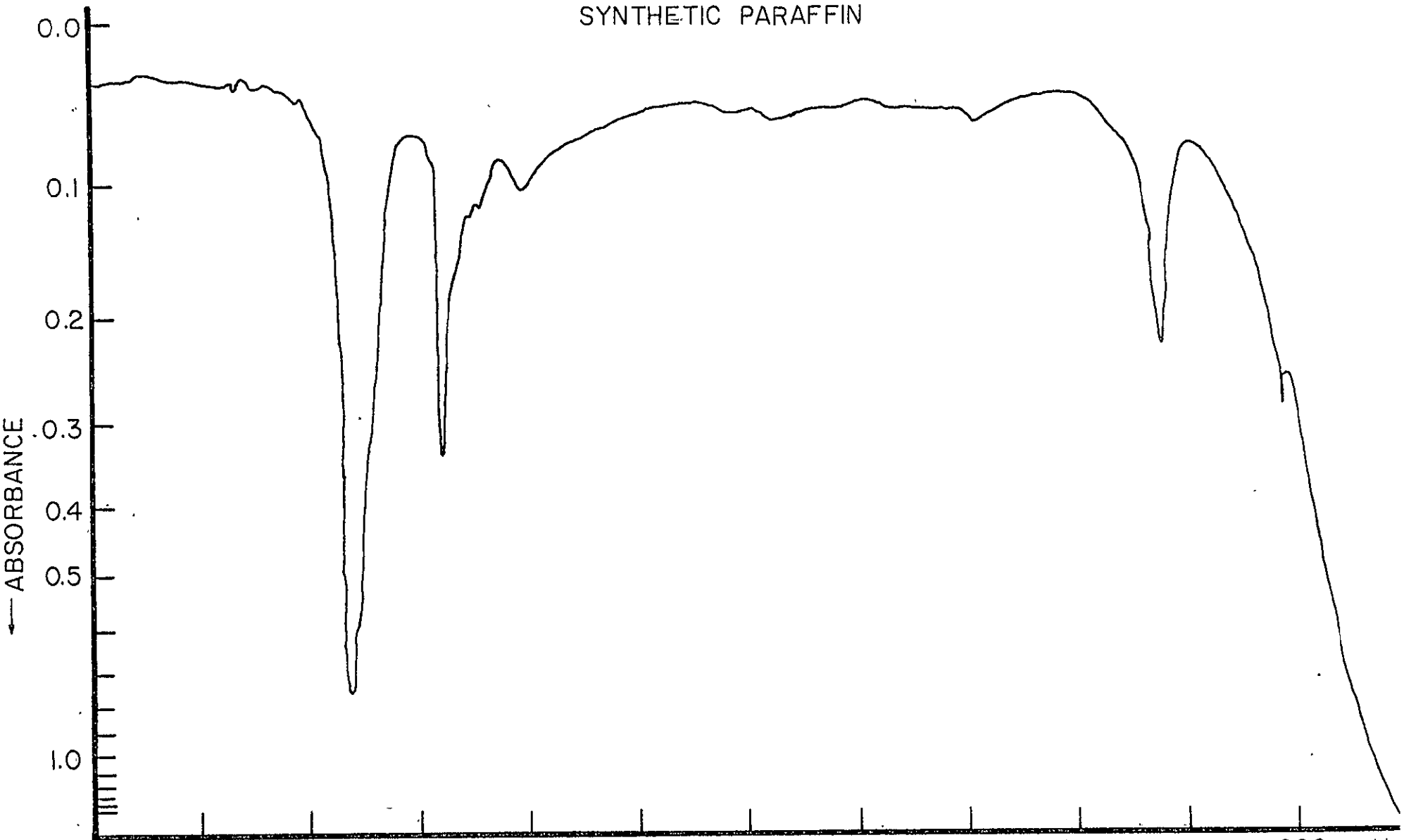
SYNTHETIC PARAFFIN
0.0
0.1
0.2
0.3
0.4
0.5
1.0
← ABSORBANCE
1600
1400
1200
1000
800
600
WAVENUMBER (cm⁻¹)

Figure 12

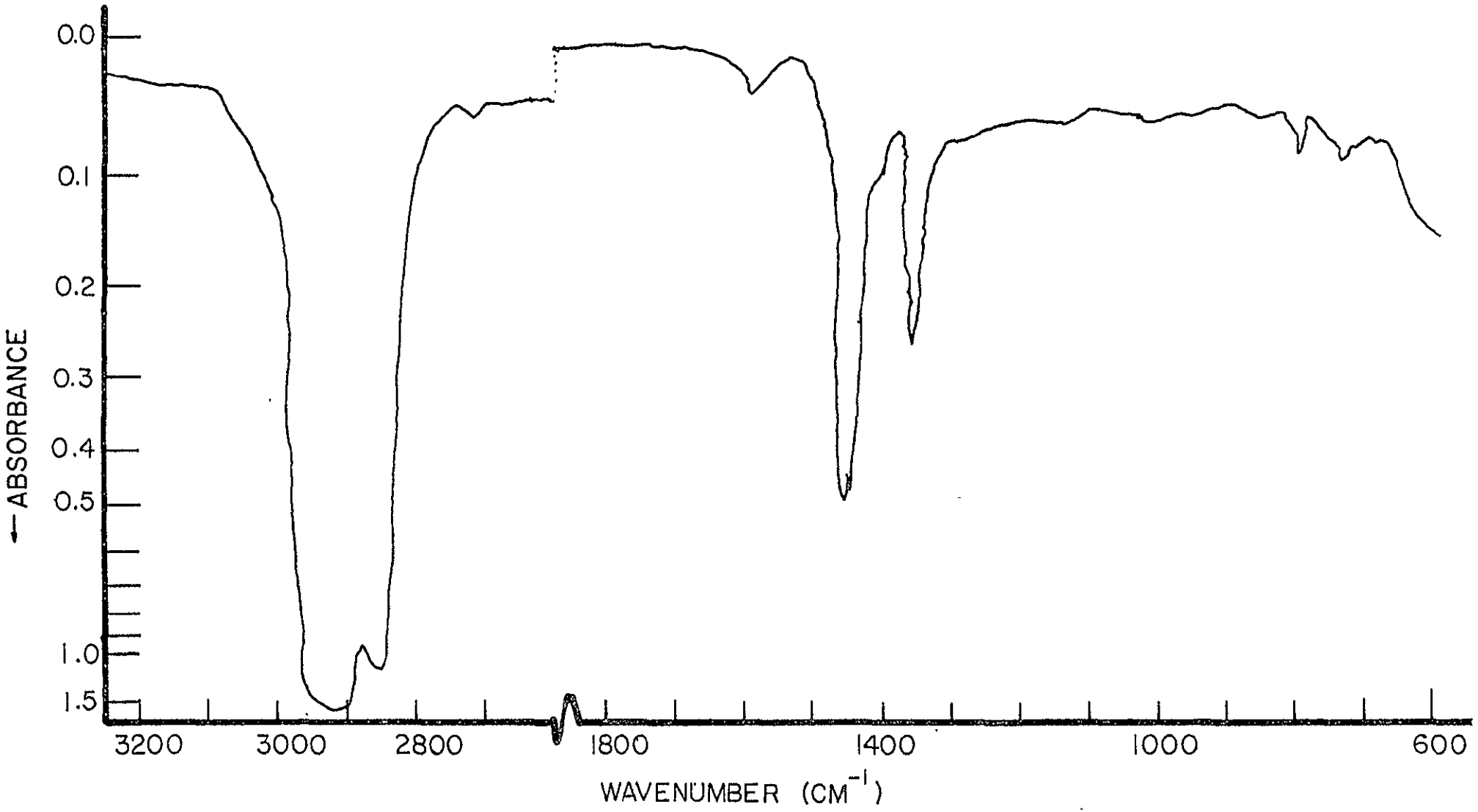
0.0
0.1
0.2
0.3
0.4
0.5
1.0
1.5
← ABSORBANCE
3200
3000
2800
1800
1400
1000
600
WAVENUMBER (CM⁻¹)

Figure 13

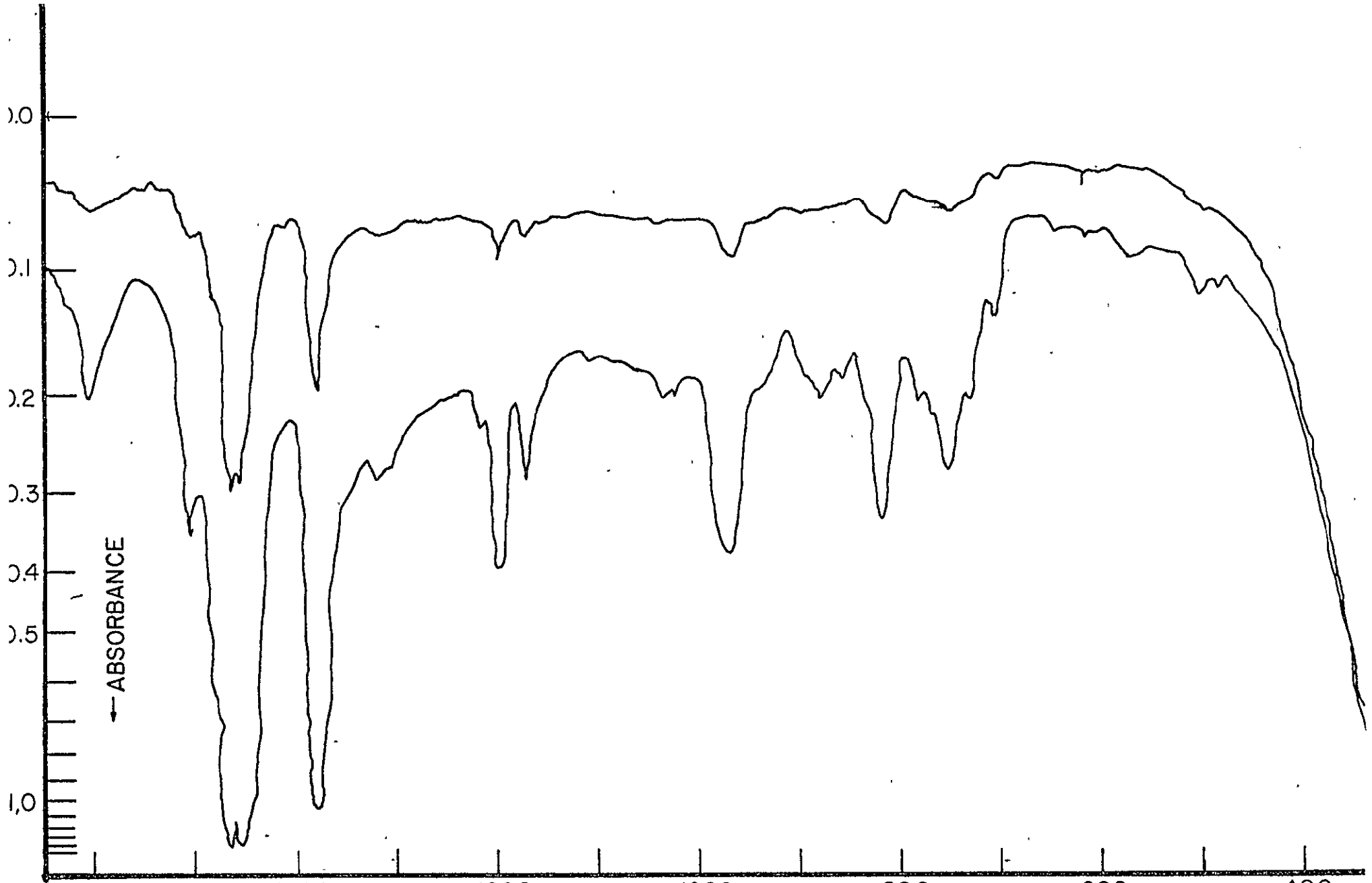
0.0
0.1
0.2
0.3
0.4
0.5
1.0
ABSORBANCE
1600
1400
1200
1000
800
600
400
WAVENUMBER (CM^{-1})

Figure 14

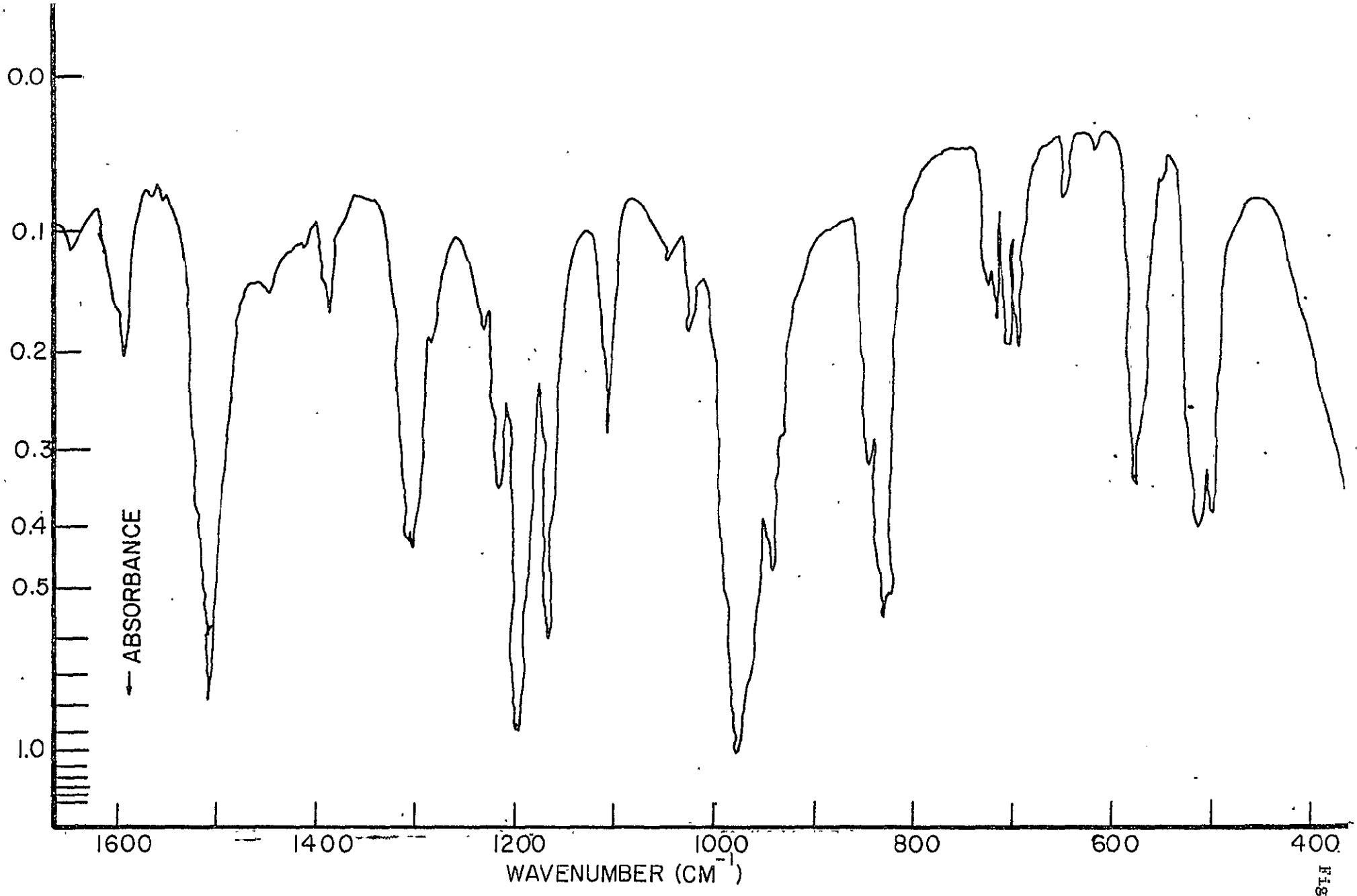
0.0
0.1
0.2
0.3
0.4
0.5
1.0
ABSORBANCE
1600
1400
1200
1000
800
600
400
WAVENUMBER (CM⁻¹)

Figure 15

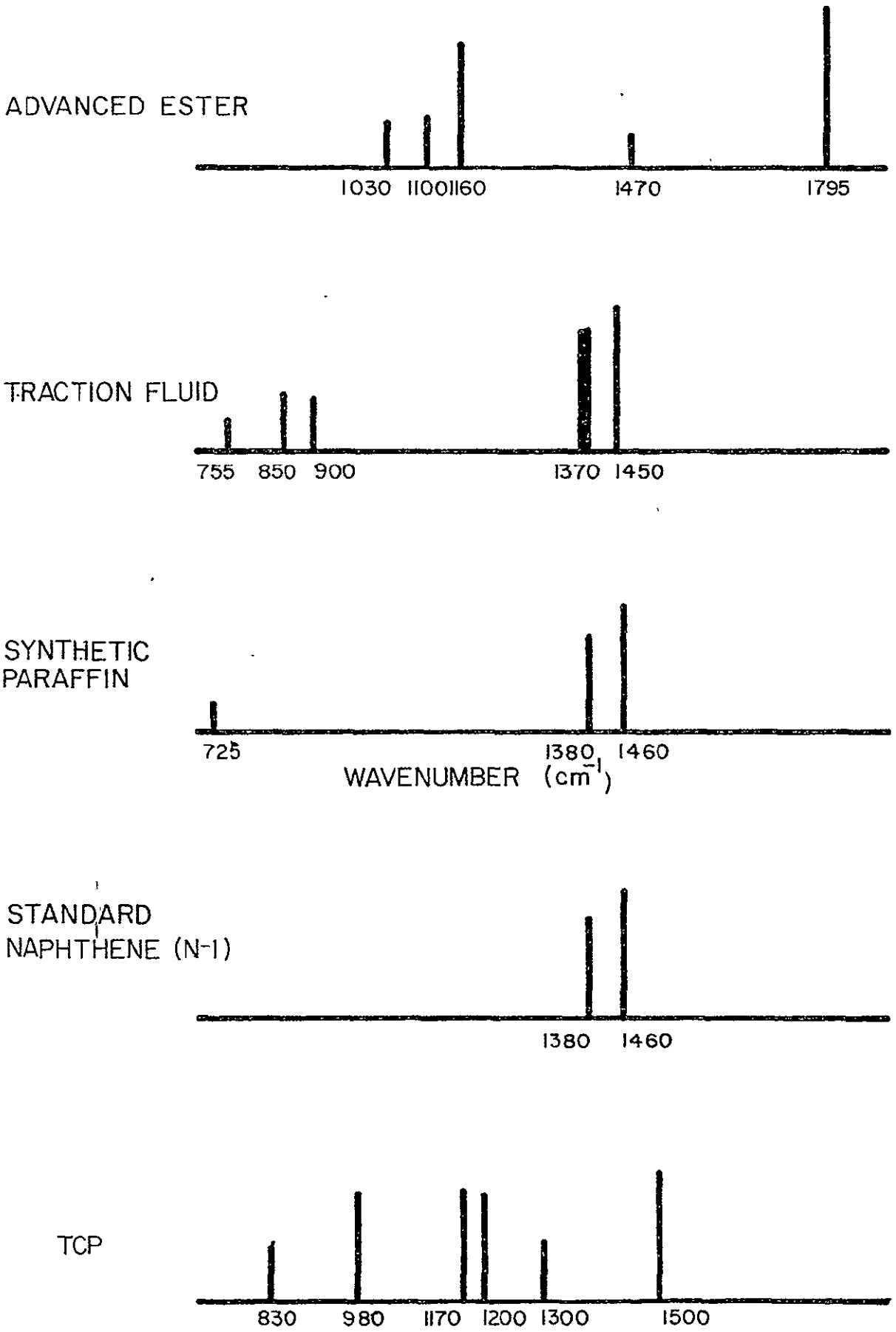

Figure 17

Figure 18

ORIGINAL PAGE IS
OF POOR QUALITY

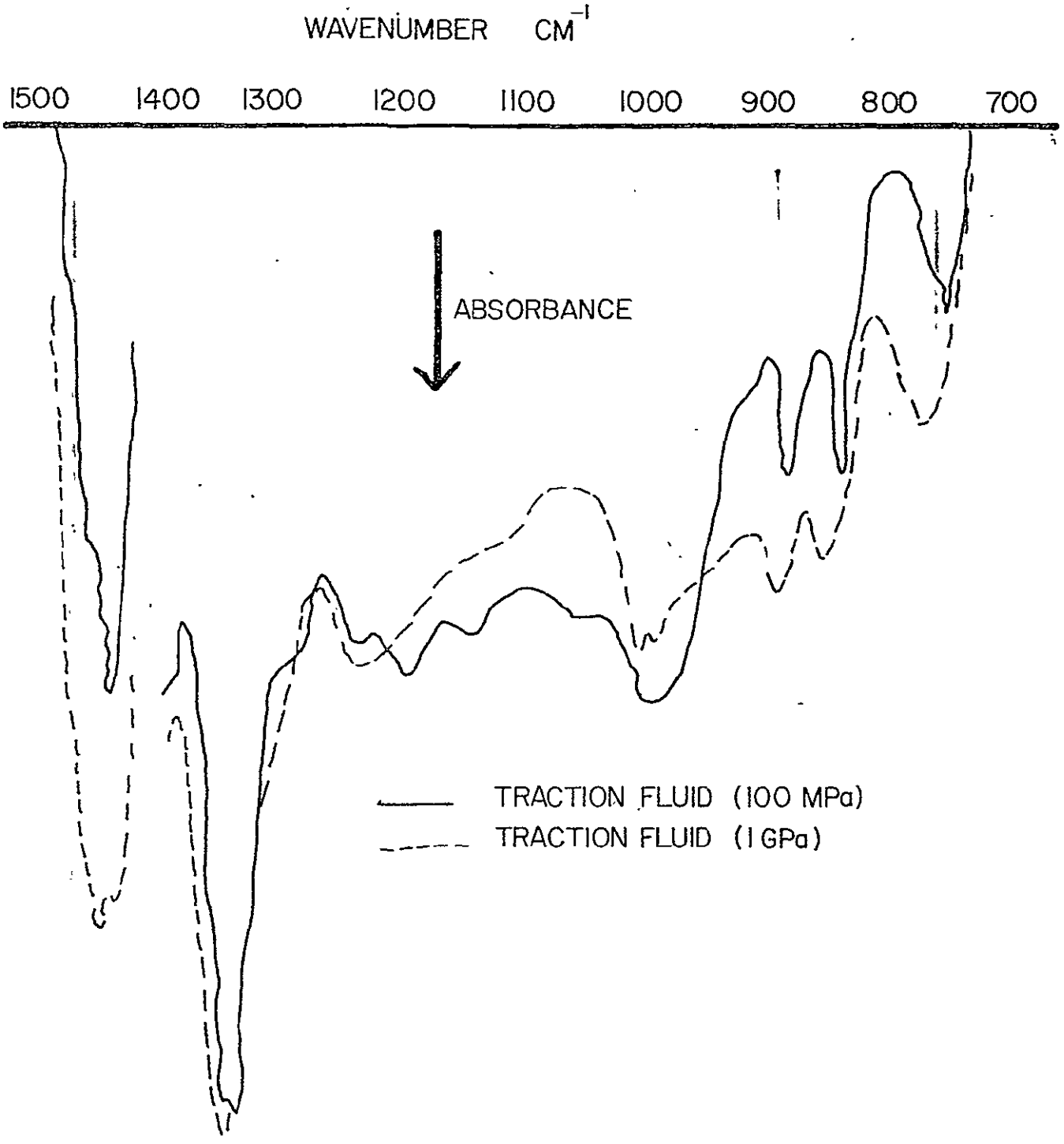

Figure 19

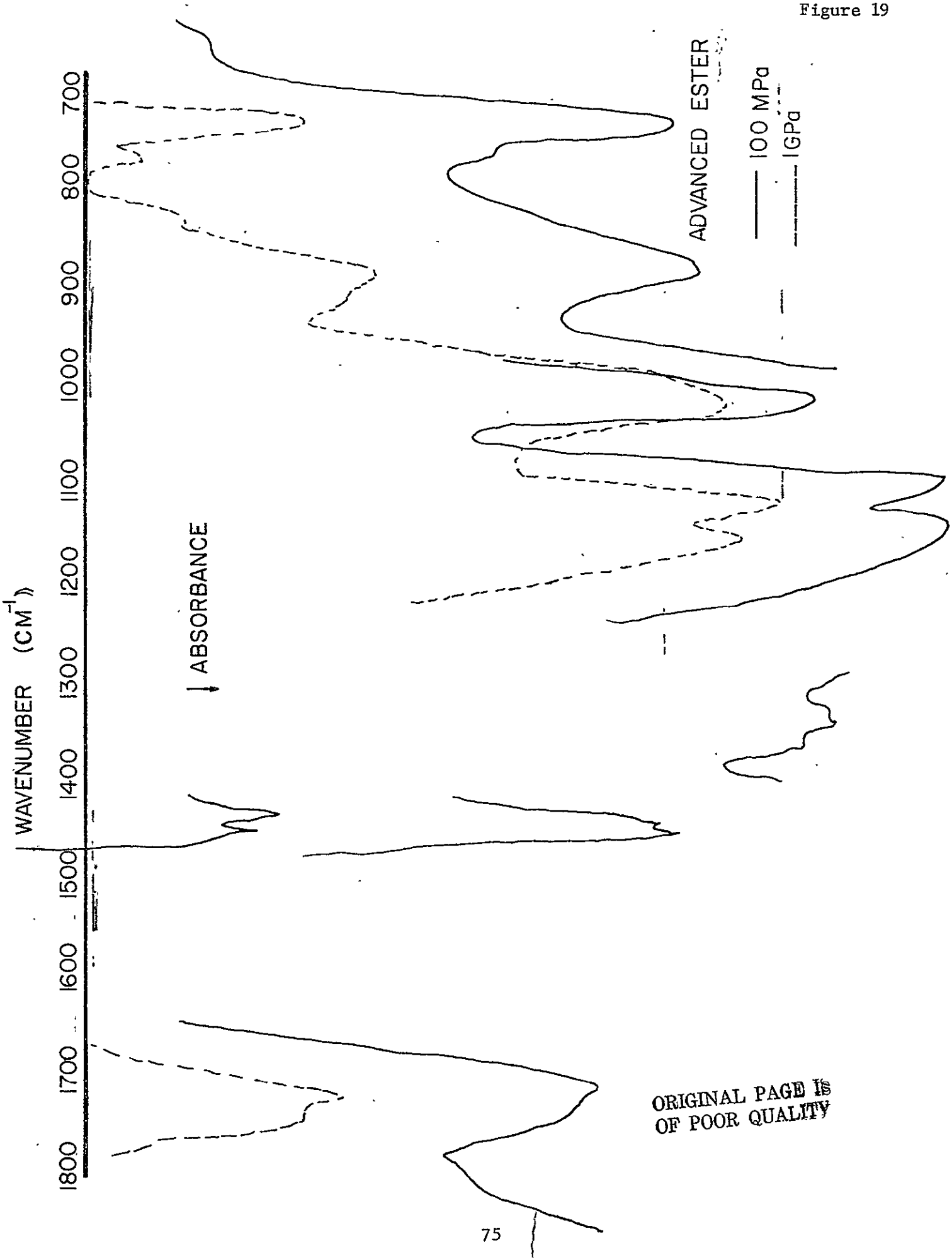

Figure 20

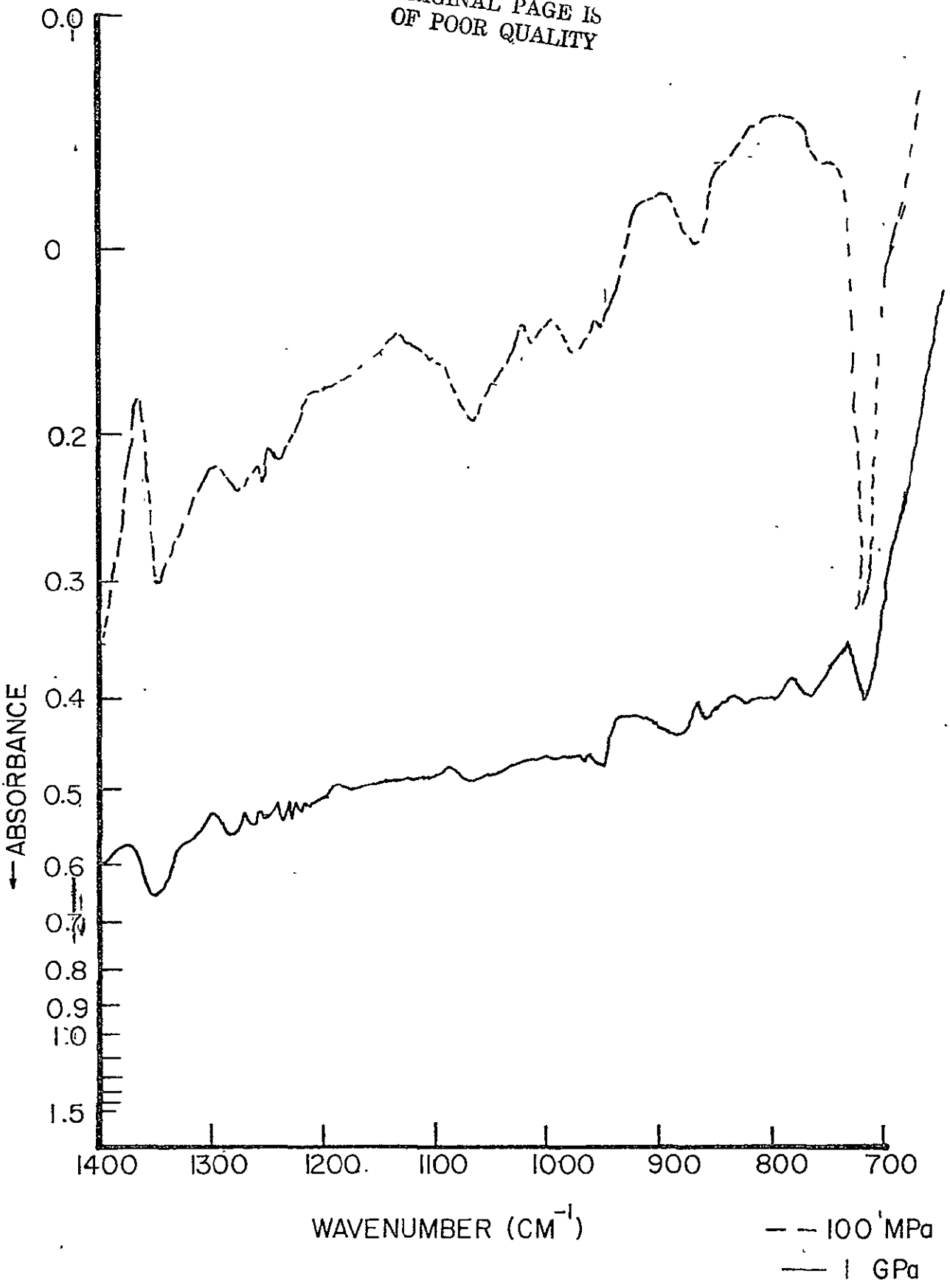

Figure 21

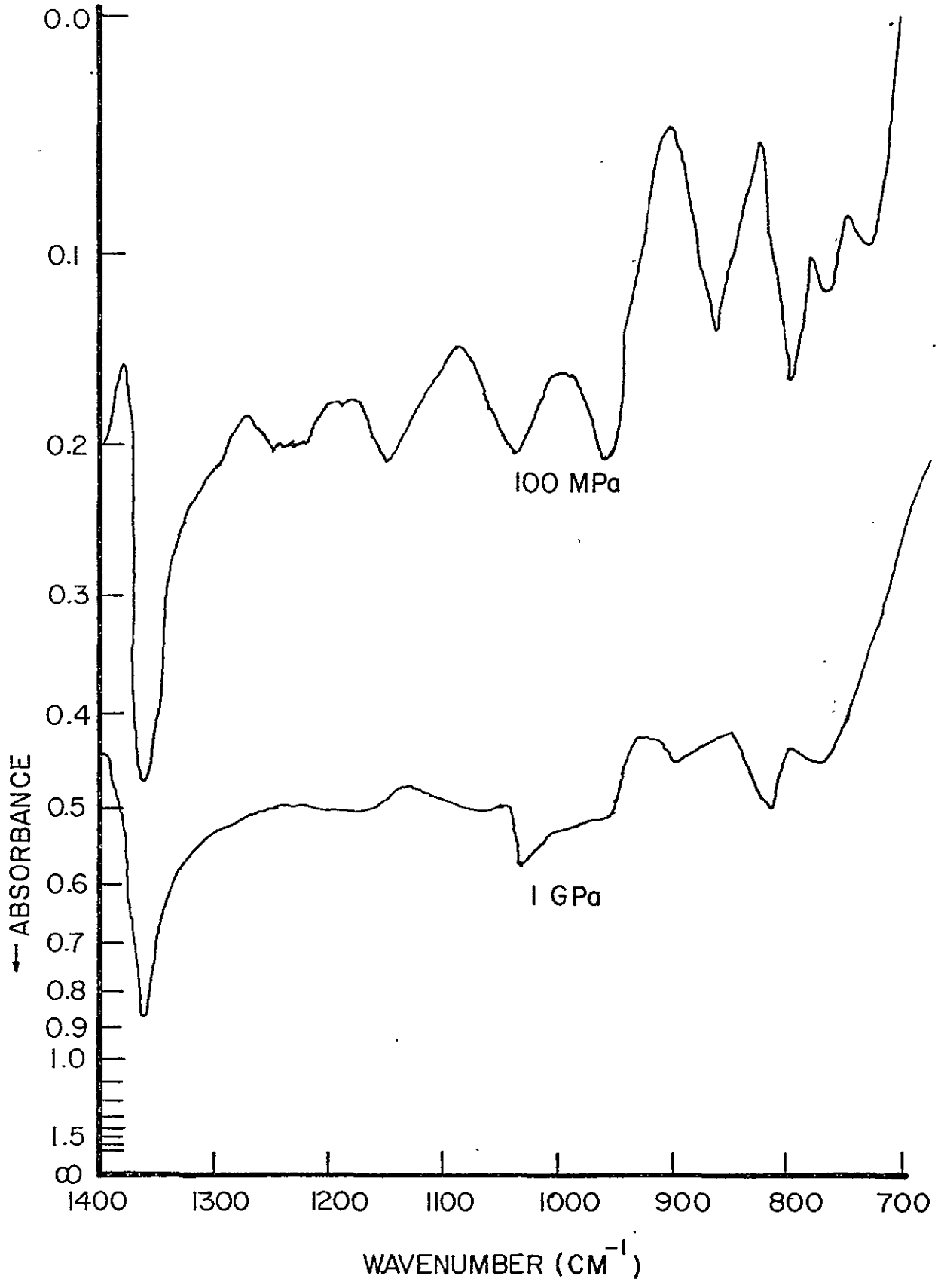
0.0
0.1
0.2
0.3
0.4
0.5
0.6
0.7
0.8
0.9
1.0
1.5
∞
ABSORBANCE
100 MPa
1 GPa
1400
1300
1200
1100
1000
900
800
700
WAVENUMBER (CM⁻¹)

Figure 22

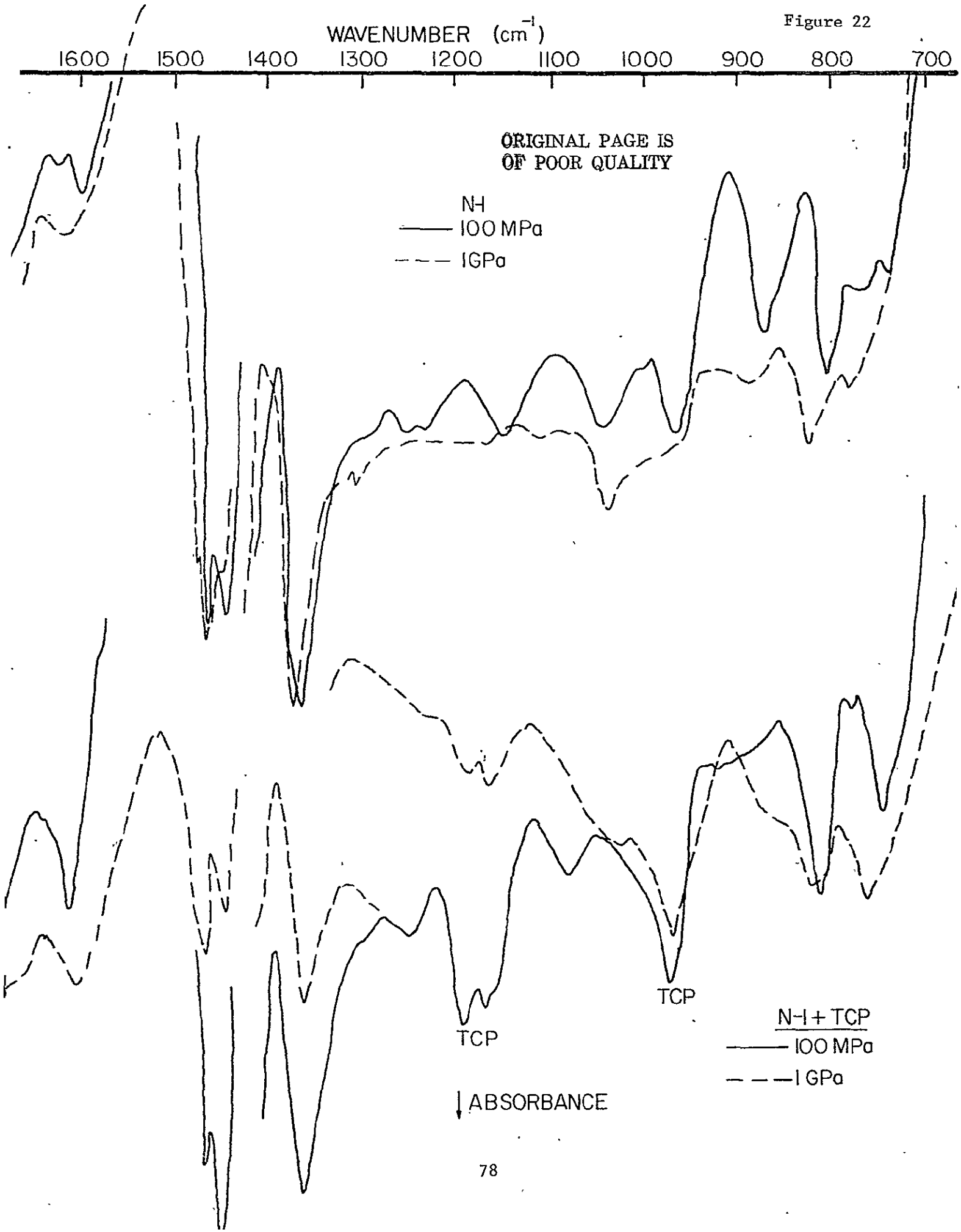
WAVENUMBER (cm⁻¹)
1600
1500
1400
1300
1200
1100
1000
900
800
700
ORIGINAL PAGE IS
OF POOR QUALITY
NH
100 MPa
1GPa
TCP
TCP
N-H + TCP
100 MPa
1 GPa
ABSORBANCE

Figure 23

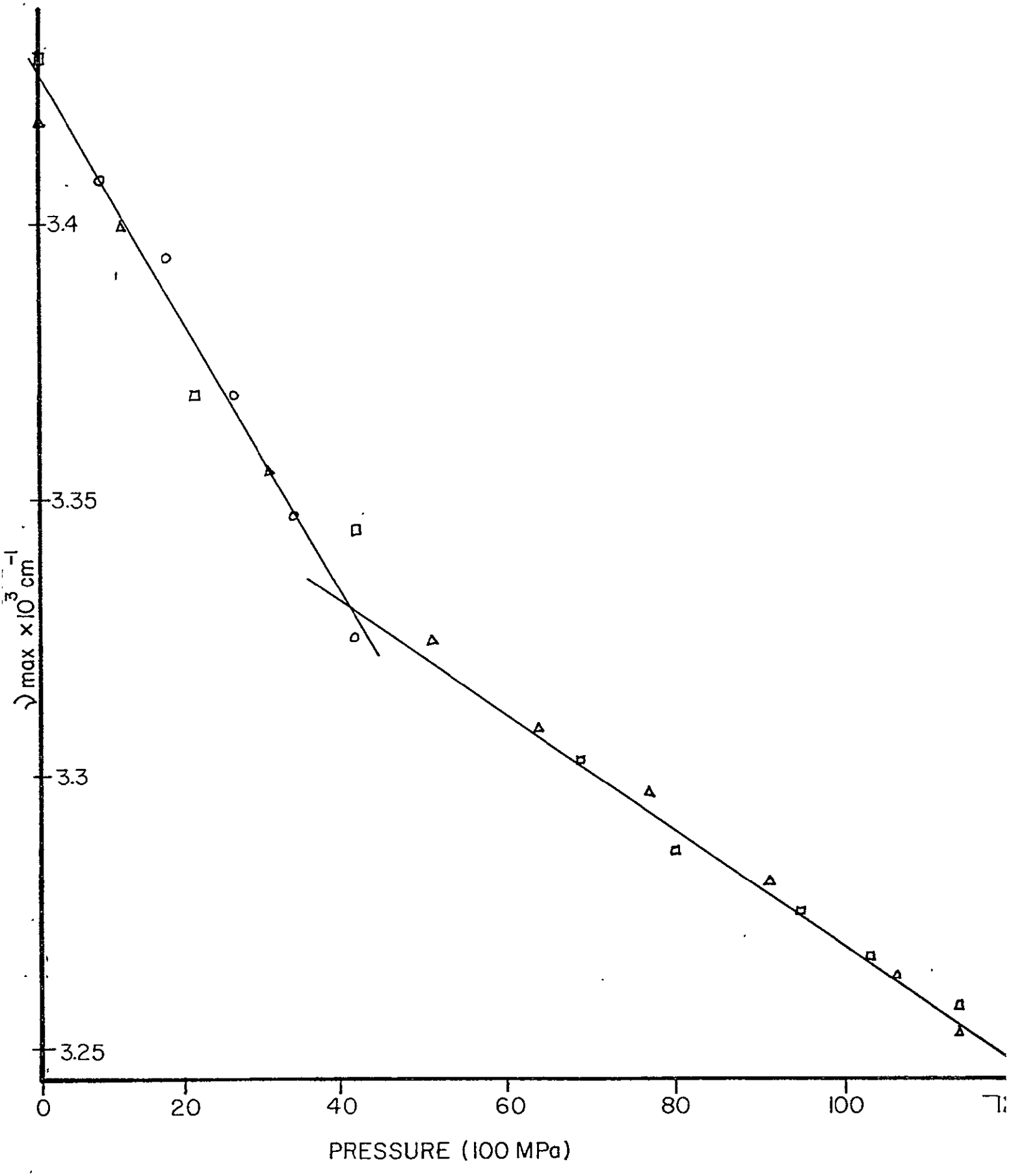
3.4
3.35
3.3
3.25
ν max $\times 10^3$ cm^{-1}
0
20
40
60
80
100
PRESSURE (100 MPa)

Figure 24

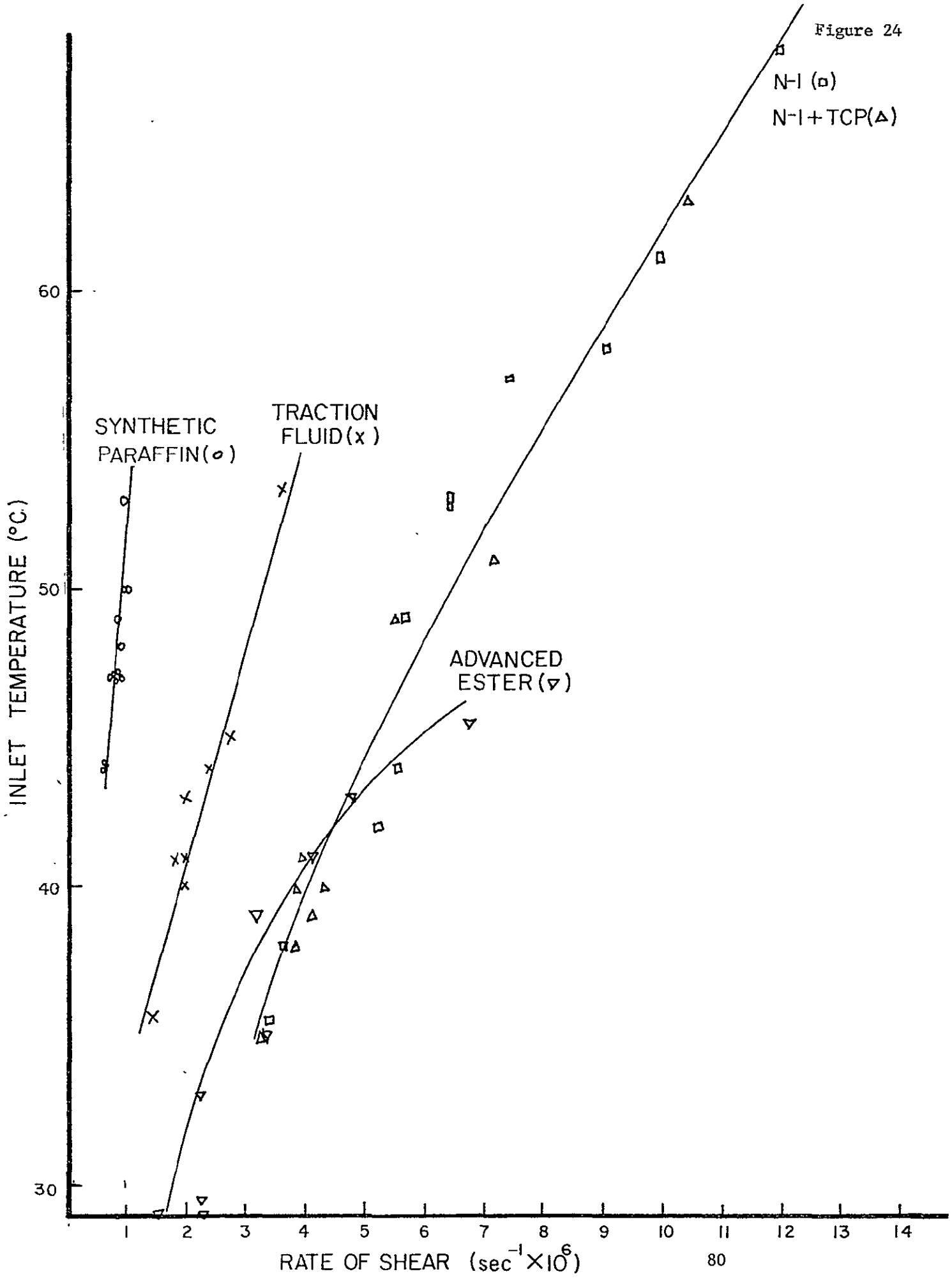
N-I (□)
N-I+TCP(△)
SYNTHETIC PARAFFIN(○)
TRACTION FLUID(×)
ADVANCED ESTER(▽)
INLET TEMPERATURE (°C.)
60
50
40
30
1
2
3
4
5
6
7
8
9
10
11
12
13
14
RATE OF SHEAR (sec^{-1} × 10^{6})

Figure 25

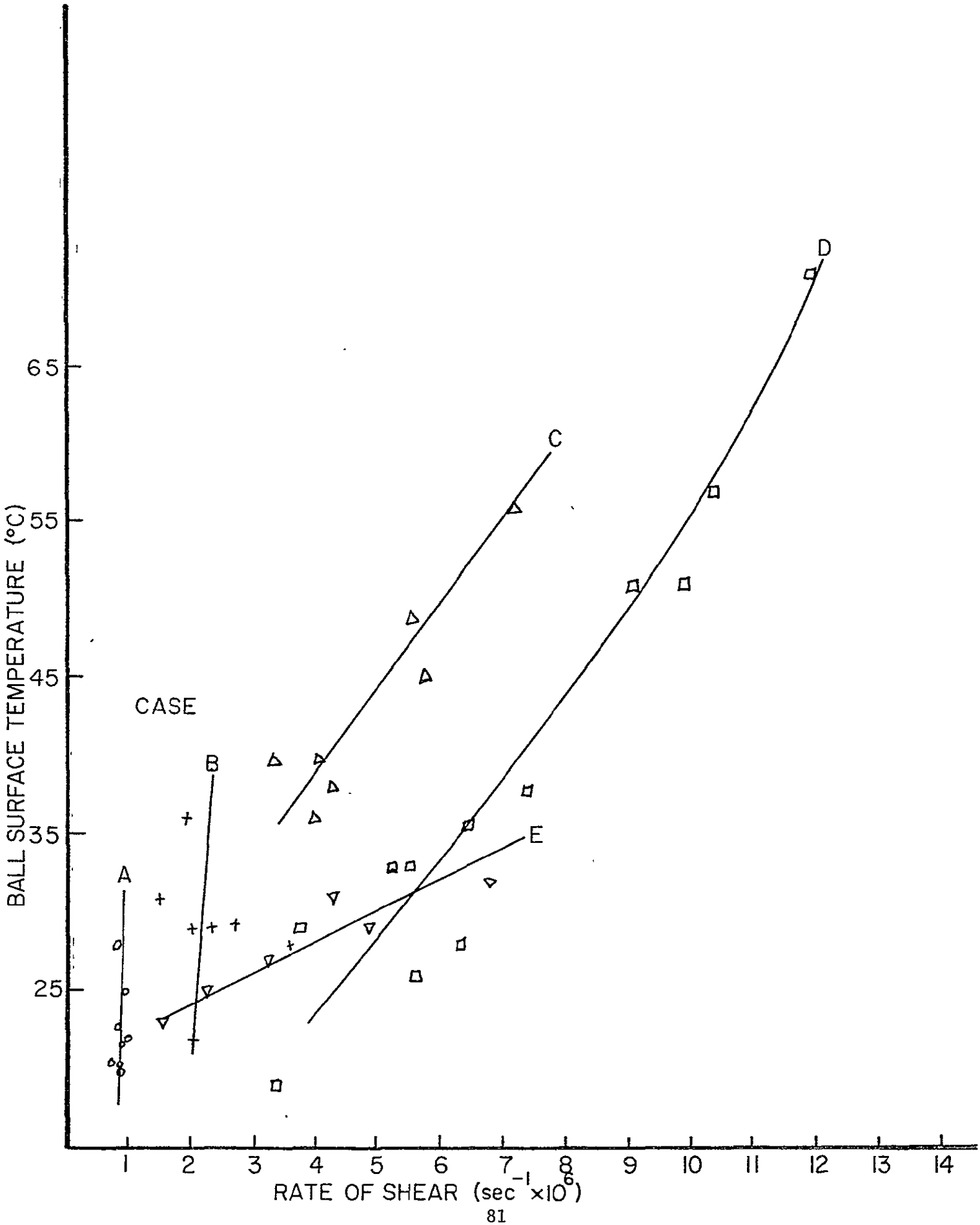
BALL SURFACE TEMPERATURE (°C)
65
55
45
35
25
CASE
A
B
C
D
E
1
2
3
4
5
6
7
8
9
10
11
12
13
14
RATE OF SHEAR (sec⁻¹ ×10⁶)

Figure 26

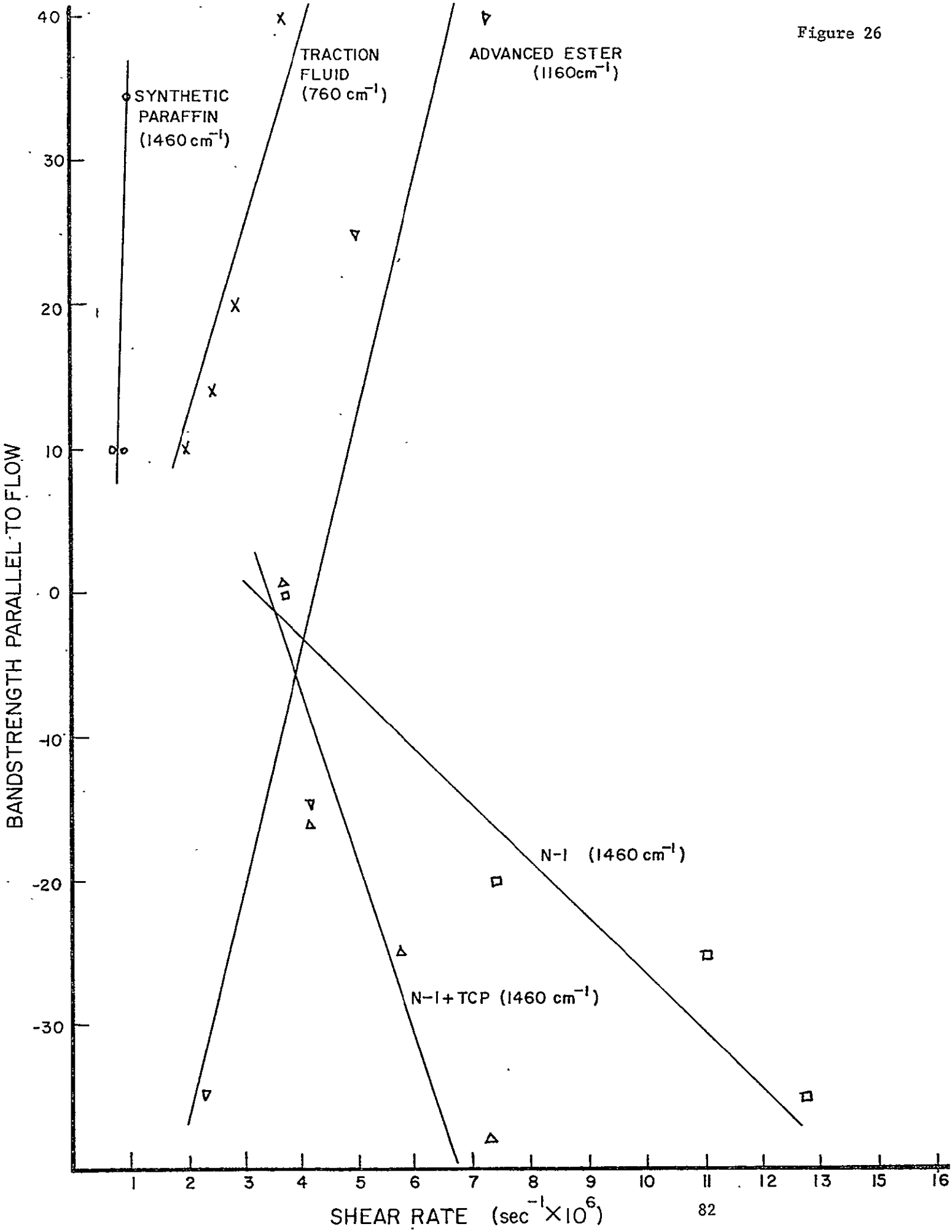
SYNTHETIC PARAFFIN (1460 cm⁻¹)
TRACTION FLUID (760 cm⁻¹)
ADVANCED ESTER (1160cm⁻¹)
N-1 (1460 cm⁻¹)
N-1+TCP (1460 cm⁻¹)
BANDSTRENGTH PARALLEL TO FLOW
SHEAR RATE (sec⁻¹ × 10⁶)
40
30
20
10
0
-10
-20
-30
1
2
3
4
5
6
7
8
9
10
11
12
13
15
16

Figure 27

TRACTION FLUID

15°C BATH TEMPERATURE
108 N LOAD
.72 meters/sec

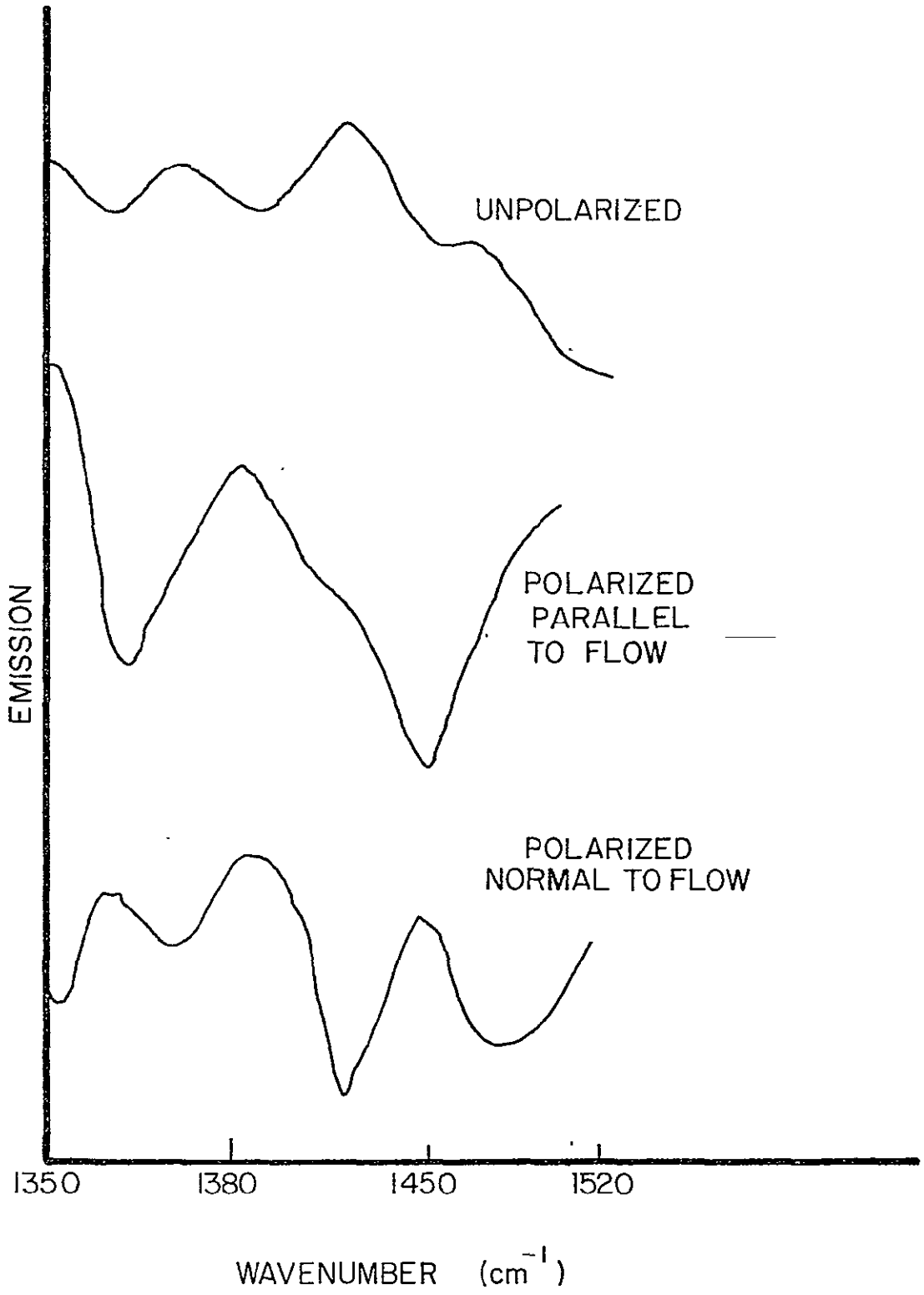

Figure 28

TRACTION FLUIDS

15 °C BATH TEMPERATURE
216 N LOAD .72 meters/sec

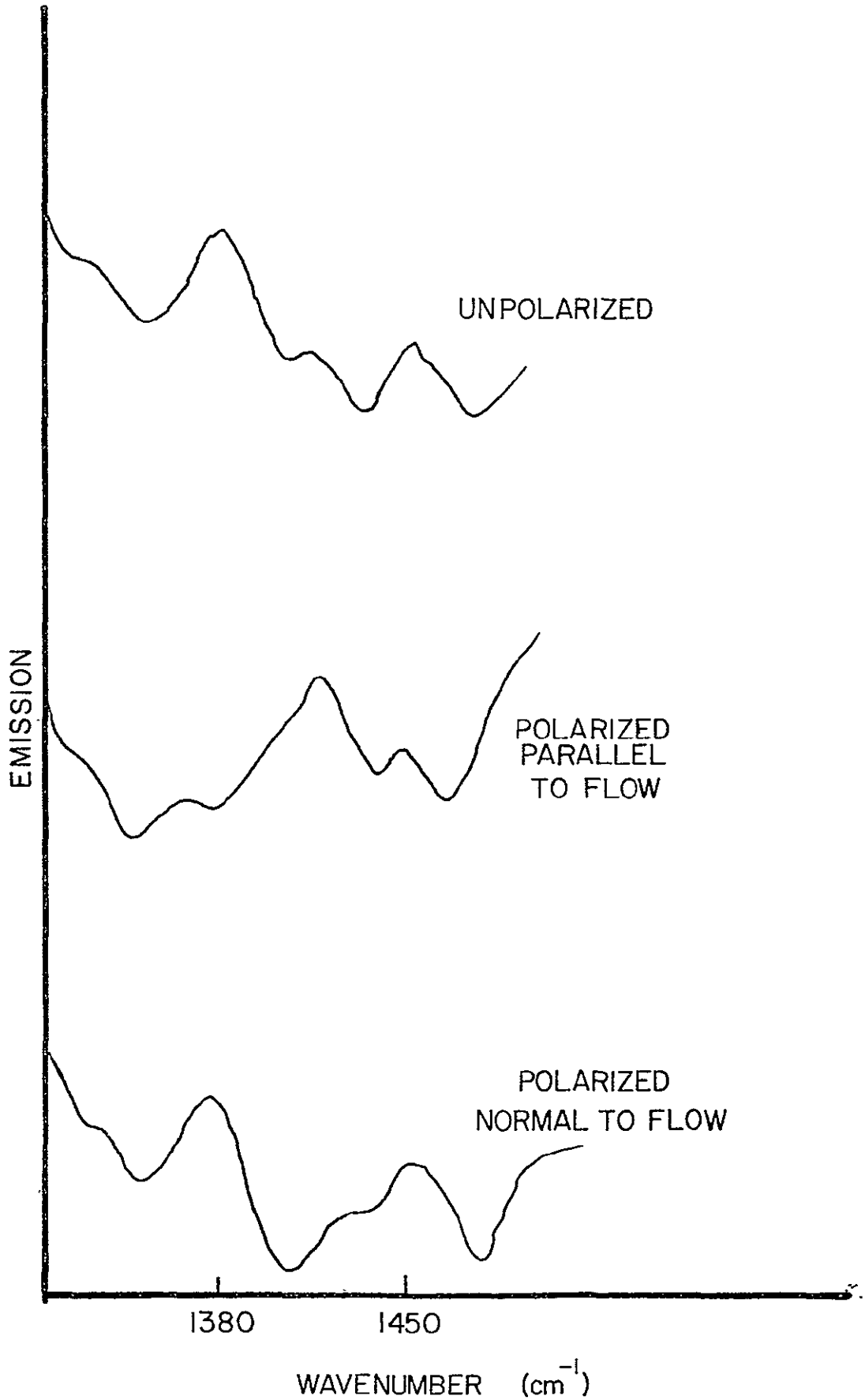

Figure 29

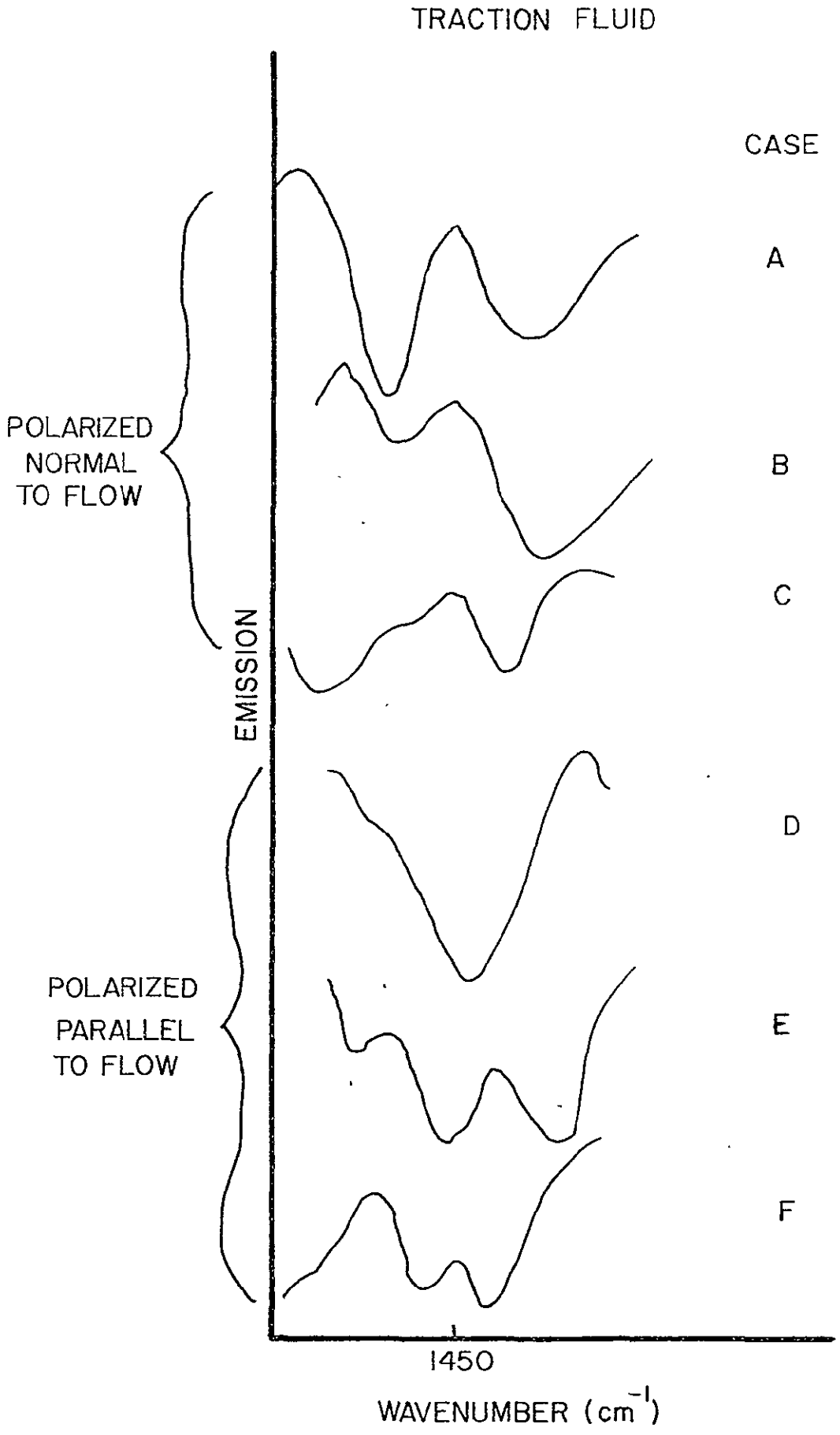
TRACTION FLUID
CASE
A
B
C
D
E
F
POLARIZED
NORMAL
TO FLOW
POLARIZED
PARALLEL
TO FLOW
EMISSION
1450
WAVENUMBER (cm⁻¹)

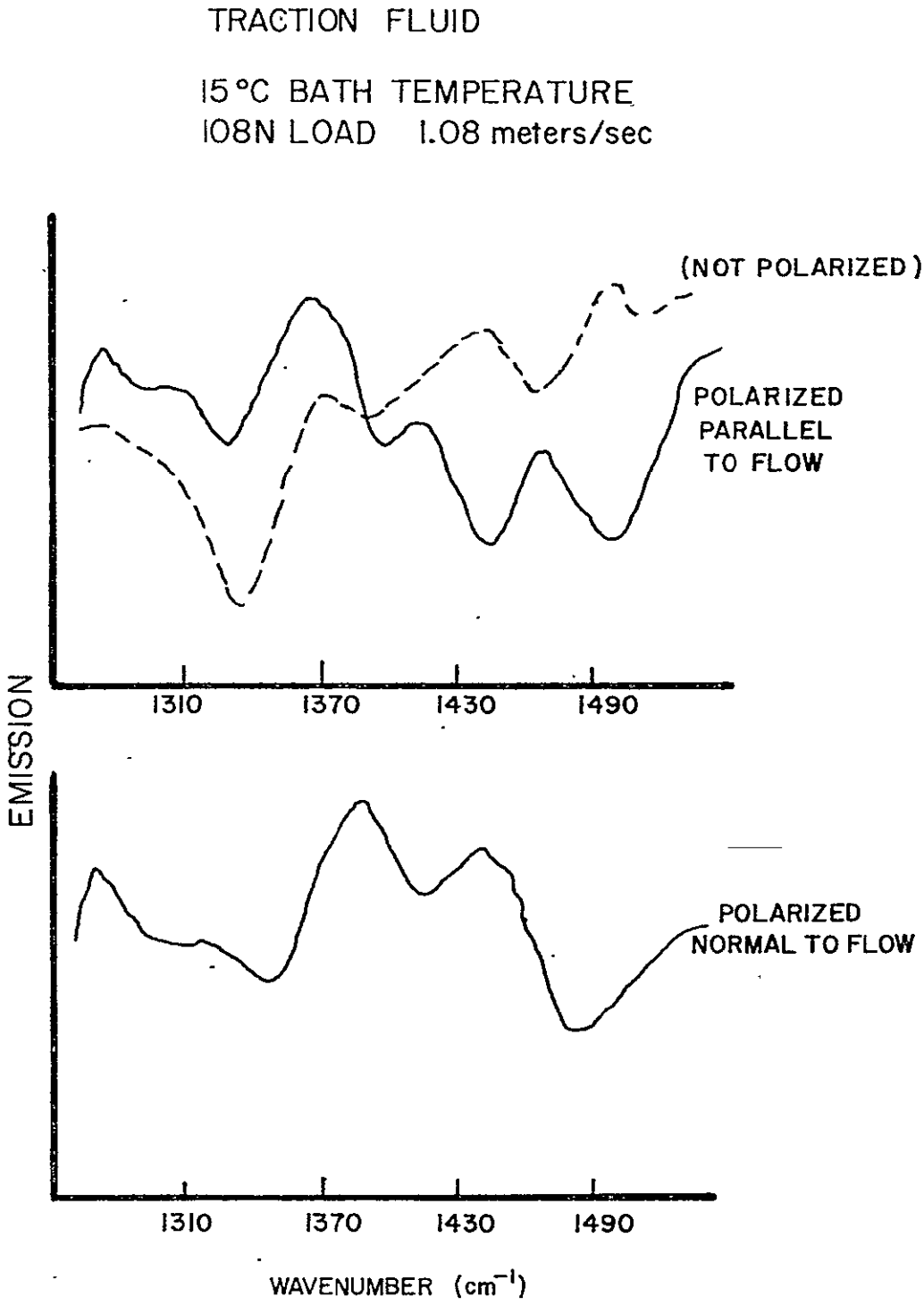
TRACTION FLUID
15°C BATH TEMPERATURE
108N LOAD 1.08 meters/sec
(NOT POLARIZED)
POLARIZED
PARALLEL
TO FLOW
1310
1370
1430
1490
EMISSION
POLARIZED
NORMAL TO FLOW
1310
1370
1430
1490
WAVENUMBER (cm⁻¹)

Figure 31

PETH

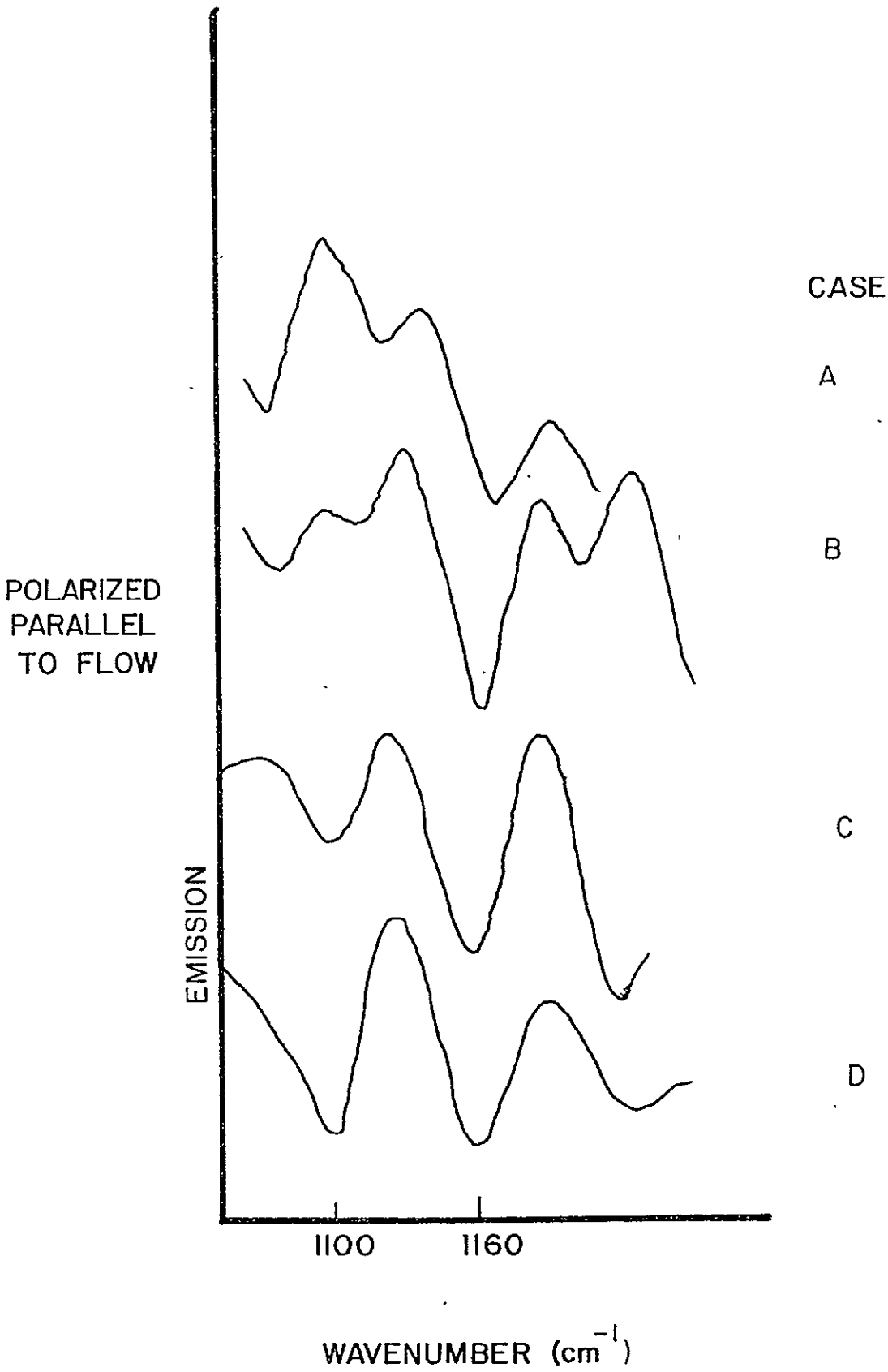

Figure 32

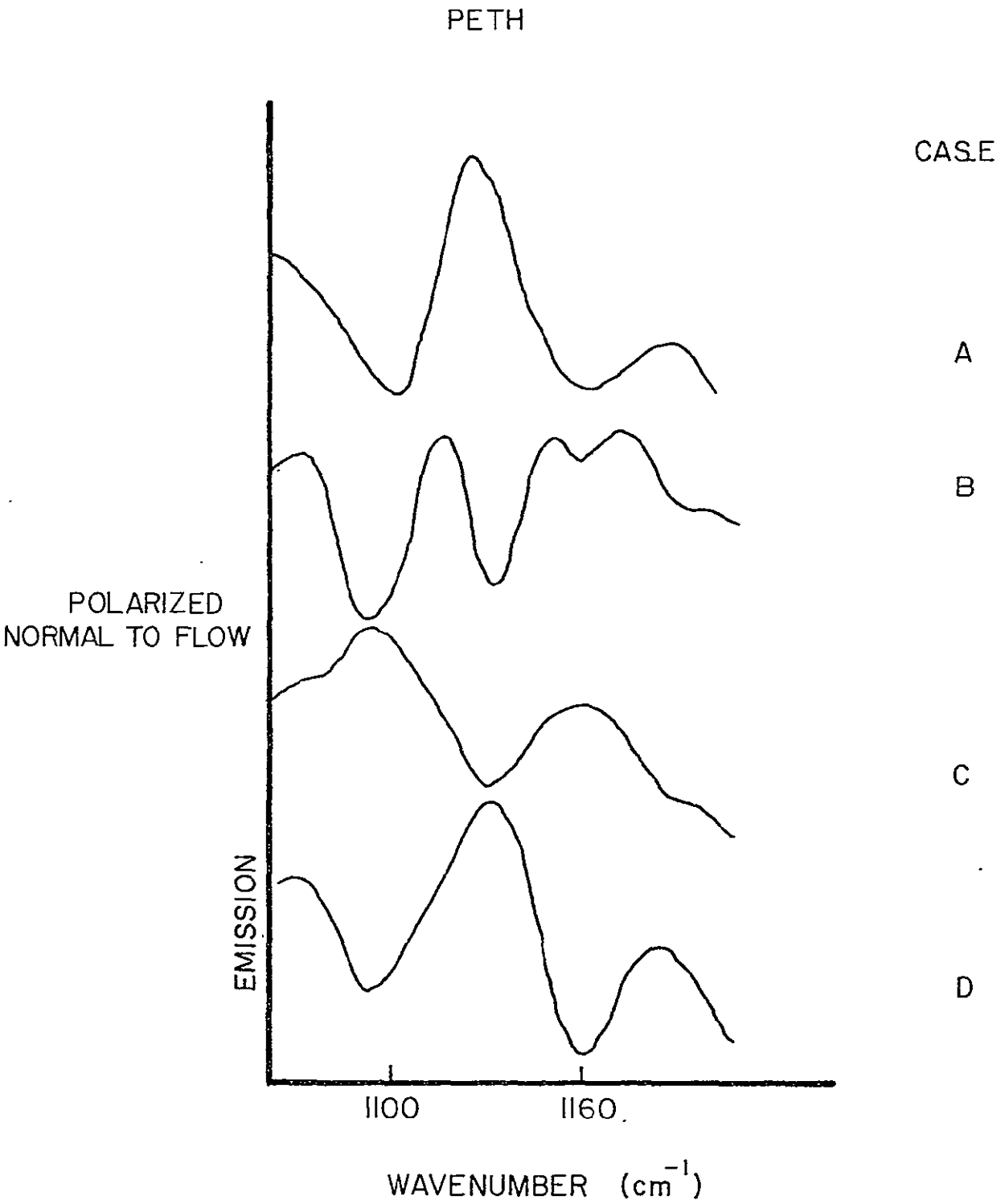
PETH
CASE
A
B
C
D
POLARIZED
NORMAL TO FLOW
EMISSION
1100
1160
WAVENUMBER (cm⁻¹)

Figure 33

PETH

15 °C BATH 216 N LOAD

.72 meters/sec 2v REFERENCE

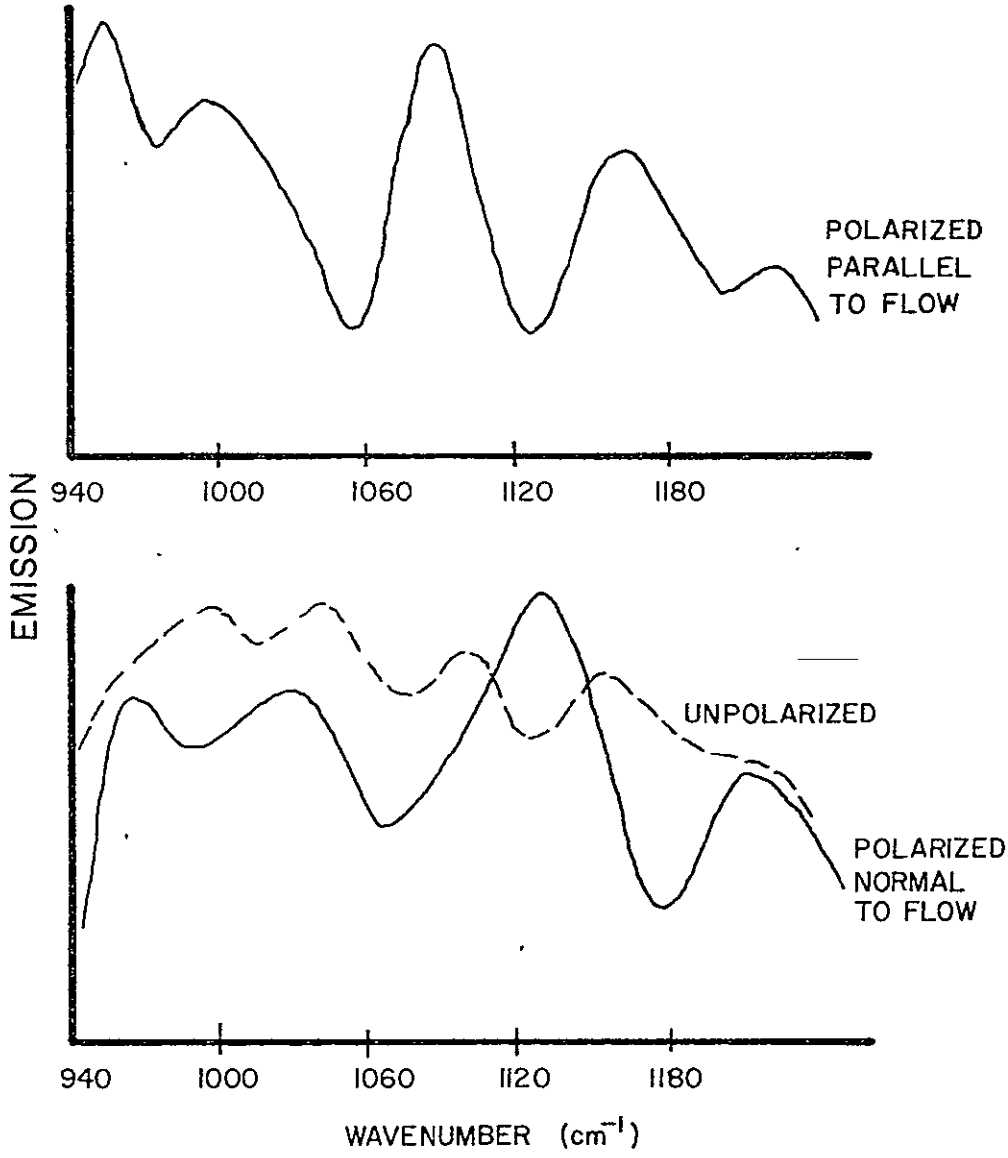

C-2

Figure 34

PETH

25 °C BATH 216 N LOAD

1.08 meters/sec 2v REFERENCE

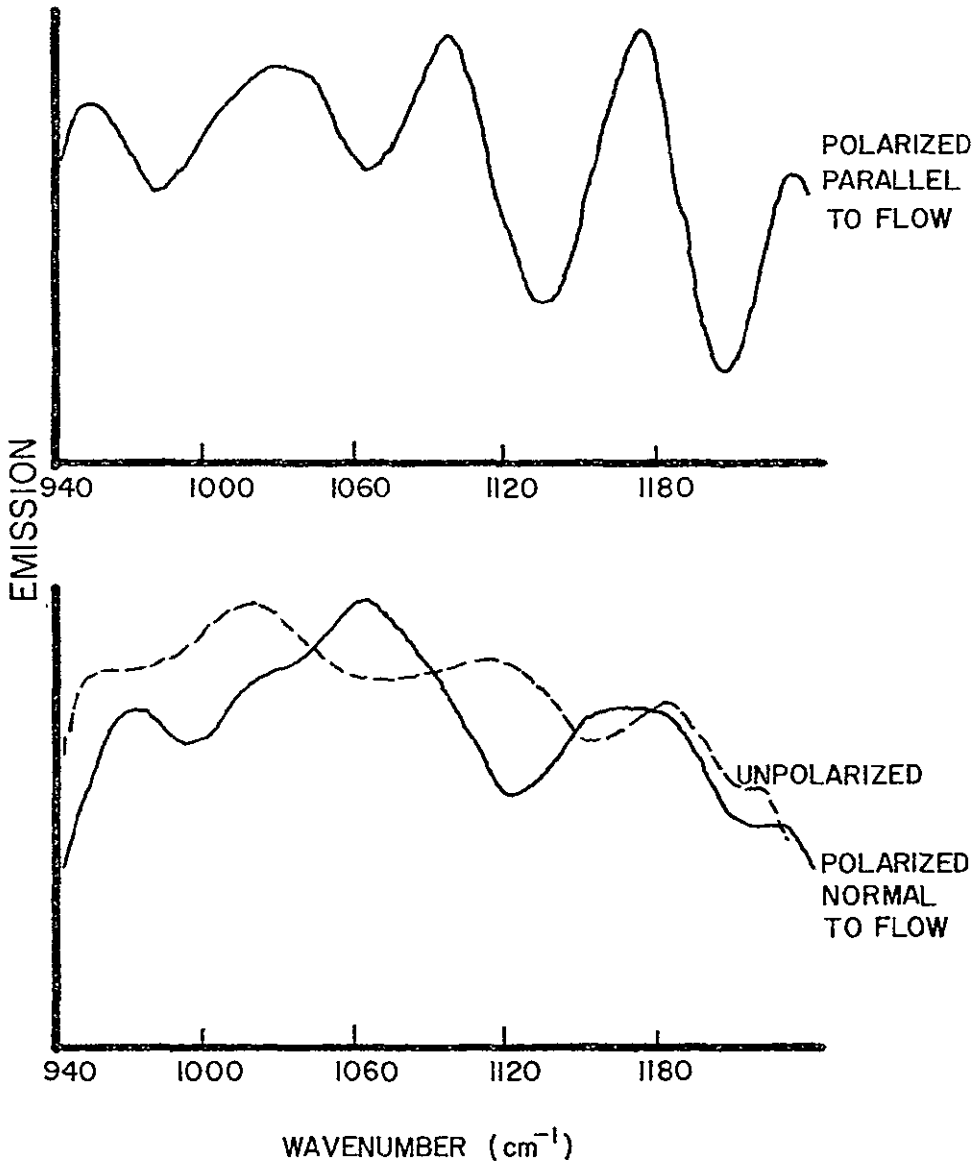

Figure 35

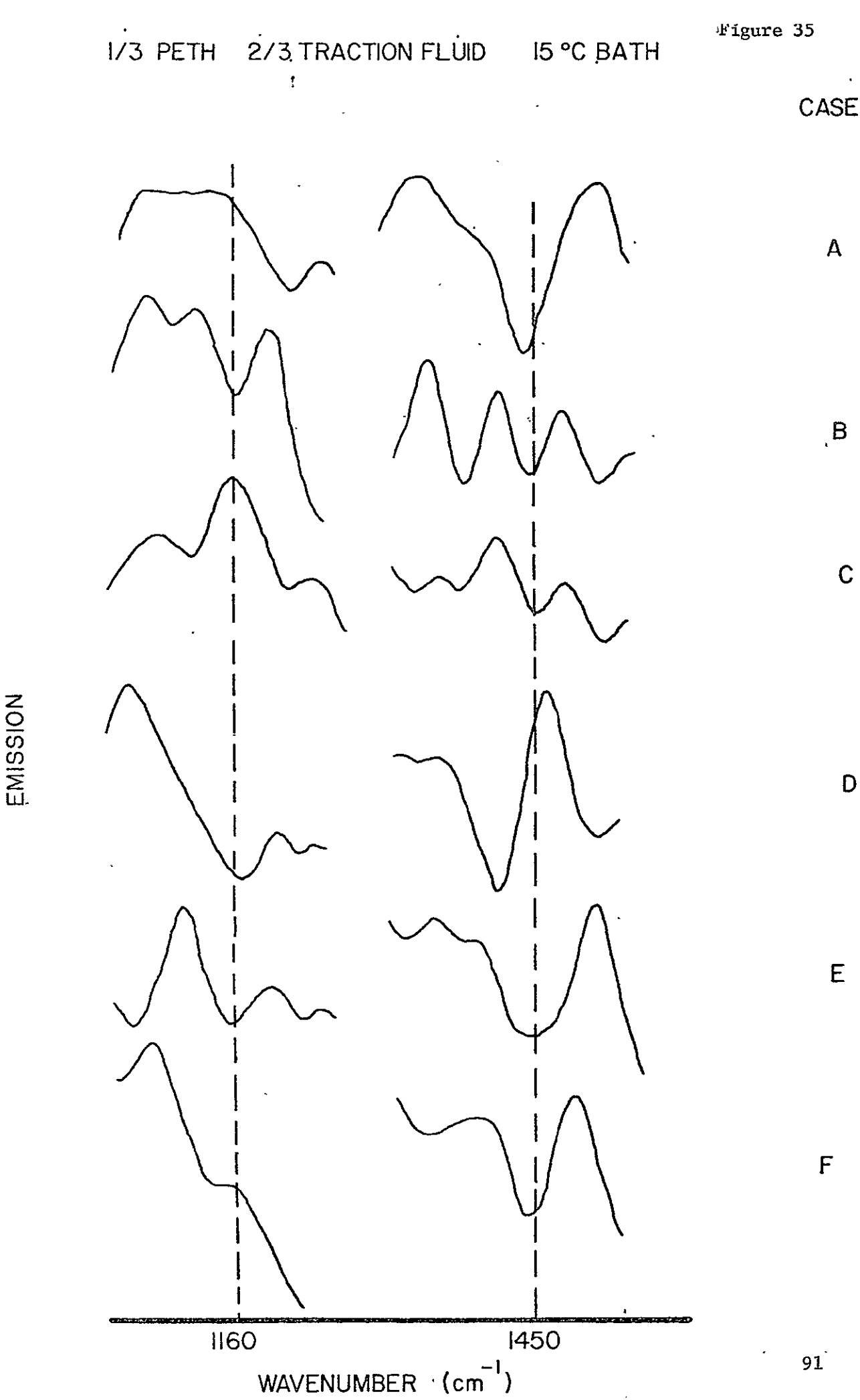
1/3 PETH 2/3 TRACTION FLUID 15 °C BATH
CASE
A
B
C
D
E
F
EMISSION
1160
1450
WAVENUMBER (cm⁻¹)

Figure 36

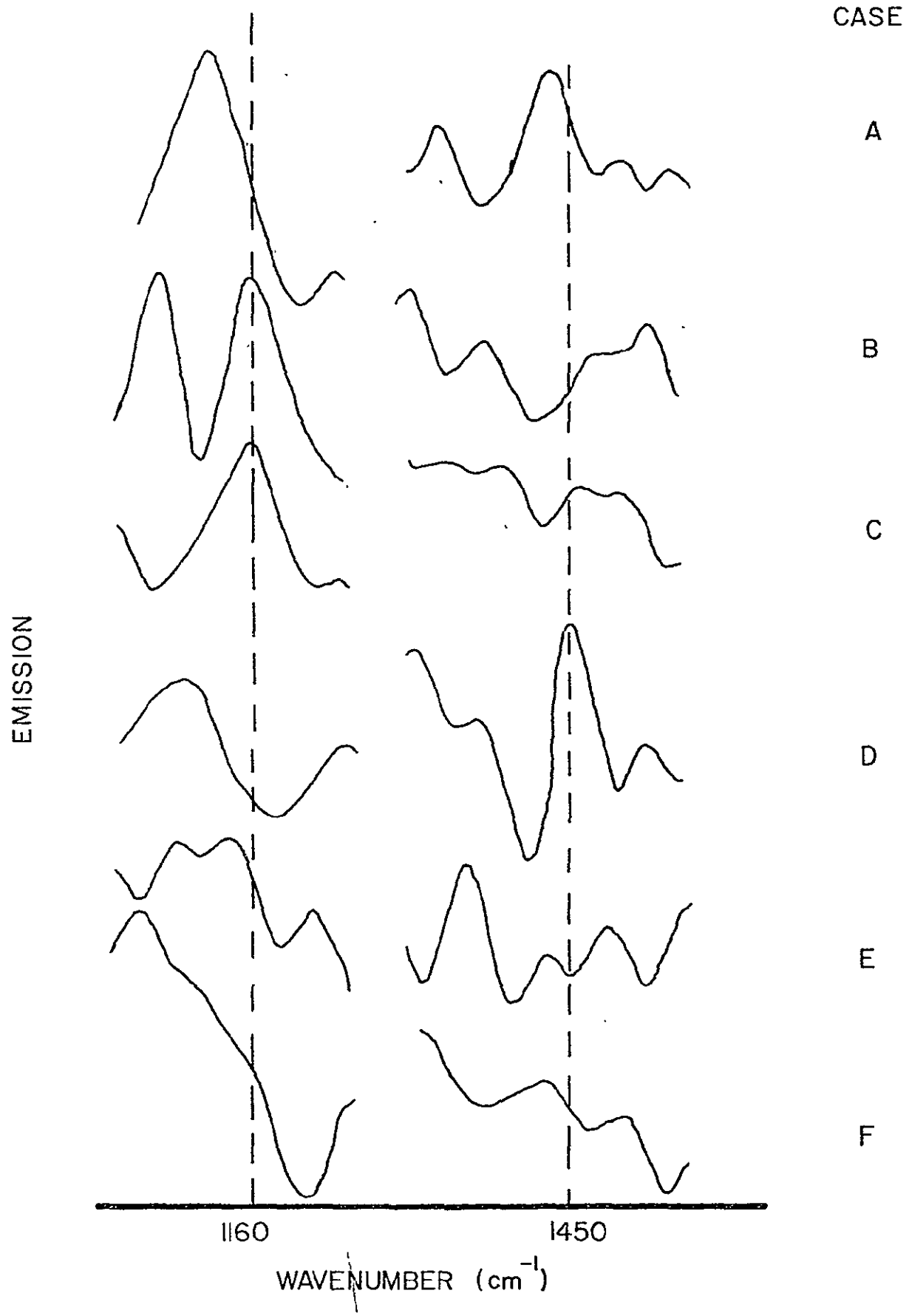
2/3 PETH. 1/3 TRACTION FLUID 15 °C BATH
CASE
A
B
C
D
E
F
EMISSION
1160
1450
WAVENUMBER (cm⁻¹)

Figure 37

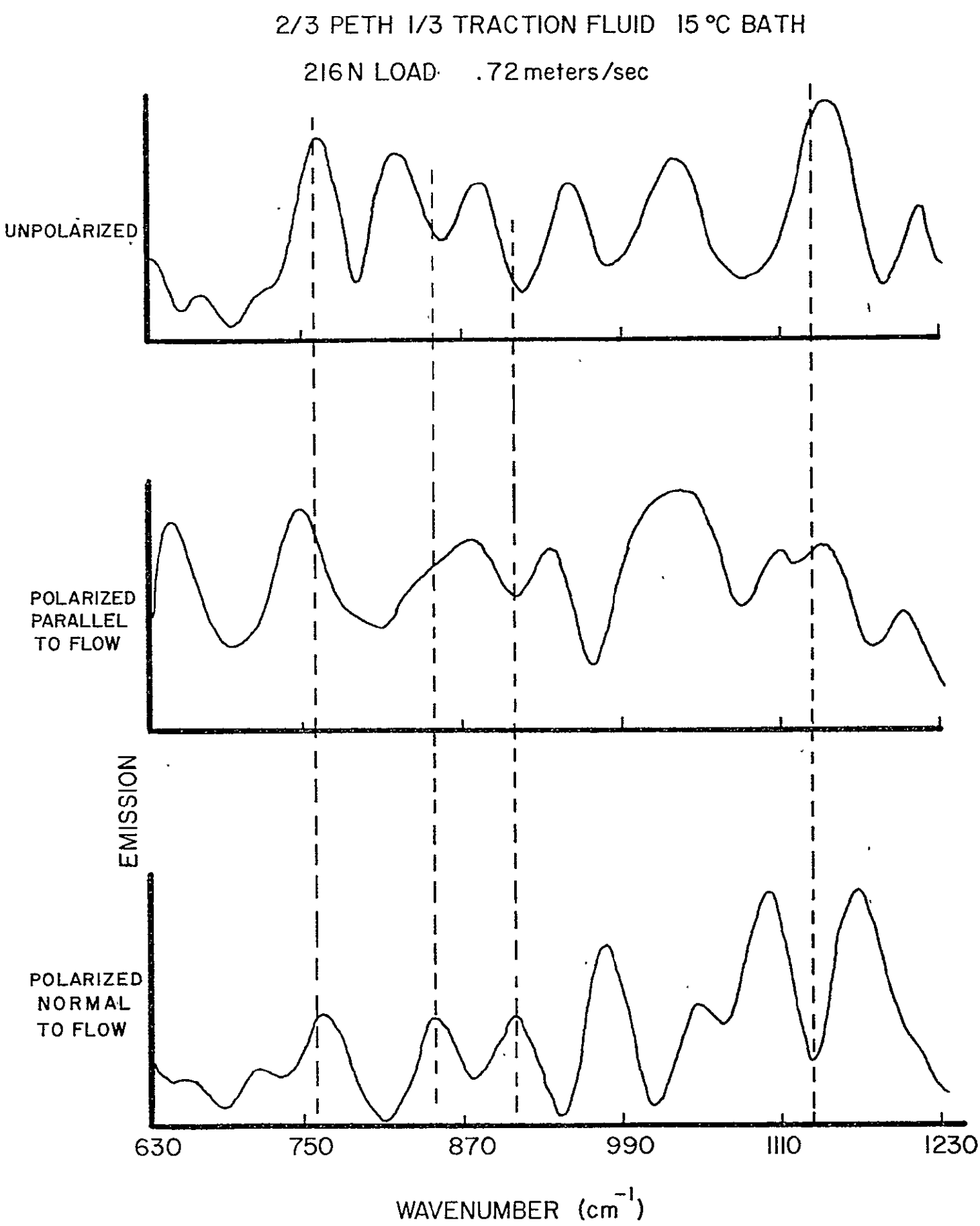
2/3 PETH 1/3 TRACTION FLUID 15 °C BATH
216 N LOAD .72 meters/sec
UNPOLARIZED
POLARIZED PARALLEL TO FLOW
POLARIZED NORMAL TO FLOW
EMISSION
630
750
870
990
1110
1230
WAVENUMBER (cm⁻¹)

Figure 38

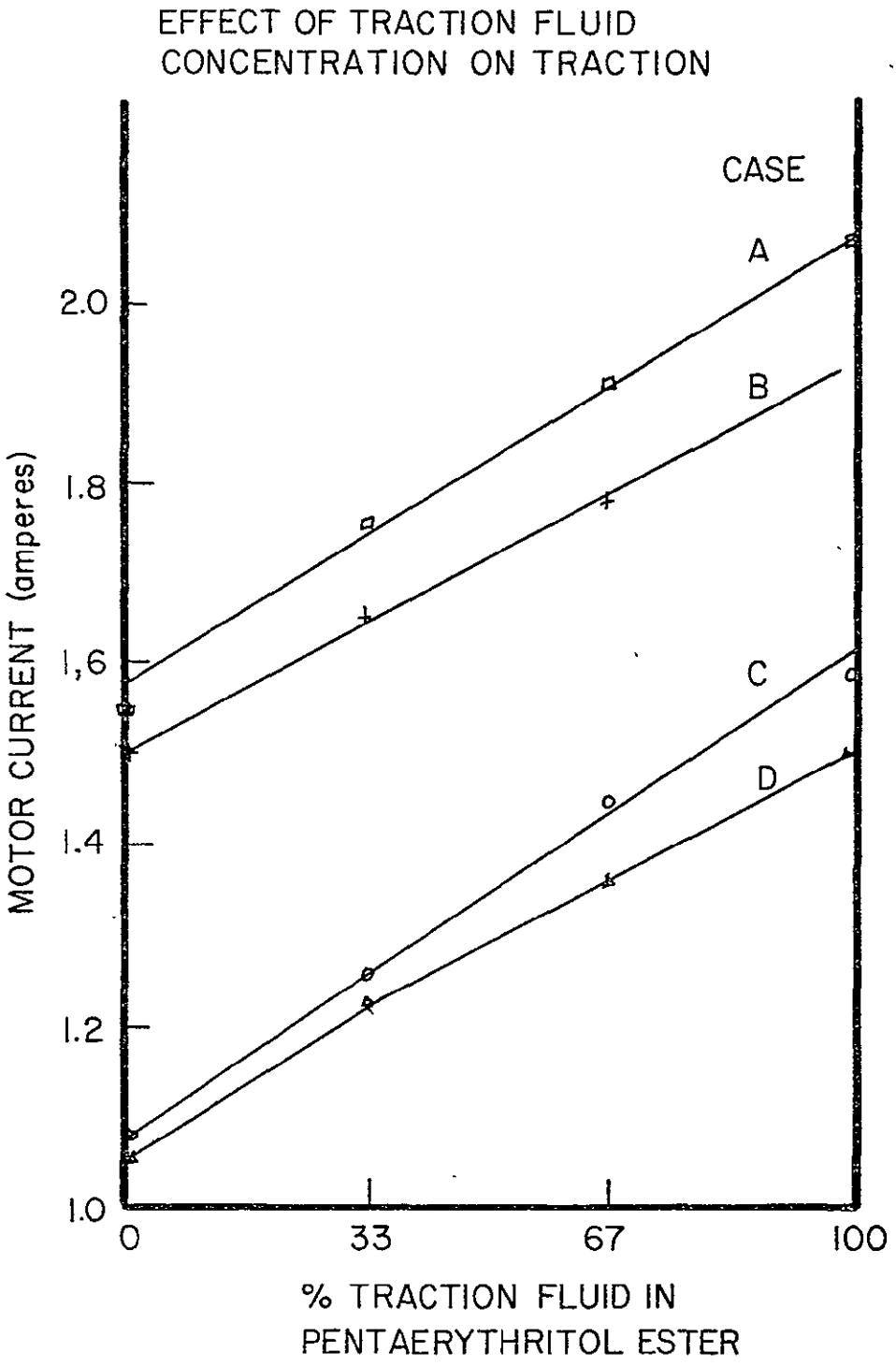
EFFECT OF TRACTION FLUID
CONCENTRATION ON TRACTION
CASE
A
B
C
D
MOTOR CURRENT (amperes)
2.0
1.8
1.6
1.4
1.2
1.0
0
33
67
100
% TRACTION FLUID IN
PENTAERYTHRITOL ESTER

Figure 39

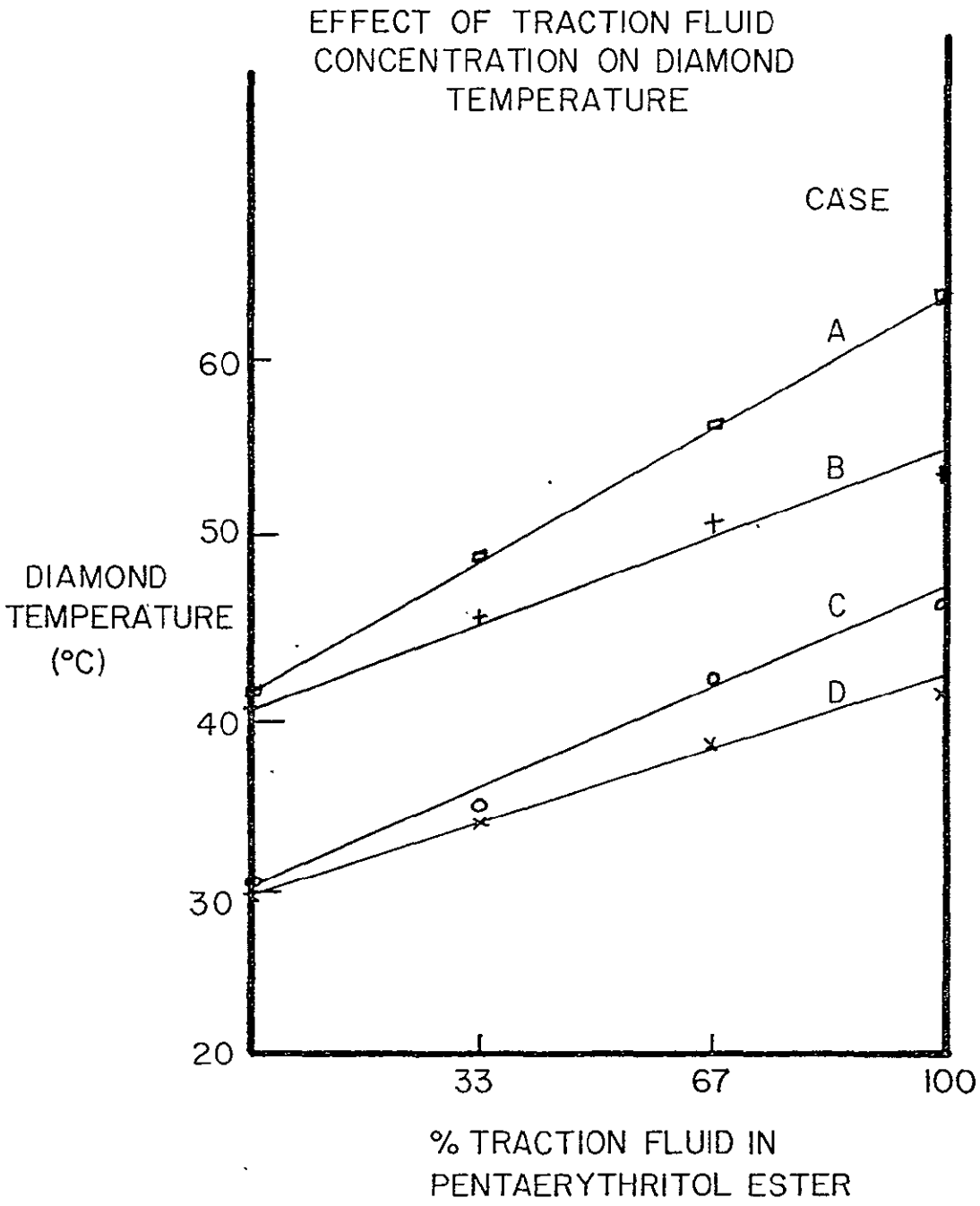
EFFECT OF TRACTION FLUID CONCENTRATION ON DIAMOND TEMPERATURE
CASE
A
B
C
D
60
50
40
30
20
DIAMOND TEMPERATURE (°C)
33
67
100
% TRACTION FLUID IN PENTAERYTHRITOL ESTER

Figure40

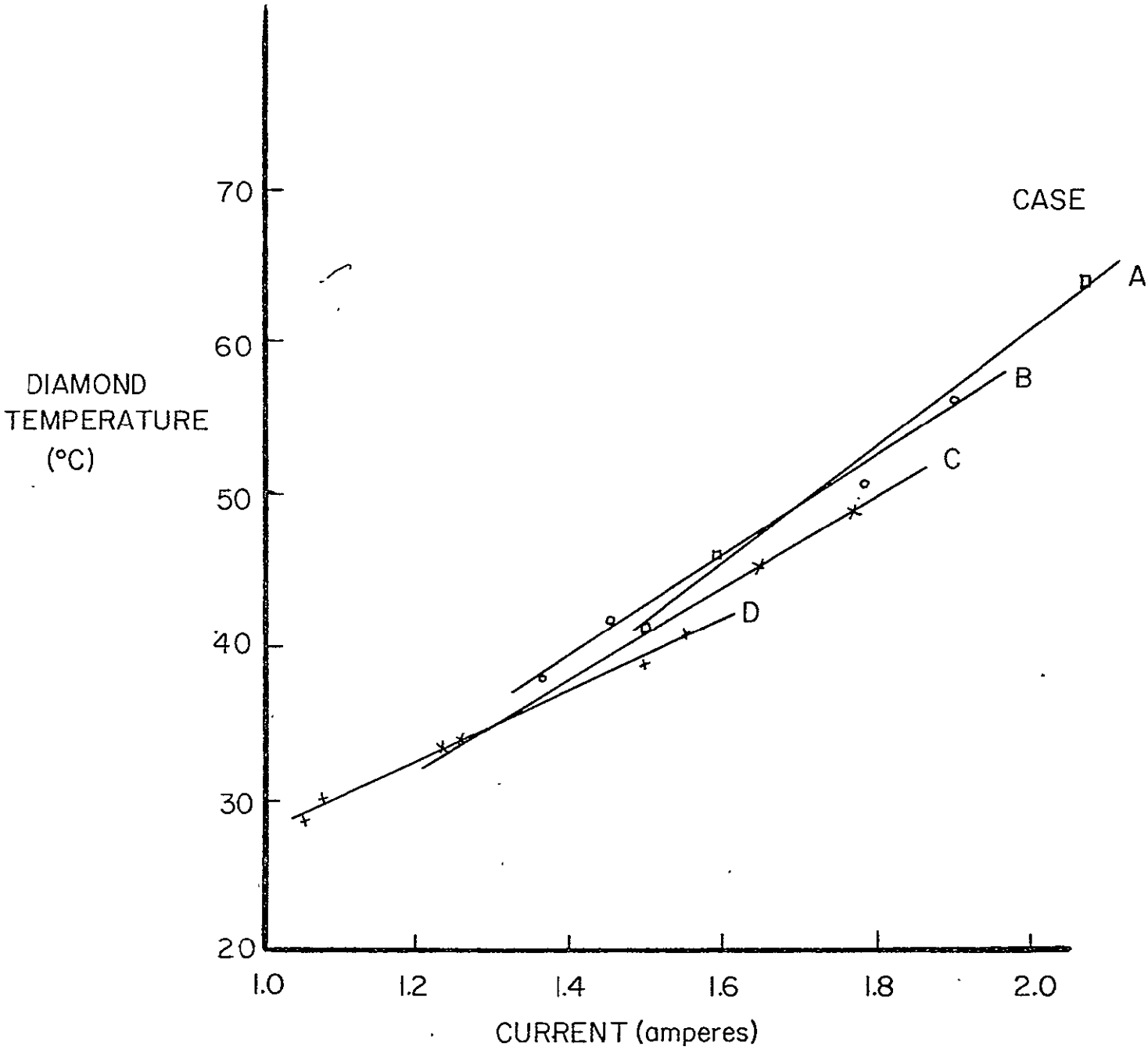
70
60
50
40
30
20
DIAMOND
TEMPERATURE
(°C)
CASE
A
B
C
D
1.0
1.2
1.4
1.6
1.8
2.0
CURRENT (amperes)

Figure 41

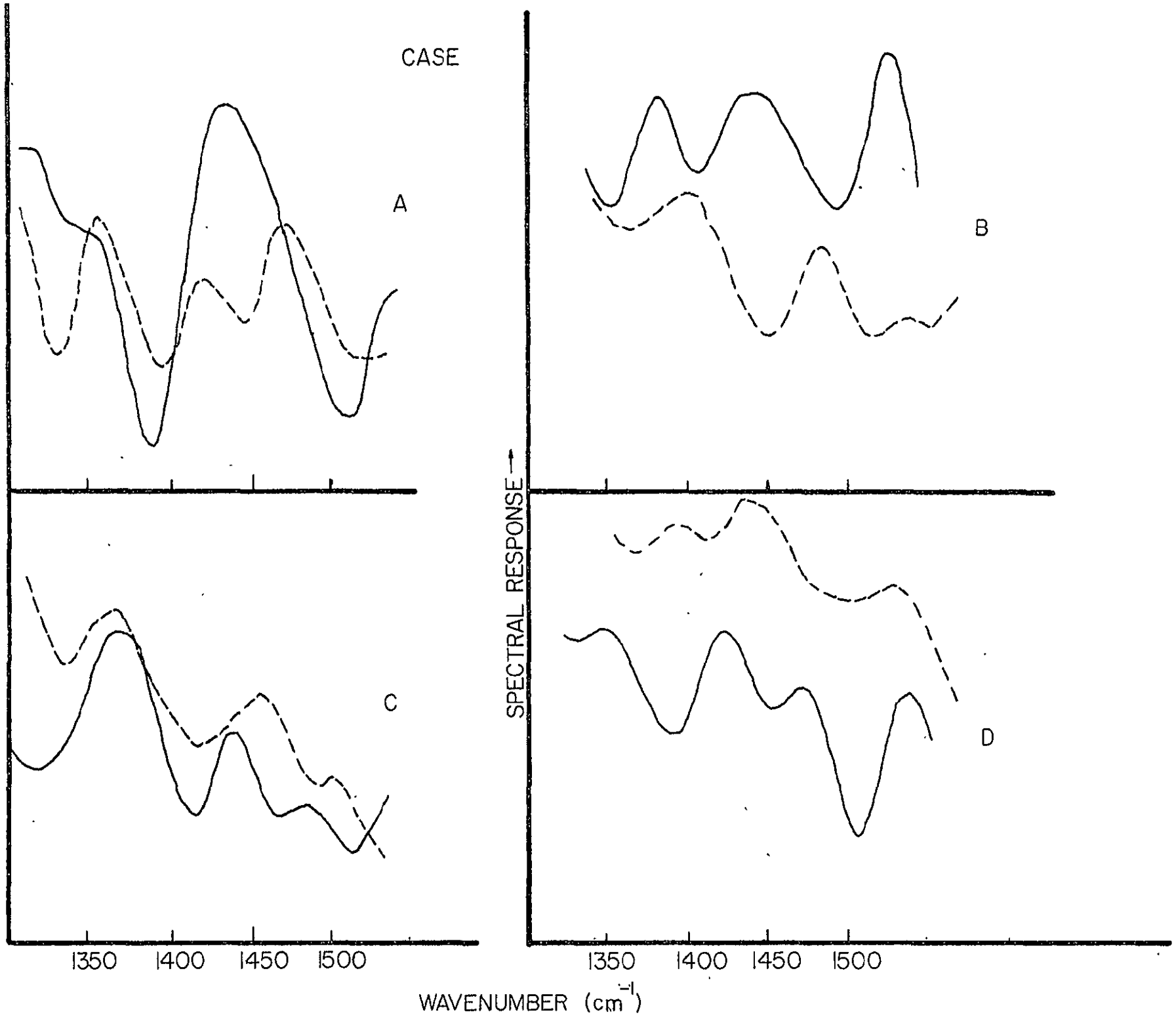
CASE
A
B
C
D
SPECTRAL RESPONSE
1350
1400
1450
1500
WAVENUMBER (cm⁻¹)

Figure 42

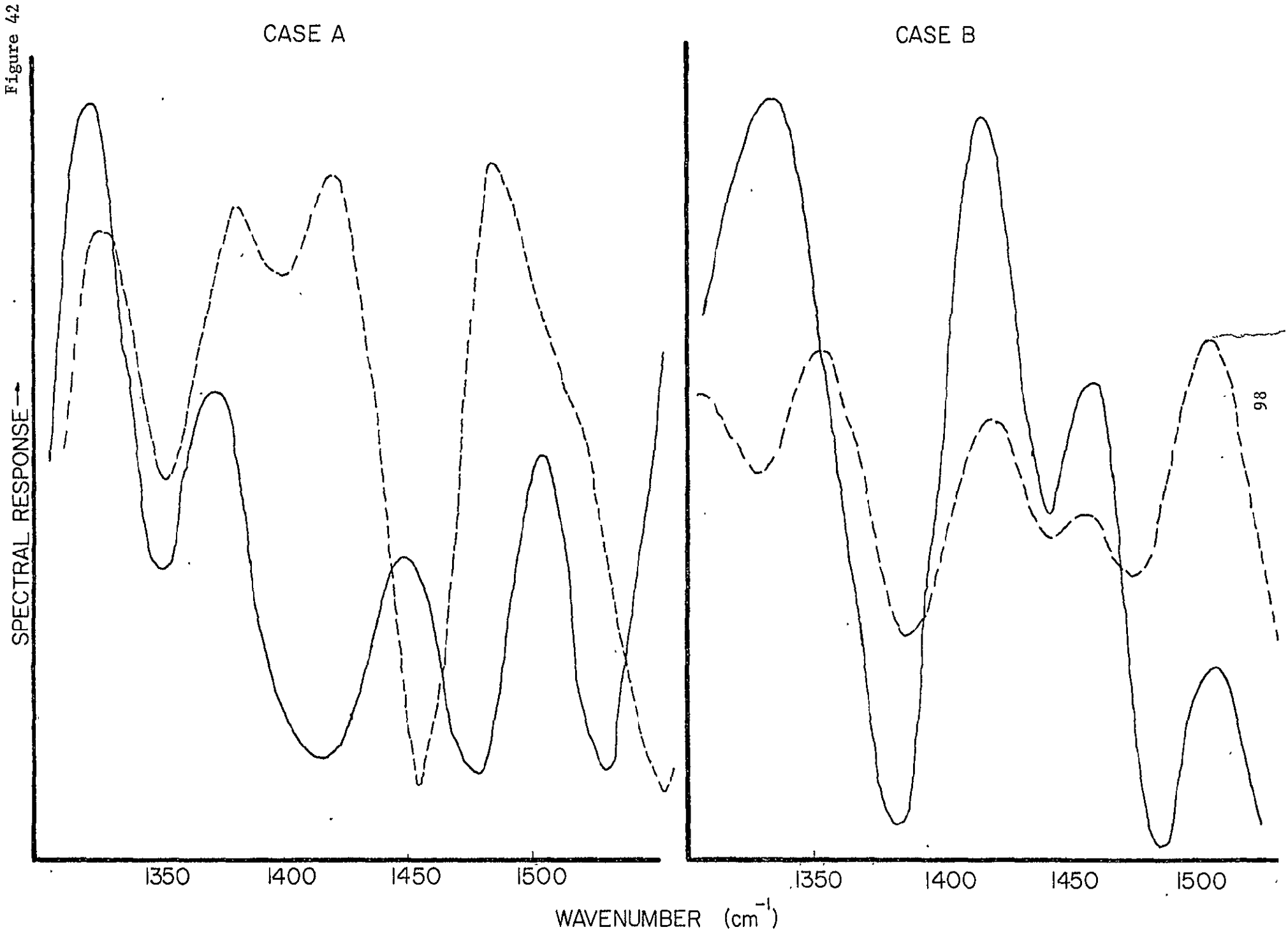
CASE A
CASE B
SPECTRAL RESPONSE →
1350
1400
1450
1500
WAVENUMBER (cm⁻¹)
98

Figure 43

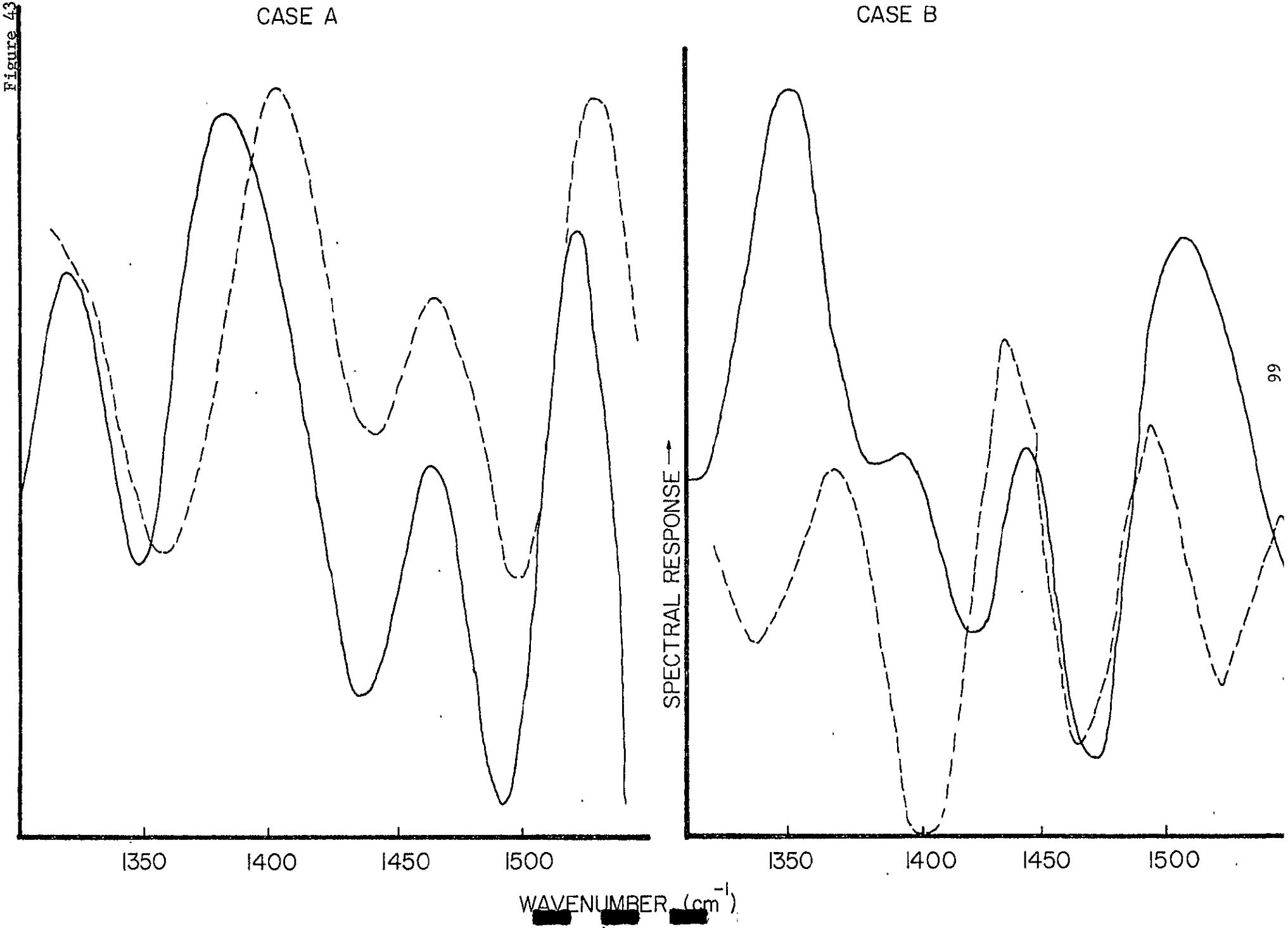
CASE A
CASE B
SPECTRAL RESPONSE →
1350
1400
1450
1500
1350
1400
1450
1500
WAVENUMBER (cm⁻¹)

Figure 44

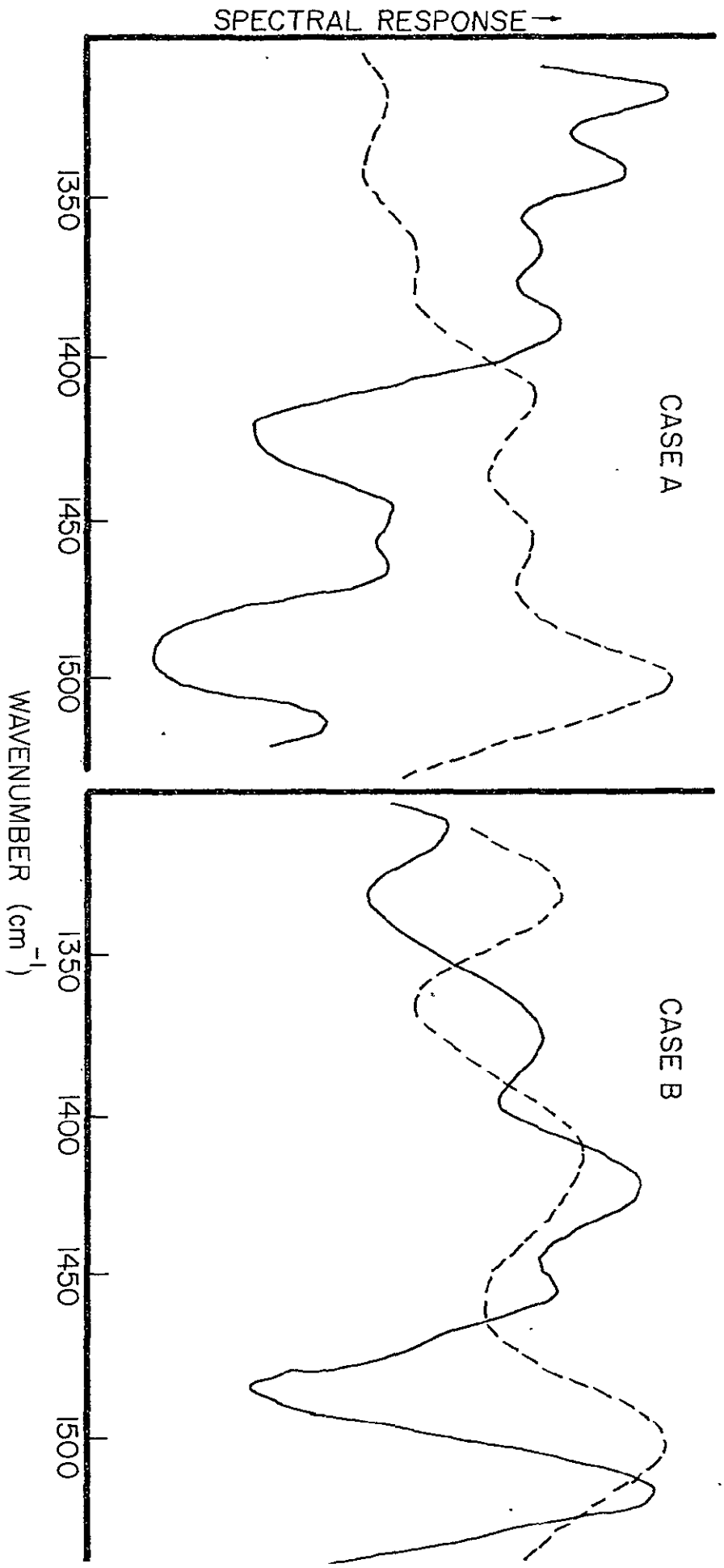
SPECTRAL RESPONSE →
1350
1400
1450
1500
WAVENUMBER (cm⁻¹)
CASE A
CASE B

Figure 45

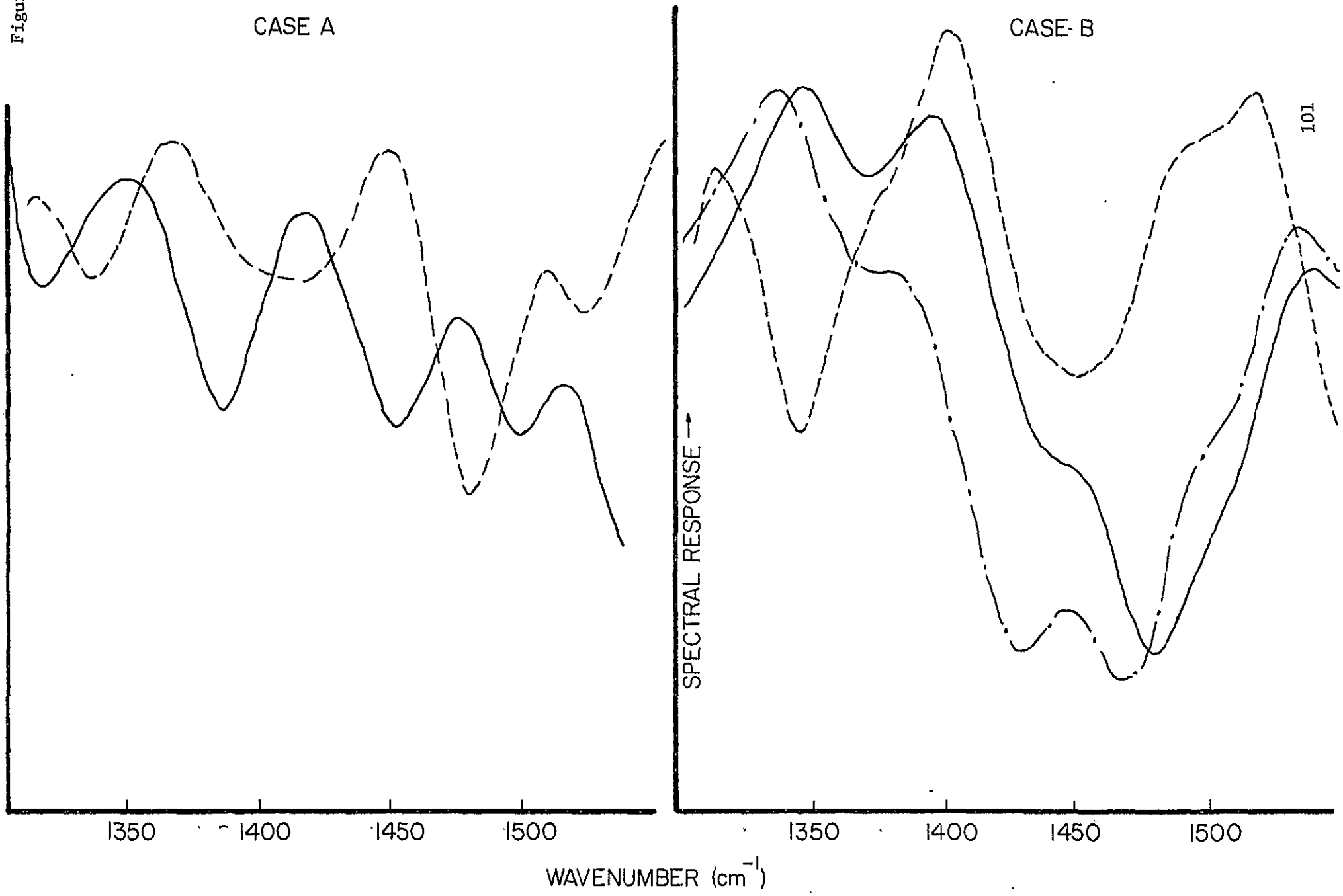
CASE A
CASE- B
SPECTRAL RESPONSE →
1350
1400
1450
1500
1350
1400
1450
1500
WAVENUMBER (cm⁻¹)

Figure 46

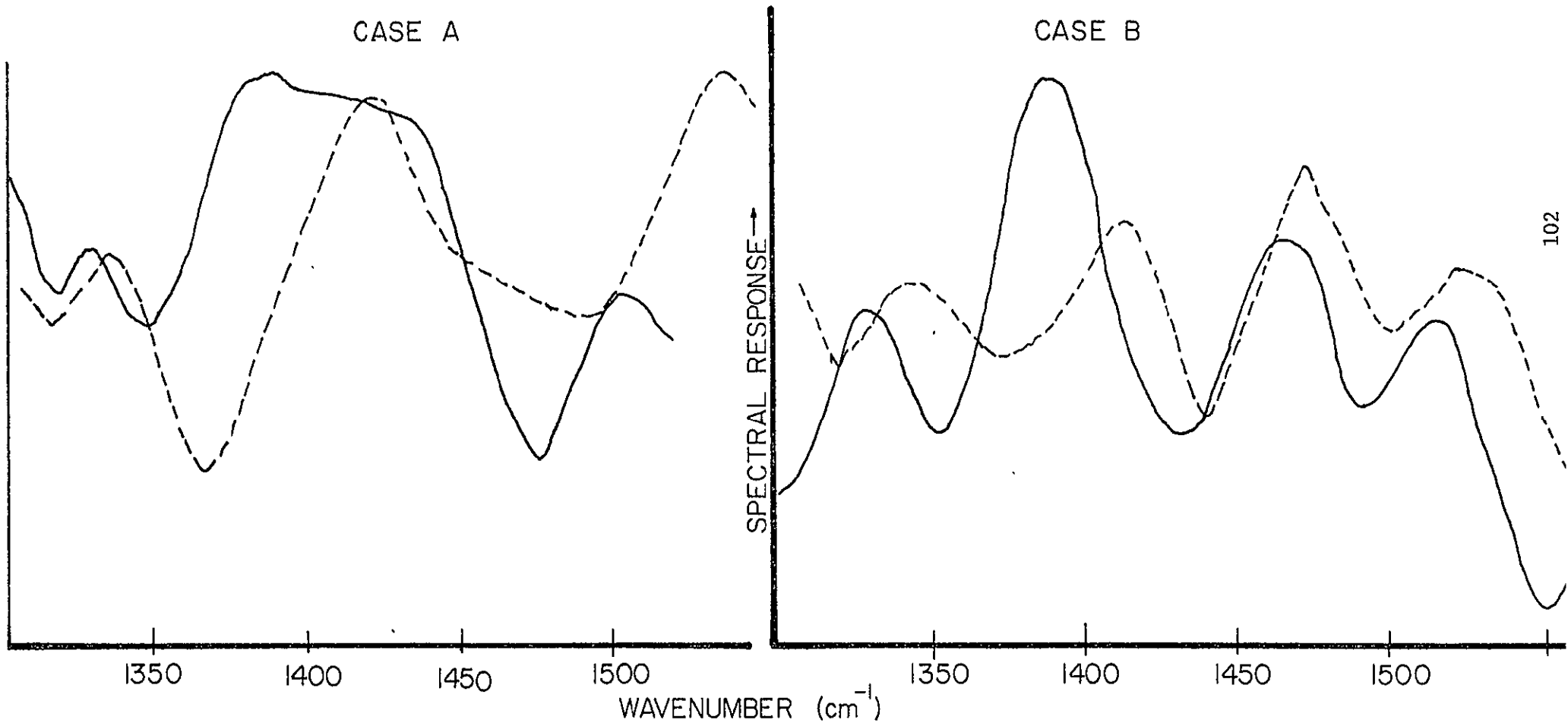
CASE A
CASE B
SPECTRAL RESPONSE
1350
1400
1450
1500
1350
1400
1450
1500
WAVENUMBER (cm⁻¹)

Figure 47

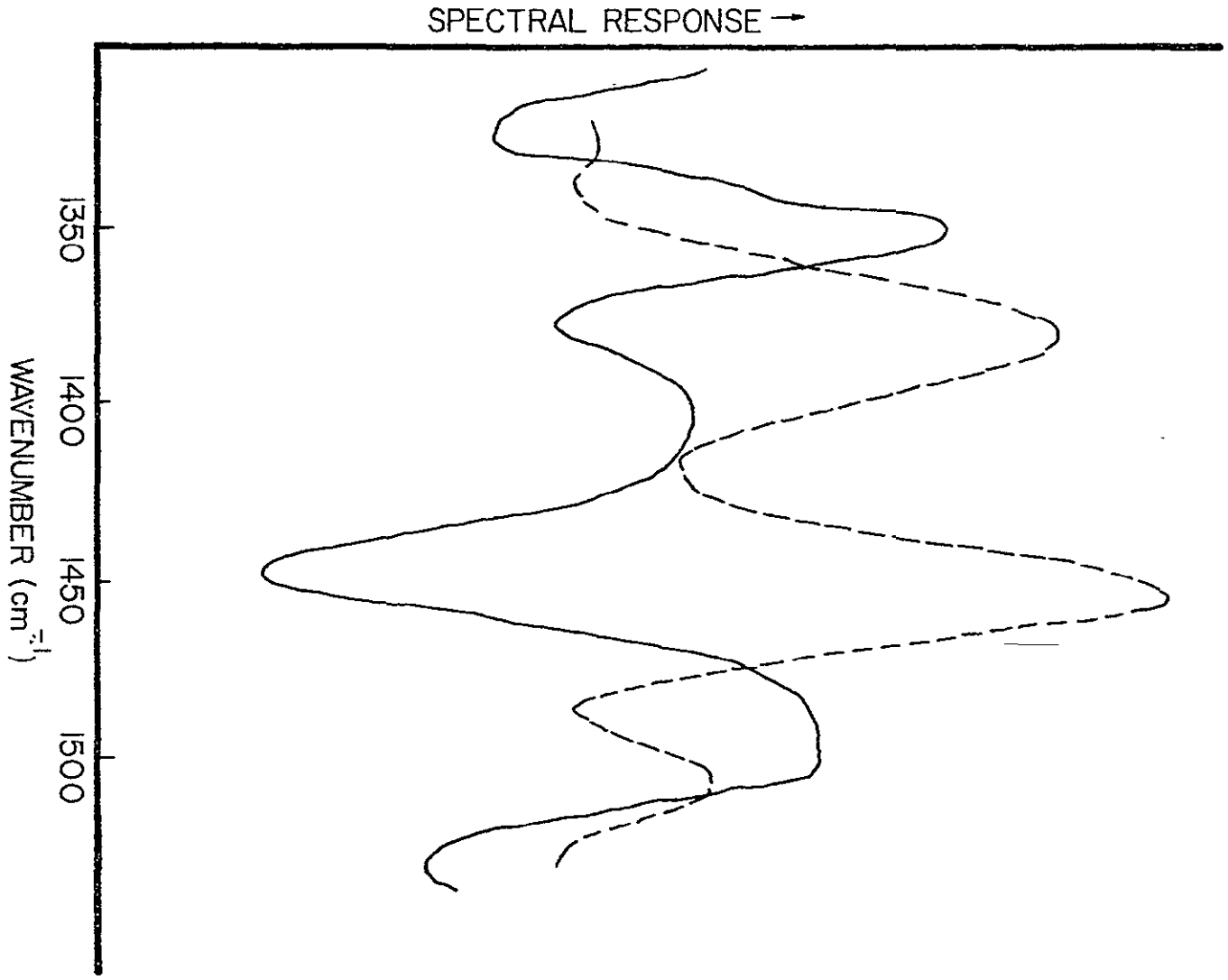

Figure 48

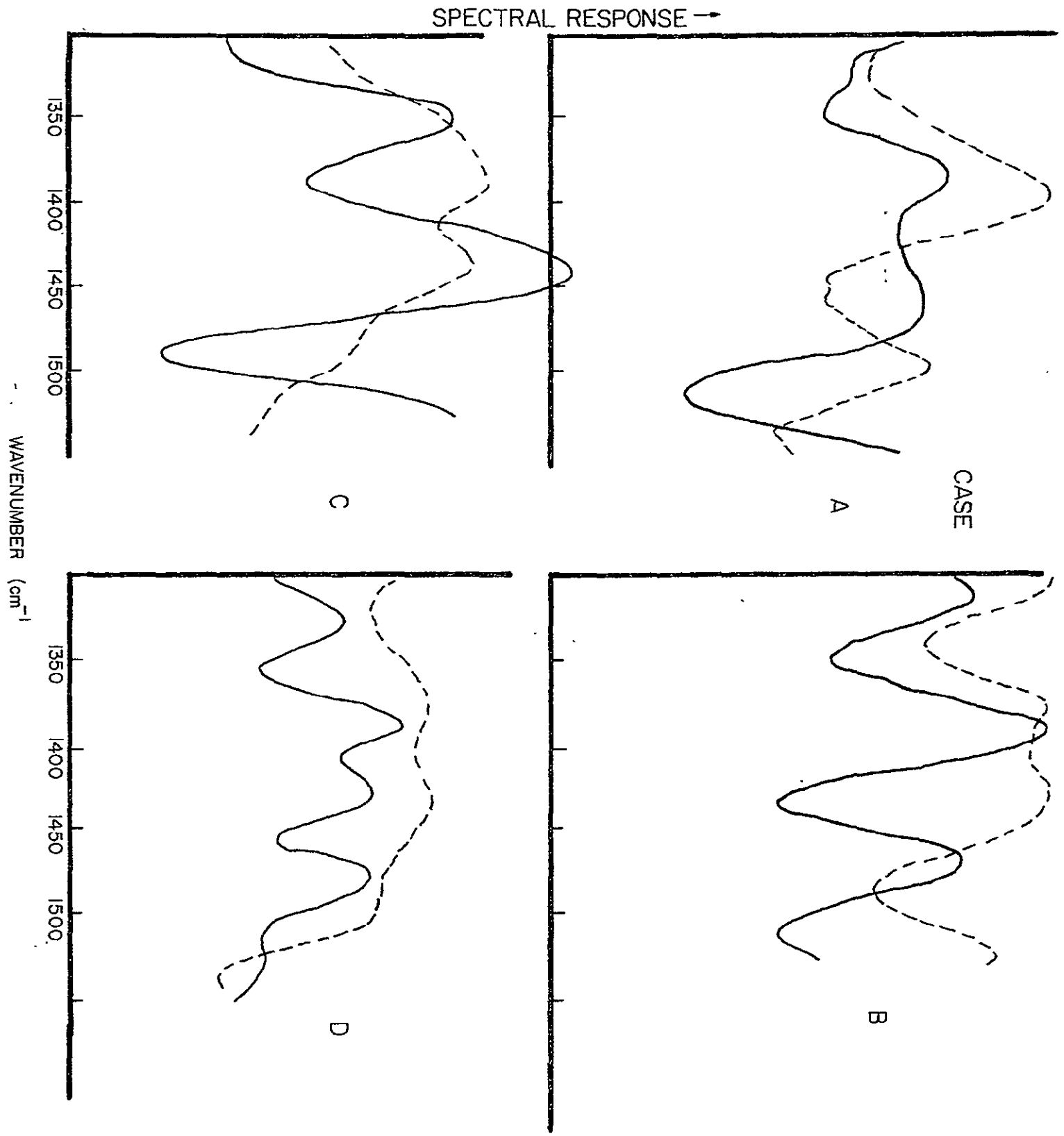
SPECTRAL RESPONSE →
CASE
A
B
C
D
1350
1400
1450
1500
WAVENUMBER (cm⁻¹)

Figure 49

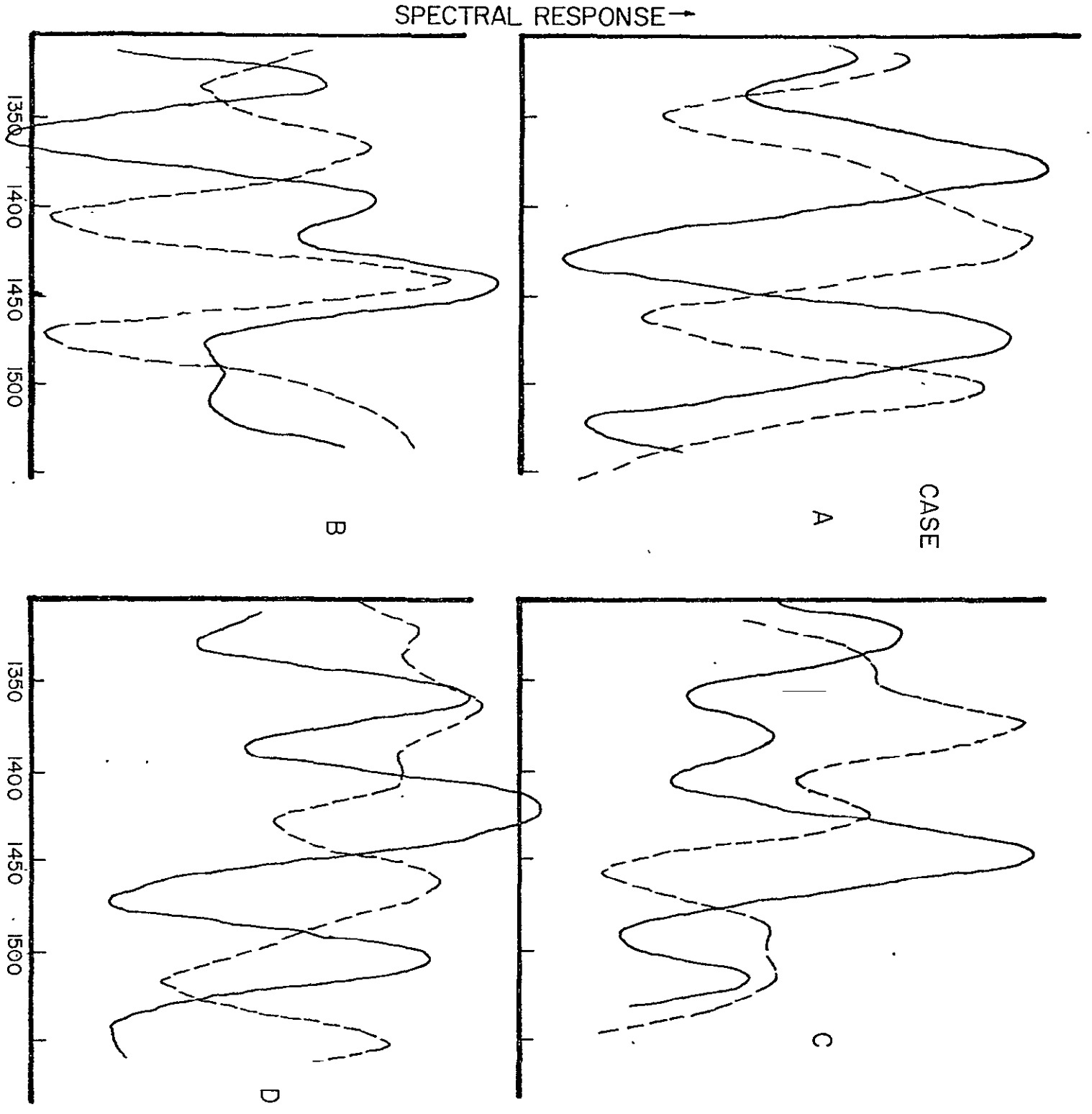
SPECTRAL RESPONSE
1350
1400
1450
1500
WAVENUMBER, cm⁻¹
A
B
C
D
CASE

Figure 50

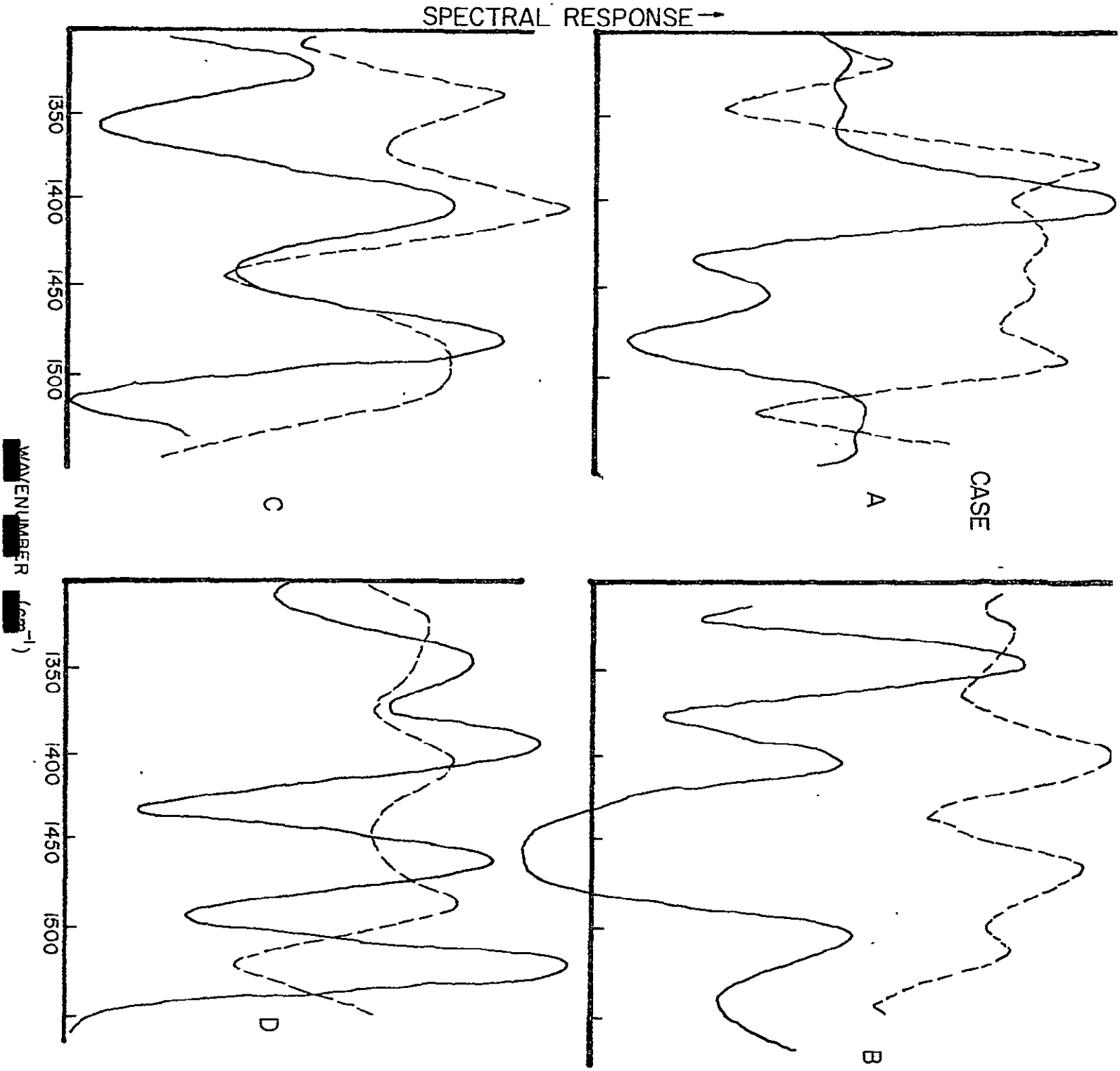
SPECTRAL RESPONSE →
1350
1400
1450
1500
WAVENUMBER (cm⁻¹)
A
B
C
D
CASE

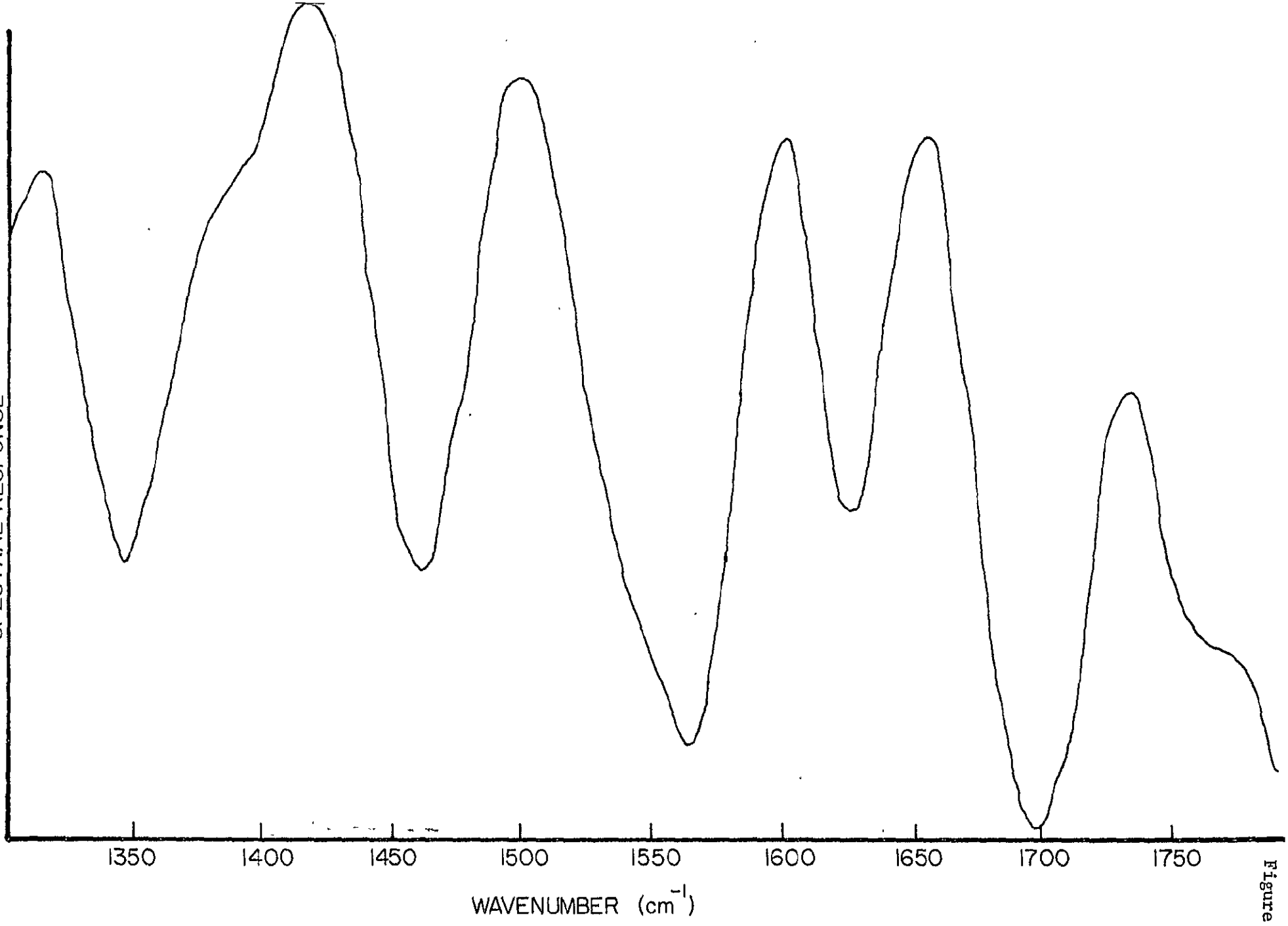
SPECTRAL RESPONSE→
1350
1400
1450
1500
1550
1600
1650
1700
1750
WAVENUMBER (cm⁻¹)

Figure 51

Figure 52

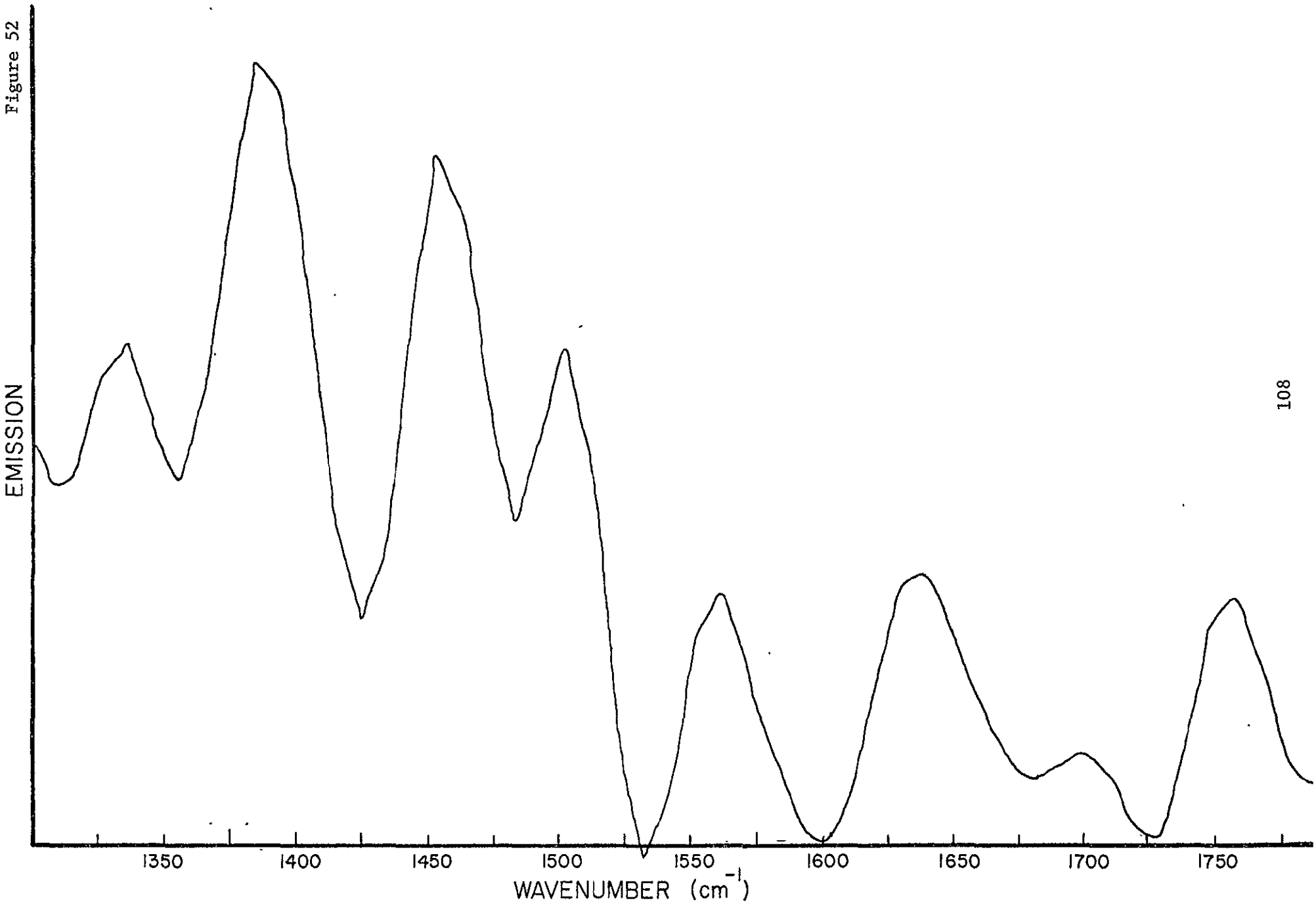
EMISSION
1350
1400
1450
1500
1550
1600
1650
1700
1750
WAVENUMBER (cm⁻¹)

Figure 53

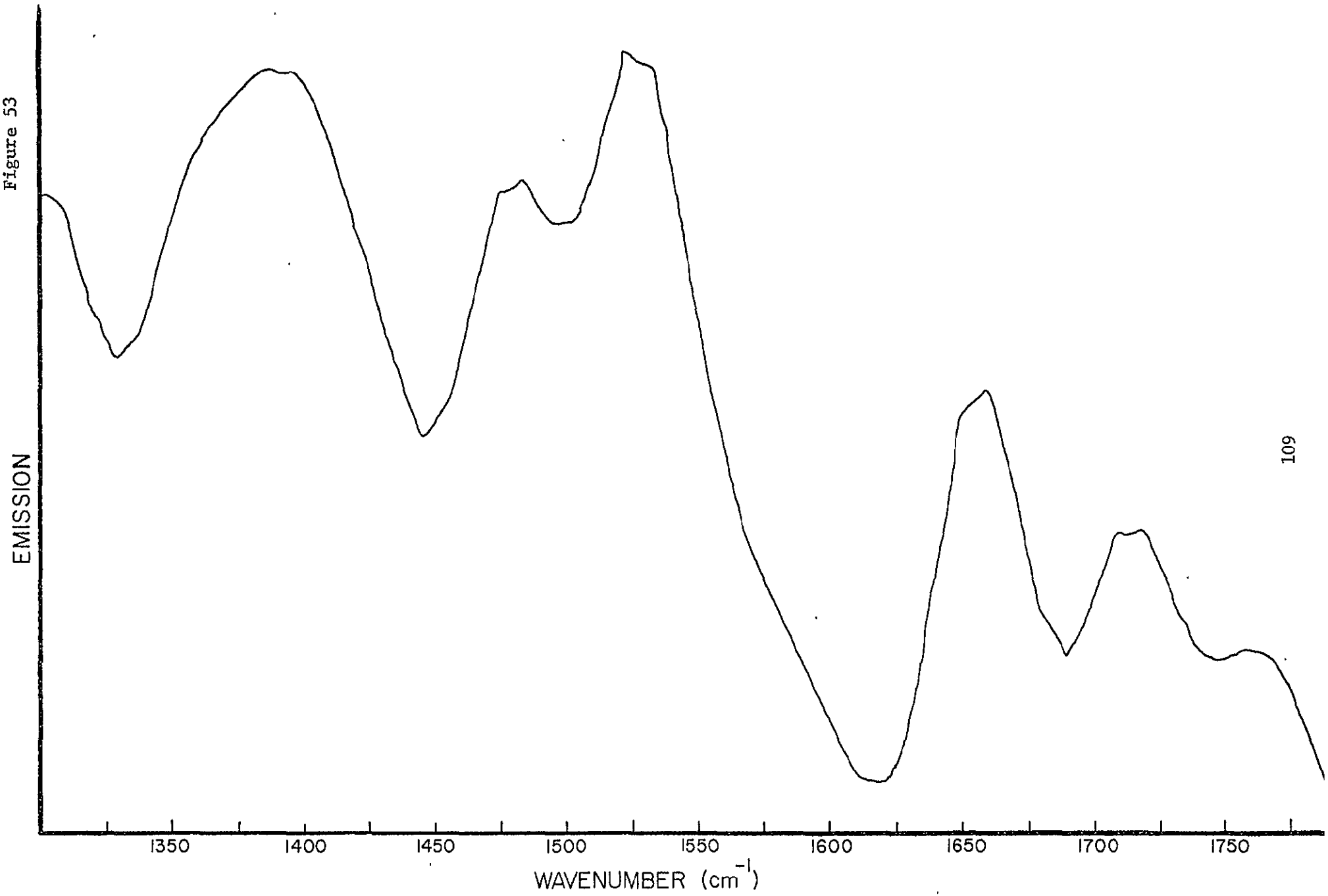
EMISSION
1350
1400
1450
1500
1550
1600
1650
1700
1750
WAVENUMBER (cm^{-1})

Figure 54

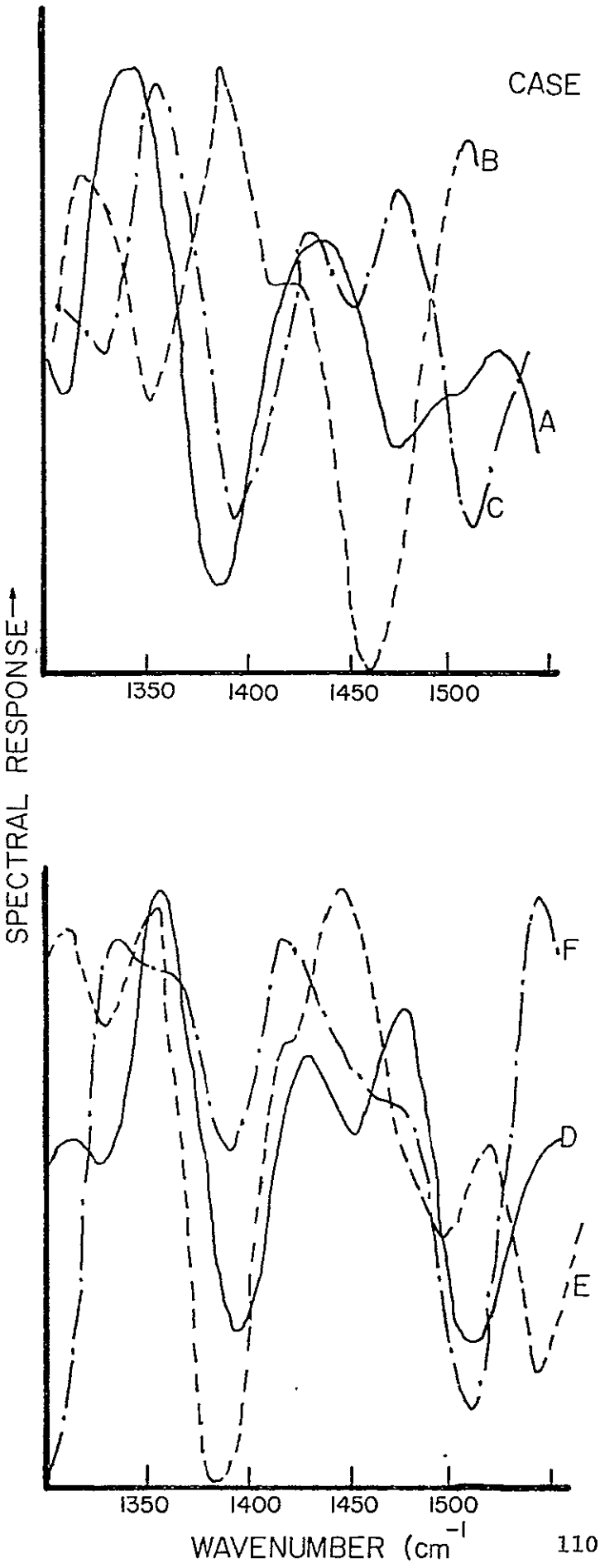

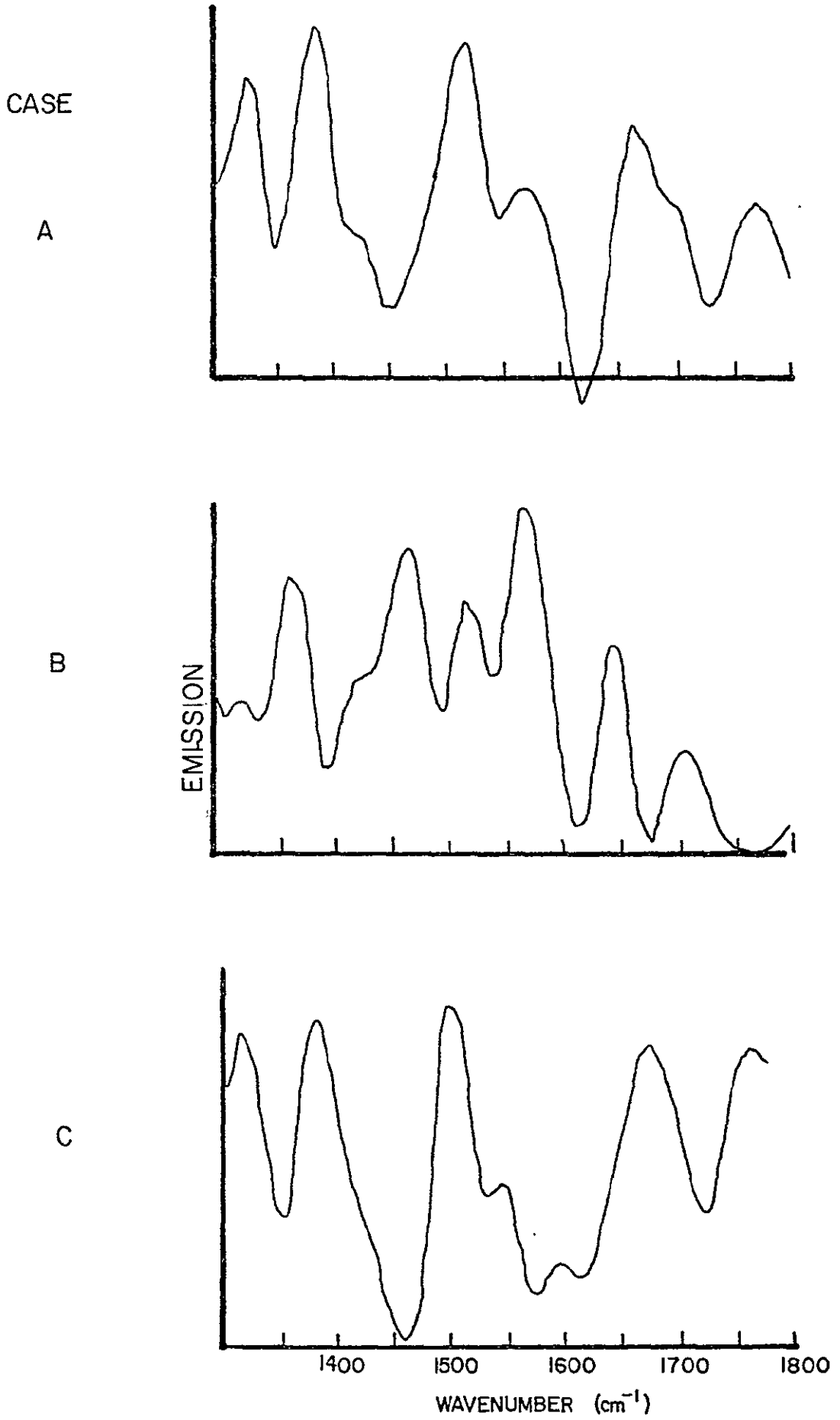
CASE
A
B
C
EMISSION
1400
1500
1600
1700
1800
WAVENUMBER (cm⁻¹)

Figure 56 .

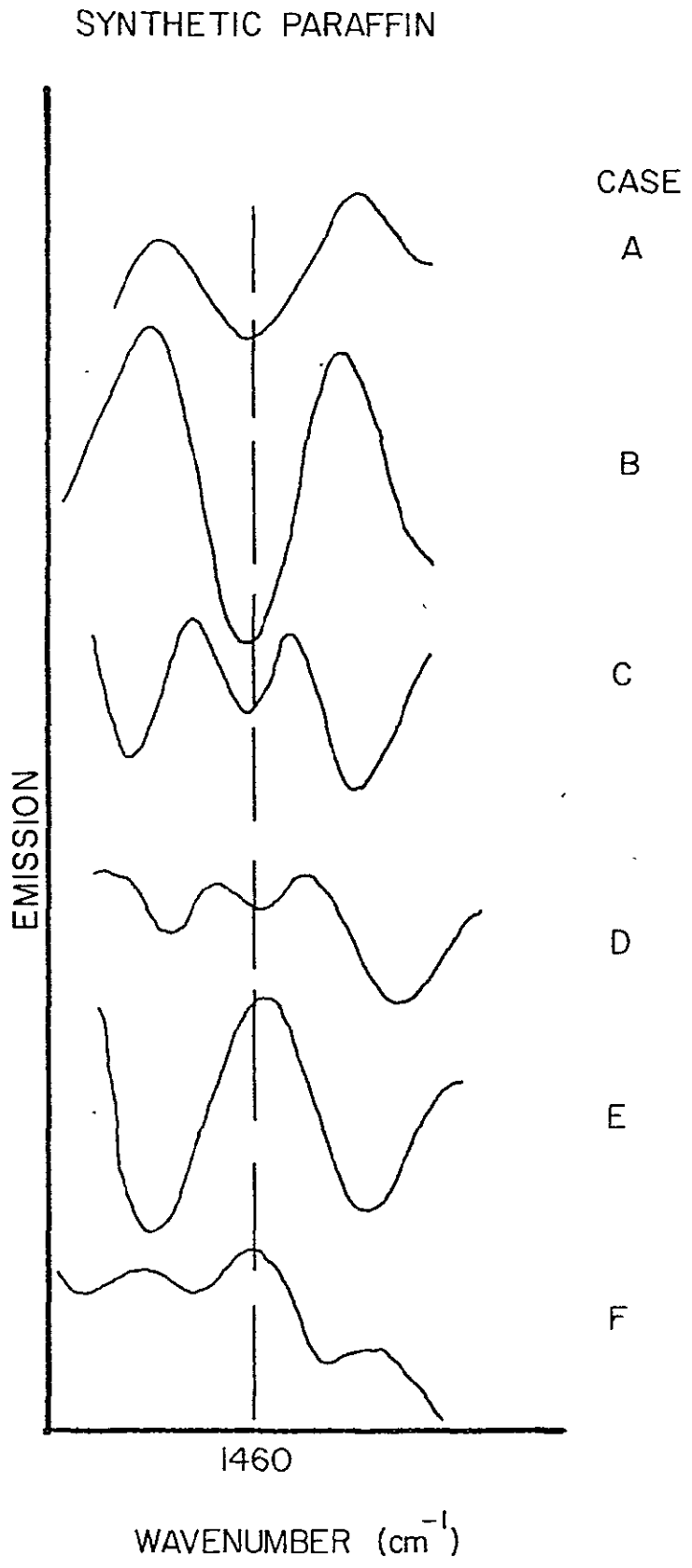
SYNTHETIC PARAFFIN
CASE
A
B
C
D
E
F
EMISSION
1460
WAVENUMBER (cm⁻¹)

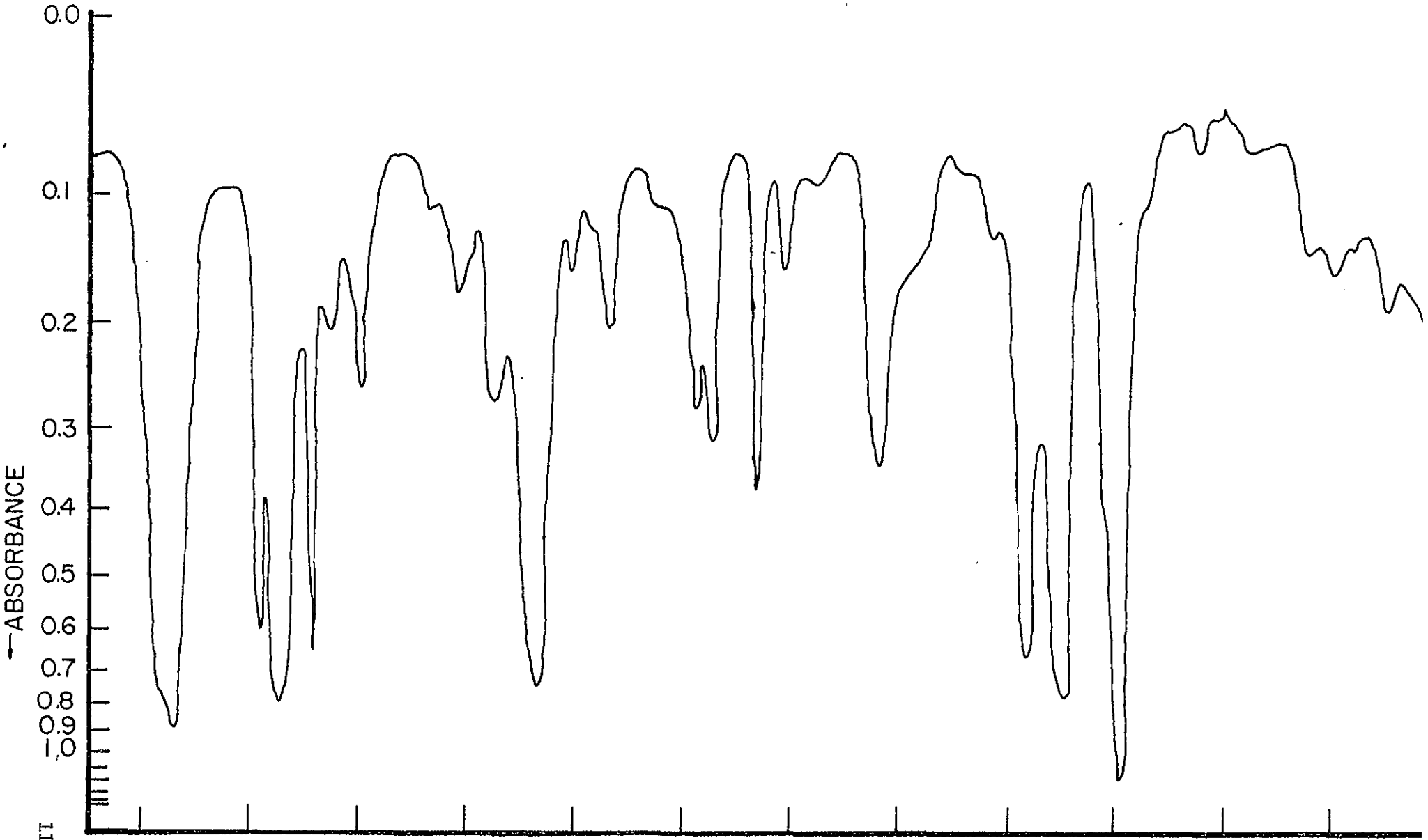
0.0
0.1
0.2
0.3
0.4
0.5
0.6
0.7
0.8
0.9
1.0
ABSORBANCE
1600
1400
1200
1000
800
600
WAVENUMBER (cm⁻¹)

Figure 57

Figure 58

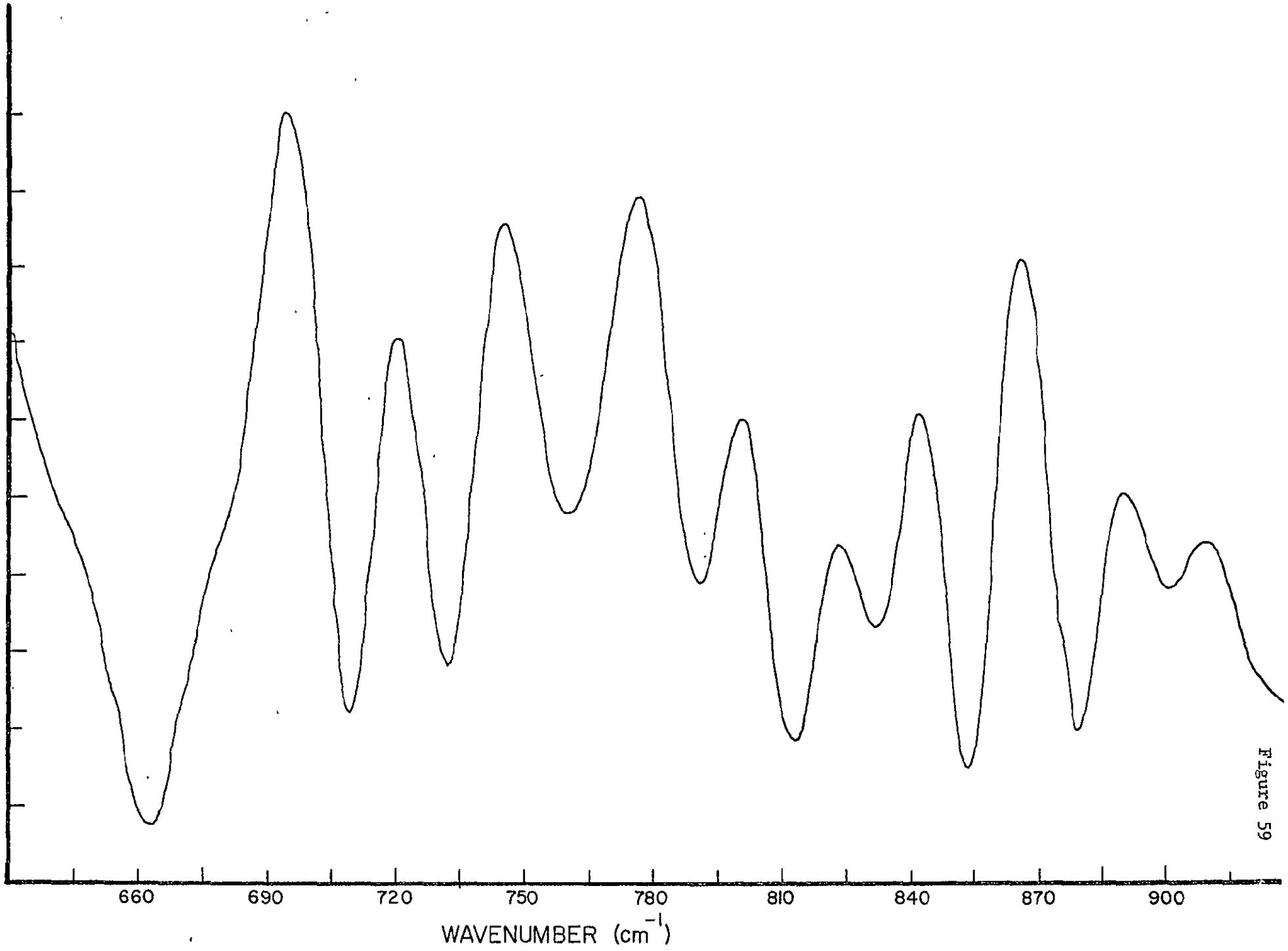

Figure 59

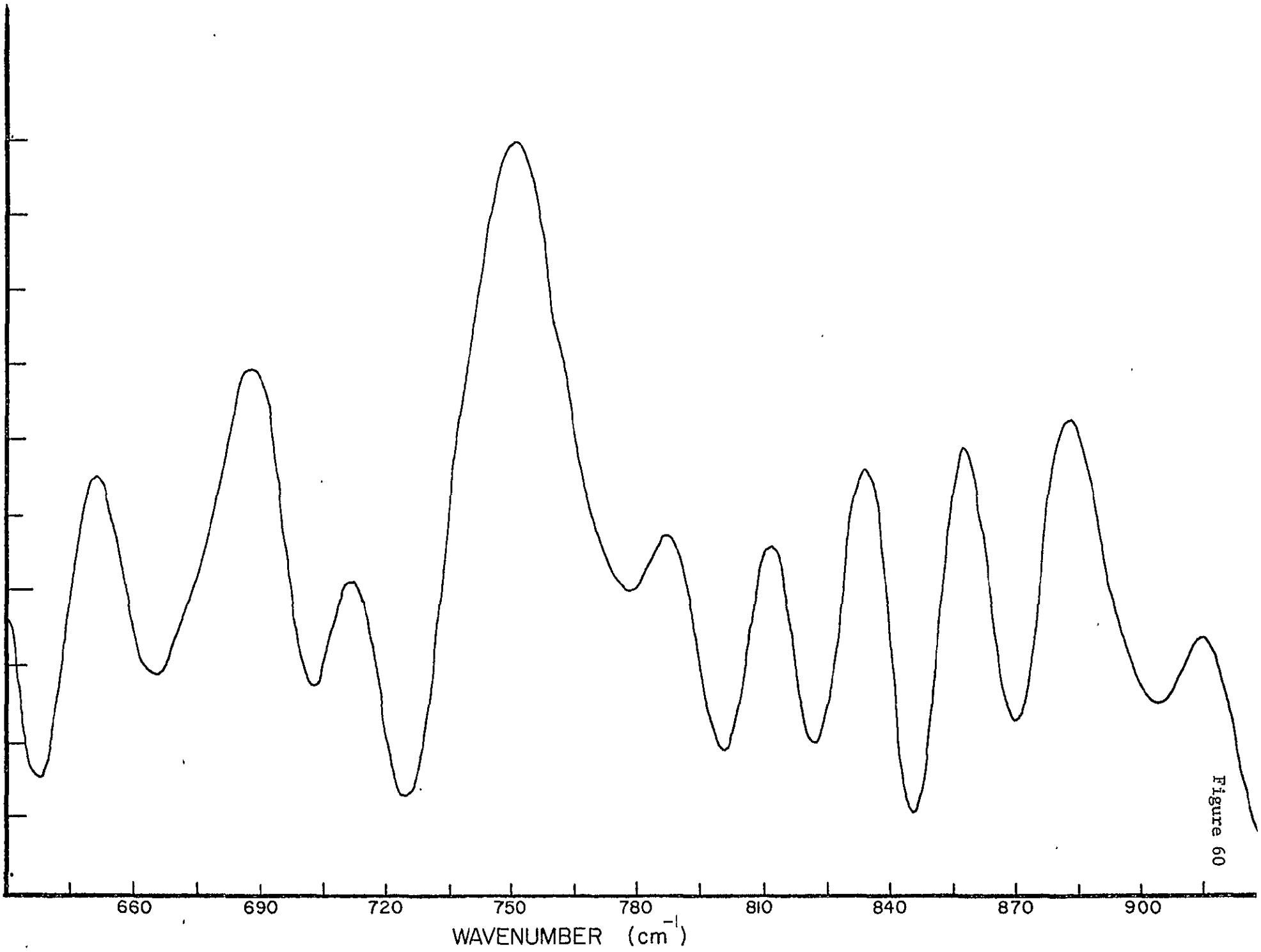

Figure 60

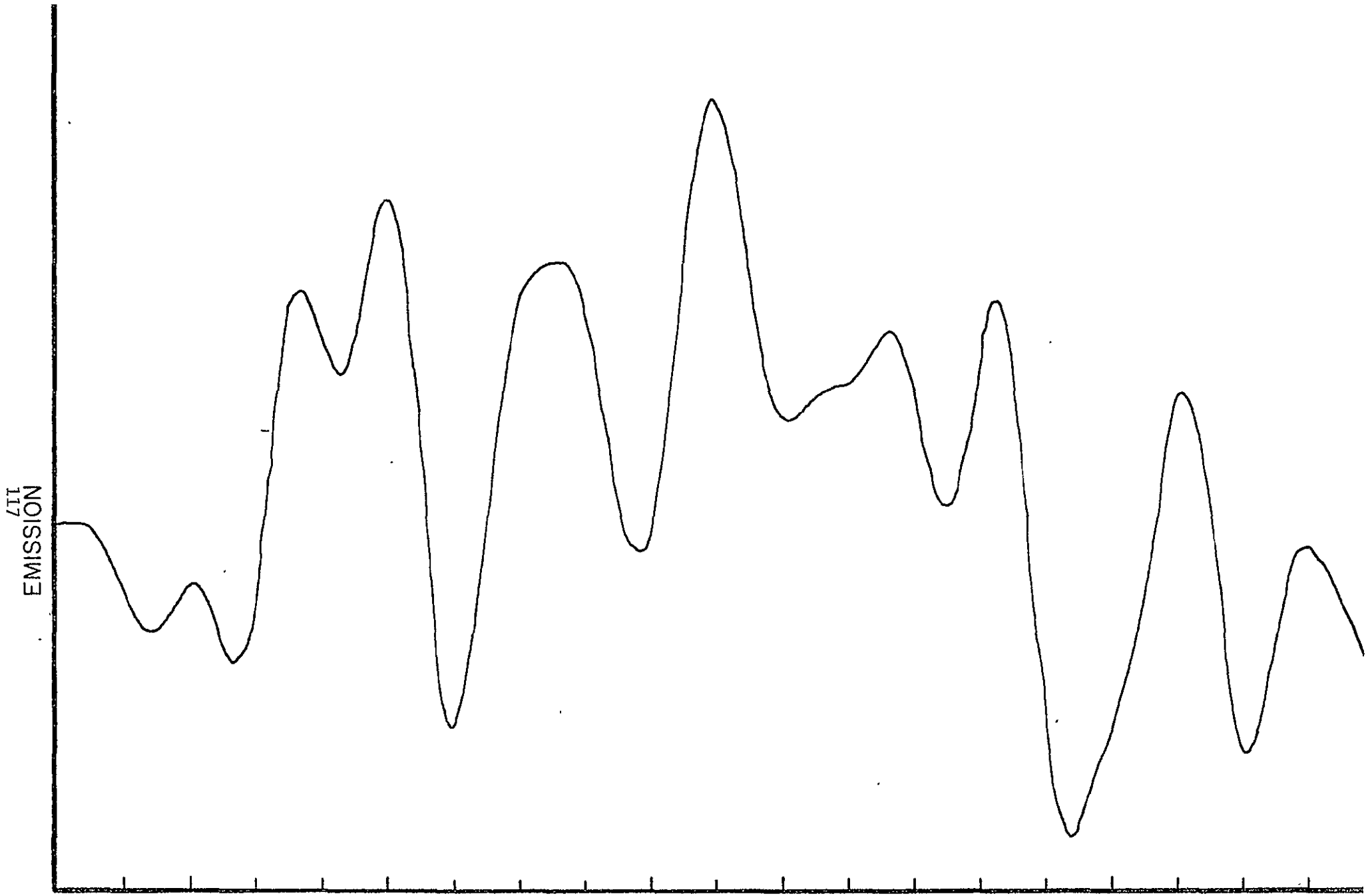
EMISSION
117
660
690
720
750
780
810
840
870
900
WAVENUMBER (cm⁻¹)

Figure 61

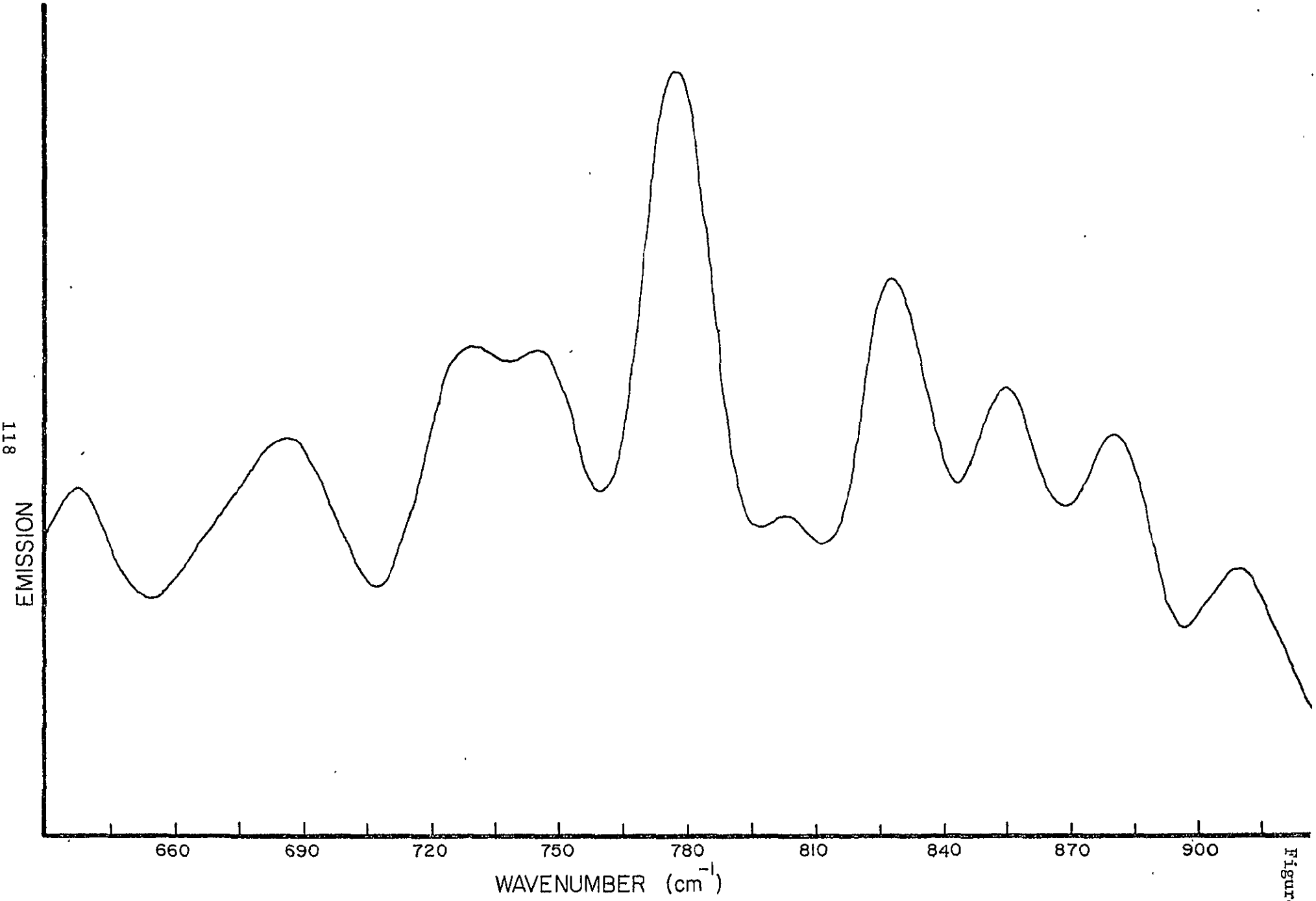

Figure 62

XIII. PUBLICATIONS RESULTING FROM THIS WORK

1. Infrared Emission Spectra of Lubricants in Operating Bearings, Presented at the 10th Middle Atlantic Regional ACS Meeting at the Marriott Hotel, Philadelphia, on February 26, 1976.

2. Infrared Emission Spectra from Lubricant Films in Operating Bearings by Fourier Methods. Paper No. 333. Presented at the 27th Pittsburgh Conference on Analytical Chemistry and Applied Spectroscopy, Cleveland, Ohio, March 1-5, 1976.

3. Analysis of Infrared Spectra of Elastohydrodynamic Lubricant Films Presented at the American Chemical Society National Centennial Meeting, Symposium on Lubricant Properties in Thin Lubricating Films. April 6, 1976, and to be published in an ACS Journal.

4. "High Pressure Infrared Interferometry," Chapter 5 in "Fourier Transform IR: Application to Chemical Systems" (J.R. Ferraro and L.J. Basile, editors). Academic Press, N.Y., pp. 169-213, April 1978.

5. Infrared Emission Spectra from Operating Elastohydrodynamic Sliding Contacts. NASA CR-134973, Final Report on Contract No. NAS 3-18531. 87 pp. March 8, 1976.

6. Traction and Lubricant Film Temperature as Related to the Glass Transition Temperature and Solidification. Preprint No. 77-AM-1A-3. Presented at the 32nd Annual Meeting in Montreal, Quebec, Canada, May 9-12, 1977.

7. Glass Transition Pressures of Fluids from the Bandwidths and Frequencies of the Fluorescence Spectrum of Ruby. Paper No. 261. Presented at 3rd Annual FACSS Meeting (Federation of Analytical Chemistry and Spectroscopy Societies), Philadelphia Civic Center, November 15-19, 1976.

8. Glass Transition and Fluid Pressure Determinations from the Fluorescence Spectrum of Ruby. Canadian J. of Spectroscopy 21, 153-158 (September, October 1976).

9. Differential Infrared Fourier Emission Microspectrometer for Lubrication Studies. Paper No. M.B.3. Presented at the 1977 International Conference on Fourier Transform Infrared Spectroscopy, University of South Carolina, Columbia, S.C., June 20-24, 1977.

10. Infrared Fourier Transform Emission Microspectrometer. Paper No. 17. Presented at the 28th Pittsburgh Conference, Cleveland Convention Center, February 28 - March 4, 1977.

11. Polarized Infrared Emission Spectrophotometry with a Microinterferometer. American Laboratory, Vol. 9, 29-40 (November 1977).

12. Polarized Infrared Emission Spectra from Operating Bearings. Paper No. 592. Invited for presentation in the Coblentz Symposium at the 29th Pittsburgh Conference, Session on Application of Fourier Transform Infrared Spectroscopy, Little Theater, Cleveland Convention Center, March 2, 1978.

XIV. REFERENCES TO THIS WORK

1. "The Diamond Cell Stimulates High-Pressure Research," by S. Clark and G. Piermarini, Physics Today, 44-55 (September 1976).

2. "The Strange World of Superpressure," by Joan Steen Wilentz, Popular Science, p. 80 (February 1977).

3. "Applications of Fourier Transform Spectroscopy," Chapter 3 by R. J. Bell in Spectrometric Techniques, Vol. 1, p. 123, (George A. Vanasse, editor), Academic Press, N.Y., 1977.

XV. PATENTS

1. Invention Disclosure, S-76G036, "Viscosity Measuring System," for early filing with the U.S. Patent Office. Submitted on February 27, 1976.

2. U.S.P. 4,009,962 (March 1, 1977). An Emission Spectroscopic System Having Compensation for Background Radiation.

3. U.S.P. 3,399,786 (December 14, 1976). System for Spectroscopic Analysis of a Chemical Stream.